

1-1-2016

Imaging Anti-Proliferative Compounds With Flt-Pet

Christopher Mchugh
Wayne State University,

Follow this and additional works at: https://digitalcommons.wayne.edu/oa_dissertations

 Part of the [Biology Commons](#)

Recommended Citation

Mchugh, Christopher, "Imaging Anti-Proliferative Compounds With Flt-Pet" (2016). *Wayne State University Dissertations*. 1561.
https://digitalcommons.wayne.edu/oa_dissertations/1561

This Open Access Dissertation is brought to you for free and open access by DigitalCommons@WayneState. It has been accepted for inclusion in Wayne State University Dissertations by an authorized administrator of DigitalCommons@WayneState.

IMAGING ANTI-PROLIFERATIVE COMPOUNDS WITH FLT-PET

by

CHRISTOPHER I. MCHUGH

DISSERTATION

Submitted to the Graduate School

of Wayne State University,

Detroit, Michigan

in partial fulfillment of the requirements

for the degree of

DOCTOR OF PHILOSOPHY

2016

MAJOR: CANCER BIOLOGY

Approved By:

Advisor

Date

**© COPYRIGHT BY
CHRISTOPHER I. MCHUGH
2016
All Rights Reserved**

DEDICATION

To Vidya and Flash

ACKNOWLEDGEMENTS

When I entered the Shields laboratory in the summer of 2013, I had just finished my first two years of medical and excluding brief summer rotations, had been away from full time laboratory work for the better part of three years. To put it mildly, I was unprepared for what was in store for me. Fortunately I received tremendous support, from conceptual help in designing my studies to technical assistance in carrying out various assays. Others simply listened while I complained about my experiments. To all those who have helped me these past few years, I want to extend my heartfelt thanks.

Advisors:

I would like to thank *Dr. Anthony Shields* for accepting me into his laboratory and supporting my research endeavors; for finding time to talk to me when I needed advice, despite his busy schedule; for reading my last minute abstracts, posters, and manuscripts (including this one); and for giving me the freedom to design and carry out my experiments independently. Mostly I would like to thank Tony for being a wonderful career mentor and a model physician-scientist.

Dr. Manohar Ratnam, thank you for all of your guidance designing my studies, for welcoming me into your lab, for helping me to learn several molecular biology techniques, and for allowing me to randomly barge into your office. Most of all I would like to give my appreciation for inviting me to collaborate with you on this project. Your hard work laid the foundation for the majority of my thesis.

Committee Members:

Dr. Shirish Gadgeel, thank you for help with our patient studies. Although we haven't been able to find our last patient as of this writing, without you we would be unable to

conduct our human studies. In addition, I would like to thank you for teaching me a lot about lung cancer, and for comments throughout the process.

Dr. Wei-Zen Wei, thank you for all your help throughout my graduate studies. You accepted me into your lab as a rotation student, served as my faculty advisor for journal club, and were nice enough to write me a recommendation letter for my F30 grant, even though I hadn't been in your lab for several years at that point.

Dr. Stanley Terlecky, thank you for your constant encouragement and enthusiasm. You taught me a lot about being a graduate student. I am confident you will do fantastic at your next destination. You will surely be missed at Wayne State.

Dr. Daniel Walz, thank you for all of your support throughout my graduate studies, and with my transition back to medical school.

Lab Members:

Jawana, thanks for teaching me how to use all of our imaging software and how to read a PET scan. Also, I would like to thank you for all of the laughs and for bringing me back food from presentations. I will miss hearing stories about your kids; I will never forget about your son asking you to mail him gum.

Kirk, thanks for all of your help with ordering lab reagents, scheduling the microPET scanner, and with our scans. Thanks for putting up with my wanting to image more and more mice per day. Also thank you for giving me someone with whom to talk about *Game of Thrones*. I will miss you during next season for sure.

Stephanie, thank you for showing me how to do tracer uptake assays and helping me interpret my animal images. Also thank you for all of your thoughtfulness and generosity over the years. I will miss your cooking and artwork.

Janice, thank you for everything. You have done so much for me over the years, from scheduling my committee meetings, helping with reimbursement from conferences, to giving me a critical reading of all my writing. I have no idea what I would have done with you. You are truly the glue that holds our laboratory (and Tony's schedule) together.

Collaborators:

Dr. Thomas Mangner, thank you for synthesizing FLT for our experiments and for accommodating my (often last-minute) requests.

Dr. Lisa Polin, thank you for teaching me how to work with mice and for spending countless afternoons in the basement of Elliman injecting mice for our experiments.

Dr. Jing Li, thank for lending your expertise in helping design the Dex treatment strategy that we used in the animals.

Dr. Mugdha Patki, thank you for teaching me how to western blots and PCR. Your patience and understanding was extremely appreciated.

Cancer Biology Program:

Dr. Larry Matherly, thank you for welcoming me into the program and helping me with my F30 grant despite being in the hospital. Although you referred to me as an orphan during my year 1 orientation, I always felt welcome in the CB program.

Dr. George Brush, thank you for your helping me to design my graduate curriculum. I definitely would have been lost without you in that regard.

Nadia Daniel, thank you for all your help with administrative matters throughout my tenure. Also thank you for your assistance with the CB symposium.

Cancer Biology Steering Committee – Thank you for keeping tabs on me throughout my training and for awarding me the DeRoy fellowship this year.

Cancer Biology Students – Thank you for being so welcoming and friendly to me throughout my studies. I will keep in contact with you for years to come and wish you the best.

Others:

Dr. Ambika Mathur, thank you for guiding me through my first years in the MD/PhD program and for helping me so much with my F30 application. Despite your rise into administration, you are still wonderfully student-centered.

Dr. Julie Boerner, thank you for allowing me to use your laboratory space and for your assistance in authenticating my cell lines.

Karri Stark, thank you for teaching me how to do IHC and tolerating my various mishaps in the tissue culture room.

Juiwanna Kushner and Kathryn White, thank you for all your help with the animals.

Family:

Lastly I would like to thank my parents for their constant support and encouragement throughout my (lengthy) education.

TABLE OF CONTENTS

DEDICATION	ii
ACKNOWLEDGEMENTS	iii
LIST OF TABLES	ix
LIST OF FIGURES	x
LIST OF ABBREVIATIONS	xii
CHAPTER 1 – INTRODUCTION	
Anatomic imaging modalities commonly used in oncology	2
Monitoring tumor proliferation	6
¹⁸ F-FLT PET	8
Imaging response to therapy with ¹⁸ F-FLT	13
Limitations of ¹⁸ F-FLT PET	14
Other fluoropyrimidine tracers	15
Glucocorticoids and their use in cancer	17
CHAPTER 2 – UTILIZING FLT UPTAKE TO MONITOR THE EFFECT OF DEXAMETHASONE ON NON-SMALL CELL LUNG CANCER	
Background	21
Materials and Methods	23
Results	28
Discussion	50
CHAPTER 3 – EFFECT OF CAPECITABINE TREATMENT ON THE UPTAKE OF THYMIDINE ANALOGS USING EXPLORATORY PET IMAGING AGENTS: FAU, FMAU, AND FLT	
Background	53
Materials and Methods	55

Results	59
Discussion	66
CHAPTER 4 - SUMMARY.....	69
REFERENCES.....	72
ABSTRACT	120
AUTOBIOGRAPHICAL STATEMENT.....	122

LIST OF TABLES

Table 2.1. Measurement of serum Dex at various time points	32
Table 2.2. Change in tumor FLT uptake in NSCLC patients after Dex.....	41
Table 3.1. Patient Characteristics	58
Table 3.2. Tumor Retention in Patients Imaged with FLT	59
Table 3.3. Tumor Retention in Patients Imaged with FMAU.....	61
Table 3.4. Tumor Retention in Patients Imaged with FAU.....	64

LIST OF FIGURES

Figure 1.1. Thymidine and related PET tracers	10
Figure 1.2. Thymidine pathways used for DNA synthesis	11
Figure 2.1. GR expression in NSCLC cell lines	29
Figure 2.2. Effect of Dex on ³ H-FLT retention in NSCLC cell lines.....	30
Figure 2.3. Dex treatment and animal imaging protocol	32
Figure 2.4A. FLT-PET images of mice with A549 xenografts.....	33
Figure 2.4B. ¹⁸ F-FLT uptake in High-GR α A549 xenografts	34
Figure 2.4C. FLT-PET images of mice with H1299 xenografts	35
Figure 2.4D. ¹⁸ F-FLT uptake in H1299 xenografts	36
Figure 2.5A. GR α expression in mouse xenografts.....	37
Figure 2.5B. GR staining in human xenografts.....	38
Figure 2.6. Interlesion heterogeneity in a NSCLC patient	40
Figure 2.7. Effect of Dex and Pem on ³ H-FLT retention in NSCLC cell lines	43
Figure 2.8A. Effect of Pem on ¹⁸ F-FLT uptake in A549 xenografts.	45
Figure 2.8B. Summary of the effect of Dex and PEM treatments on ¹⁸ F-FLT retention in A549 tumors.....	46
Figure 2.9A. Effect of Pem on ¹⁸ F-FLT uptake in H1299 xenografts.	47
Figure 2.9B. Summary of the effect of Dex and PEM treatments on ¹⁸ F-FLT retention in H1299 tumors.....	48
Figure 2.8C. Summary of the effect of Dex and PEM treatments on ¹⁸ F-FLT retention in H1299-GR α tumors.....	49
Figure 3.1: Tumor FLT Uptake in Patient 3.....	60
Figure 3.2: Tumor FMAU Uptake in Patient 7	62
Figure 3.3: Tumor FAU Uptake in Patient 15.....	65

LIST OF ABBREVIATIONS

Abbreviation	Definition
5-FU	5-fluorouracil
AP-1	Activator protein 1
AUC	Area under the curve
AZT	3'-azidothymidine
CT	Computed tomography
Dex	Dexamethasone
DHFR	Dihydrofolate reductase
dUMP	Deoxyuridine-monophosphate
FAU	1-(2'-deoxy-2'-fluoro- β -D-arabinofuranosyl) uracil
FAU-MP	FAU-monophosphate
FDG	2'-deoxy-2'-fluoro-D-glucose
FLT	3'-deoxy-3'-fluorothymidine
FLT-DP	FLT-diphosphate
FLT-MP	FLT-monophosphate
FLT-TP	FLT-triphosphate
FMAU	1-(2'-deoxy-2'-fluoro- β -D-arabinofuranosyl) thymidine
FMAU-MP	FMAU-monophosphate
GC	Glucocorticoid
GR	Glucocorticoid receptor
GRE	Glucocorticoid response element
hCNT	Human concentrative nucleoside transporter

hENT1	Human equilibrative nucleoside transporter 1
hENT2	Human equilibrative nucleoside transporter 2
HPLC	High-performance liquid chromatography
IHC	Immunohistochemistry
LDCT	Low-dose computed tomography
MI	Mitotic index
MRI	Magnetic resonance imaging
NF- κ B	Nuclear factor kappa-light-chain-enhancer of activated B cells
NSCLC	Non-small cell lung cancer
PBS	Phosphate-buffered saline
PCFT	Proton-coupled folate transporter
Pem	Pemetrexed
PET	Positron emission tomography
RECIST	Response evaluation criteria in solid tumors
RFC	Reduced folate carrier
ROI	Region of interest
SPF	S-phase fraction
SUV	Standardized uptake value
TDP	Thymidine-diphosphate
TdR	Thymidine
TK1	Thymidine kinase 1
TK2	Thymidine kinase 2

TMP	Thymidine-monophosphate
TP	Thymidine phosphorylase
TRR	Tumor retention ratio
TS	Thymidylate synthase
TTP	Thymidine-triphosphate
US	Ultrasonography

CHAPTER 1 INTRODUCTION

Cancer is a heterogeneous group of diseases characterized by the uncontrolled growth and migration of abnormal cells. Cancers arise due to the accumulation of genetic and epigenetic alterations leading to aberrant cellular proliferation and/or reduced cell death (1, 2). At the time of this writing, cancer is the second leading cause of death in the United States, with an approximately 600,000 deaths predicted in 2016; it accounts for nearly 1 in every 4 deaths (3, 4). Since 1990, a decline of roughly 1% per year in overall cancer mortality has been observed, due to a reduction in cancer risk factors, improved early-detection methods, and better therapies (5, 6). Critical to the latter two points have been advances in the field of cancer imaging.

Technical progress in ultrasonography (US), computed tomography (CT) and magnetic resonance imaging (MRI) has greatly improved the diagnosis and staging of solid tumors by enhancing visualization of the anatomic details of tumors (7, 8). Improved detection and staging, in turn, allows for the optimization of therapy and potentially the use of curative approaches, such as surgical resection (9, 10). Furthermore, anatomic tumor measurements obtained from CT or MRI remain the basis for Response Evaluation Criteria in Solid Tumors (RECIST), used widely today in both clinical trials and routine oncologic practice (11). Anatomic imaging, however, is not without its limitations. Conclusions regarding tumor growth rate and cellularity cannot be drawn from CT or MR images. Moreover, it can be difficult to determine the efficacy of anti-neoplastic treatment using only measurements of tumor size. For instance, the slow growth rate of many solid tumors means that it may take weeks or months for treatment failure to become evident (12). Alternatively, successful treatment may leave a fibrotic mass that may persist for weeks or months.

To overcome these shortcomings, anatomic imaging is now regularly combined with molecular imaging techniques, which facilitate the non-invasive monitoring of cellular and subcellular processes, allowing for a greater understanding of cancer physiology (13, 14). Perhaps the most salient example is the use of positron emission tomography (PET) with ^{18}F -labeled 2'-deoxy-2'-fluoro-D-glucose (FDG). PET imaging with FDG exploits increased glycolysis in tumors, providing a way to discriminate between malignant and normal tissue (15-19).

Anatomic imaging modalities commonly used in oncology

The focus of this dissertation will be the use of PET imaging in cancer models, and while PET can provide important information on tumor physiology and biochemistry, relatively low spatial resolution means that important anatomical information is often not present in PET images (20). For that reason, PET is often combined with anatomic imaging modalities, allowing for the visualization of both tumor structure and molecular biology. Therefore, anatomic imaging techniques including CT, MRI, and US will be briefly reviewed, followed by an emphasis on PET imaging.

CT scans utilize a series of x-ray images taken from multiple angles to produce a three-dimensional reconstruction of patient anatomy (21-23). Because of its speed, cost-effectiveness, and high resolution, CT is one of the most commonly used imaging modalities for the detection of solid tumors (9, 13). Further, the use of CT is now a critical element of routine cancer screening (24-27). The National Lung Screening Trial demonstrated that annual screening with low-dose CT (LDCT) reduced lung cancer mortality by 20% in current and former smokers (28, 29). CT can also be used to complement the metabolic images obtained with PET and correct for attenuation of the

radioactive probes used with PET. The major disadvantage of CT is that because tissues are distinguished based solely on differences in x-ray attenuation, soft tissue resolution is relatively poor, and little molecular information can be obtained.

The basis of MRI is nuclear spin. Atoms with an odd number of protons and neutrons, such as ^1H , ^3He , ^{23}Na or ^{31}P have a non-zero nuclear spin, and therefore exhibit a magnetic moment (30). Following excitation by a strong external magnetic field, these atoms emit a radio frequency signal as they return to equilibrium (31, 32). Cancers can be distinguished from normal tissues by the difference in the rate at which atoms return to their equilibrium state (33, 34). A key advantage of MRI over other modalities is that it offers excellent spatial resolution and anatomic detail without exposing patients to ionizing radiation. Aside from its use in cancer diagnosis, screening MRI has been shown to improve overall survival in patients with hereditary breast cancer syndromes (35-37). Recent approaches allow for one to visualize tumor physiology in addition to tumor anatomy. For example, diffusion-weighted MRI uses the slow diffusion of water molecules in tumors to generate contrast (38). Moreover, the use of contrast agents can allow for the detection of tissue vascularization, and iron oxide nanoparticles can be conjugated with targeting molecules to serve as direct imaging probes (39-41). Despite its wide applications, MRI has significant limitations. The strength of the magnetic field precludes the use of MRI in patients with metallic instruments, such as pacemakers; cancer diagnosis can be hampered the presence of air or calcifications; and benign and malignant disease are difficult to distinguish on MRI alone (42). This has led to the recent introduction of scanners combing PET and MRI.

In US imaging, a transducer is used to generate sound pulses that propagate through tissue and are reflected back based on tissue density (43). US is commonly used for cancer detection and to aid in the collection of biopsy samples. The main benefits of US imaging, compared to other imaging techniques used in oncology, are its low cost, portability, and its ability to collect imaging data in real-time, which makes it ideal for repeated measurements (44, 45). When used with specialized probes such as microbubbles, US is able to provide information regarding tumor vasculature in addition to anatomic data (46). Major limitations of US include poor penetration into bone, disruption of sound waves by air or gas, and difficulty in imaging obese patients (47).

The focus of this thesis is the use of PET imaging. PET is a functional imaging technique that uses positron-emitting radionuclides to monitor specific physiologic processes. As the radionuclide decays, it emits a positron, which collides with an electron, resulting in the annihilation of both particles and the production of a pair of gamma photons, which are subsequently detected by the scanning device (48, 49). PET can be used to generate either static or dynamic images. In static PET, data is acquired at a single time point after the injection of a tracer and is used to generate a single frame that represents the average amount of radioactivity during the scan period. Tracer uptake in tissue is frequently expressed using the semi-quantitative measurement Standardized Uptake Value (SUV), which corresponds to the amount of radioactivity in the tissue divided by the injected dose per bodyweight (50). By contrast, in dynamic PET, images collection starts immediately after tracer injection, and tracer activity is monitored over time using a series of continuous acquisitions. Dynamic PET

enables the generation of time-activity curves of the tissue concentration of the radiotracer allowing for the measurement of its pharmacokinetic properties (51).

Classically, PET has been conducted using ^{18}F -FDG, which allows for the detection of malignancies due to increased glucose metabolism compared to normal tissue (17-19). ^{18}F -FDG PET is indicated for the diagnosis and staging of several neoplasms including breast, lung, and gastrointestinal cancers, and is now used to adjust treatment in lymphoma (52-57). Additionally, the use of PET has been explored as a tool for breast cancer screening (58-61). A limitation of ^{18}F -FDG is that non-specific tracer uptake in reactive lymph nodes or infiltrating macrophages can lead to false-positive results (62, 63). Newer approaches using different small molecules, as well as radiolabeled peptides, nanoparticles, and antibodies, allow for the assessment of a variety of cellular receptors and pathways (64-68). In addition, several radionuclides have been explored, such ^{11}C , ^{13}N , ^{15}O , ^{18}F , ^{64}Cu , ^{68}Ga , ^{82}Rb , and ^{89}Zr , with half-lives ranging from 1.3 minutes (^{82}Rb) to 3.3 days (^{89}Zr) (69-74). Although it provides excellent functional information, the major weakness of PET is poor spatial resolution.

Each of these imaging modalities has distinct set of advantages and disadvantages. Combined multimodal imaging enables the visualization of both tumor structure and biological processes at the molecular level, allowing for greater personalization of cancer therapy. For example, in patients with stage III lung cancer, for example, combined PET/CT can be used to detect residual cancer in mediastinal lymph nodes following chemotherapy, allowing physicians to determine which patients are eligible for surgical resection (75, 76). For that reason, imaging plays a prominent

role in several facets of modern cancer care: screening, diagnosis, and assessment of treatment response.

Monitoring tumor proliferation

Given that one of the defining characteristics of cancer is uncontrolled cellular proliferation, it is critical to develop methods to measure the proliferative capacity of tumors. Assessments of tumor proliferation have been found to have prognostic value and have been incorporated into tumor grading systems (77-79). Several techniques have been developed to monitor tumor proliferation, including analysis of fixed tissue as well as imaging approaches.

One of the first methods for measuring tumor aggressiveness was mitotic index (MI), which refers to the proportion of cells undergoing mitosis in a tumor specimen, and is expressed as mitotic bodies per high-power field-of-view (80). MI relies on inexpensive and simple tissue processing methods, and has been shown to predict survival in breast cancer (77, 81). However, poor tissue processing, inaccurate counting, and difficulty in identifying mitotic cells has led to concerns over the reproducibility of MI (82). Moreover, because of variability in the duration of mitosis, the number of mitotic bodies and the rate of cell proliferation may not be correlated (83). Rates of proliferation can be more effectively determined by measuring the fraction of cells in the S-phase of the cell cycle (SPF) using techniques such as flow cytometry to measure the phase distribution of cells, ³H-thymidine labeling, or incorporation of 5-bromodeoxyuridine into DNA (84-86).

The most common current method for measuring proliferation in patient samples is the Ki-67 labeling index. Ki-67 is a nuclear protein expressed in cells in the G1, S, G2,

and M phases, but not in resting (G0) cells (87-89). Staining of tumor specimens with antibodies directed against Ki-67 can be used to measure the percentage of proliferating tumor cells. While its exact function remains unknown, Ki-67 has been shown to be a robust biomarker for tumor aggressiveness, correlating with tumor recurrence and poor prognosis in numerous studies (90-93).

The major weakness of these approaches to assessing tumor proliferation is that they require a biopsy samples, or repeated biopsies in order to gauge treatment response. For many malignancies, the transition from a single progenitor cell to detectable mass takes several years (94). During this time, distinct tumor microenvironments form, in which cells are exposed to different environmental stressors, and have access to different levels of nutrients and growth factors (95-97). The result is significant intratumoral genetic heterogeneity (98, 99). Hence, small biopsy specimens used assess proliferation may not provide an accurate sample from a large tumor mass. Furthermore, they do not provide information with regards to metastatic foci in patients with advanced disease (100).

The shortcomings of biopsy-based metrics have led many to pursue the use of imaging. Studies comparing tumor uptake of FDG and cell proliferation rate showed some promise, but ultimately yielded mixed results (101, 102). Early attempts to image DNA replication, and thus cellular proliferation, involved the use of ^{11}C -labeled thymidine (TdR) (103). ^{11}C -TdR was found to be retained by tumors and other proliferating tissues, and incorporated into DNA (104). Several studies have evaluated the use of ^{11}C -TdR in human cancers, with one study finding a reduction in tracer uptake after chemotherapy to be predictive of clinical treatment response (105).

However, logistical challenges such as the short half-life of ^{11}C (20.3 minutes), difficult synthesis, and rapid degradation *in vivo* by plasma and cytosolic thymidine phosphorylase (TP), ultimately prevented regular clinical use of ^{11}C -TdR (106, 107).

^{18}F -FLT PET

Imaging with 3'-deoxy-3'-fluorothymidine (FLT) was developed to address the drawbacks of imaging with ^{11}C -TdR (108). FLT was originally introduced as an anti-neoplastic agent due to its inhibition of DNA synthesis via chain termination (109). It was later found to be an effective anti-viral compound and used in the treatment of HIV, following the success of a similar drug, 3'-azidothymidine (AZT) (110, 111). However, unacceptable hematologic and hepatic toxicity halted the clinical use of FLT. Although toxic at therapeutic doses, imaging studies typically use less than 1% of a single clinical dose of FLT, and therefore toxicity is not a concern. The structure of FLT is nearly identical to TdR, except that fluorine has been substituted for the hydroxyl group at the 3' position of the sugar, which increases the *in vivo* stability of FLT compared to TdR (Figure 1.1). As a PET tracer, FLT can be labeled with ^{18}F instead of ^{11}C , which greatly improves tracer half-life and therefore makes clinical use more feasible.

Cellular uptake and retention of FLT follows the TdR salvage pathway. FLT enters the cell via human nucleoside transports 1 and 2 (hENT1 and hENT2), human concentrative nucleoside transporter (hCNT), as well as passive diffusion (112, 113) (Figure 1.2). Phosphorylation by the thymidine kinase 1 (TK1) leads to the intracellular trapping of FLT, primarily as FLT-monophosphate (FLT-MP) (114, 115). FLT is subject to glucuronidation in the liver followed by renal excretion in humans (116-118). Early studies conducted in humans and dogs noted that FLT accumulates in proliferative

tissues (e. g. bone marrow, tumors) and has been found to be strongly correlated with Ki-67 (108, 119).

It should be noted that cells have two ways of obtaining TdR for DNA synthesis: the previously described salvage pathway, and the *de novo* pathway, in which the enzyme thymidylate synthase (TS) catalyzes the methylation of deoxyuridine monophosphate (dUMP) to TdR-monophosphate (TMP) (120). Broadly speaking, the balance of *de novo* TdR synthesis and TdR salvage determines the rate of FLT retention within an individual cell (121, 122). Tumors more reliant on salvage will be FLT avid, whereas tumors that primarily utilize *de novo* TdR biosynthesis will exhibit low tracer retention, irrespective of their proliferative capacity (123).

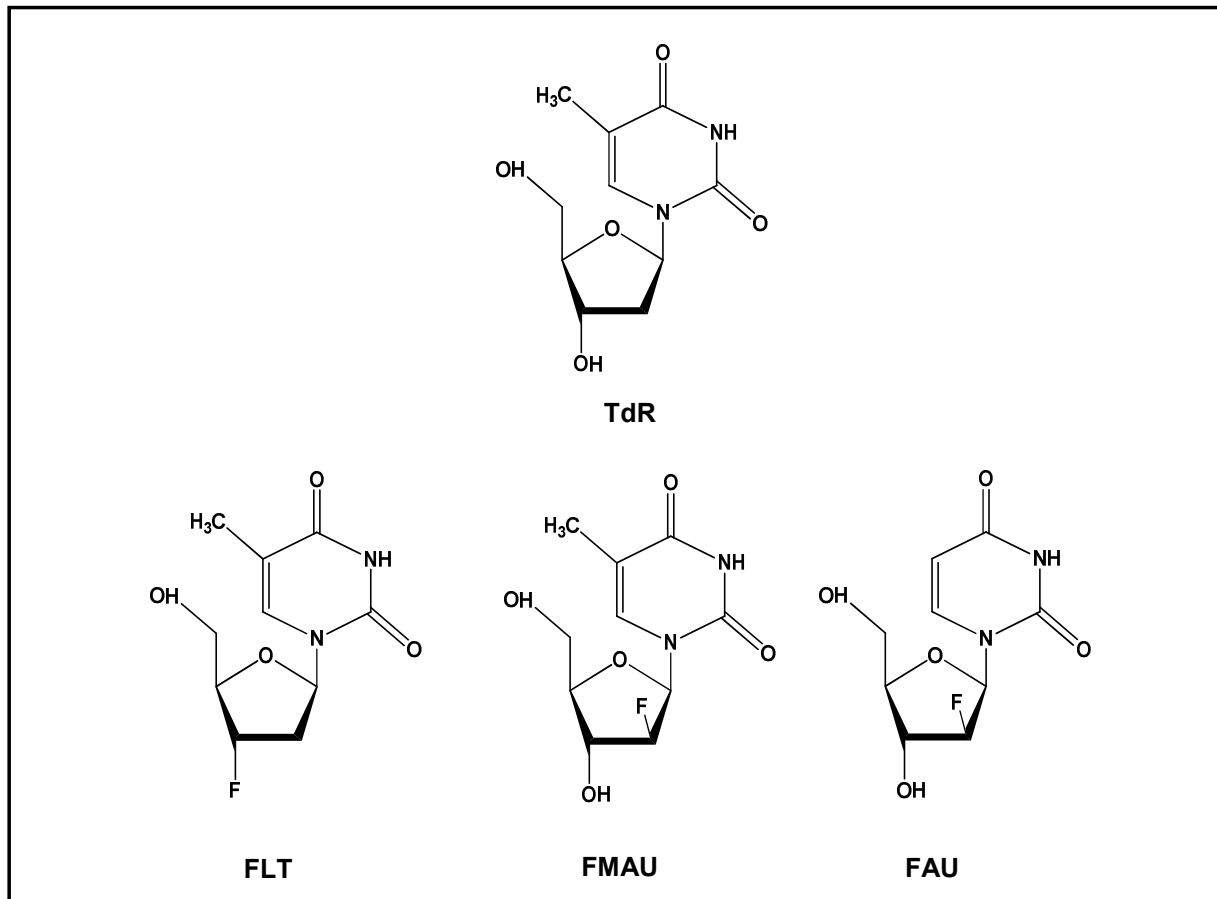


Figure 1.1: Thymidine and related PET tracers. TdR can be labeled at the methyl and ring-2 position with ^{11}C . Analogues of TdR can be labeled with ^{18}F in the 3' or 2' position of the ribose, and are resistant to cleavage by TP. FMAU and FAU can be incorporated into DNA after phosphorylation by TK1. Due to the lack of a 3' hydroxyl group, FLT functions as a chain terminator when incorporated into DNA.

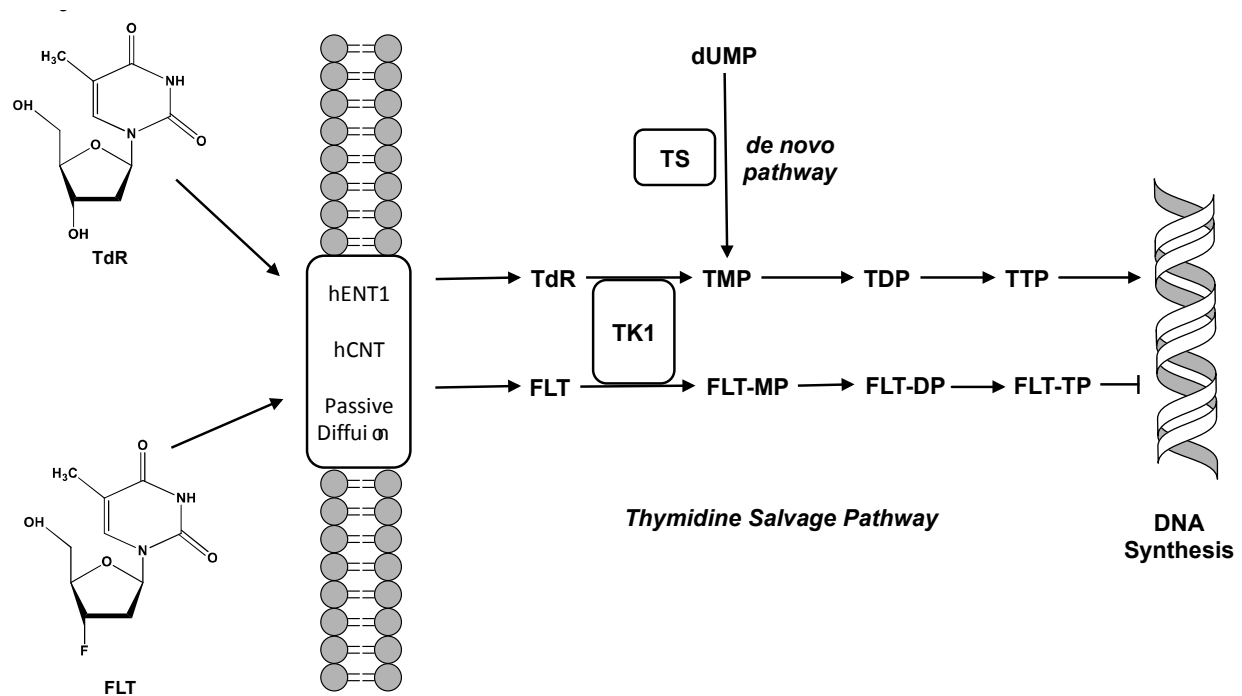


Figure 1.2: Thymidine pathways used for DNA synthesis. In the salvage pathway, TdR and FLT enter the cell via nucleoside transporters (primarily hENT1) and diffusion. Inside the cell, TdR and FLT are phosphorylated by the ATP-dependent enzyme TK1 to TdR-monophosphate (TMP) and FLT-monophosphate (FLT-MP), respectively. TdR is further phosphorylated to TdR-diphosphate (TDP) and TdR-triphosphate (TTP) and then incorporated into DNA. Similarly, FLT-MP can be further phosphorylated into FLT-diphosphate (FLT-DP) and FLT-triphosphate (FLT-TP), but causes chain termination if incorporated into DNA. Alternatively, cells can obtain TdR using the *de novo* pathway, in which TS methylates deoxyuridine monophosphate (dUMP) to TMP.

Within the TdR salvage pathway, several factors impact FLT uptake. Expression of FLT transporters, especially hENT1, has been shown to have profound impact on tumor FLT accumulation. Tumors with low hENT1 activity, either due to natural tumor physiology or inhibition, exhibit poor retention of FLT despite normal TK1 function (124, 125). Moreover, studies incorporating autoradiography and immunohistochemistry (IHC) have shown a strong correlation between expression of hENT1 and FLT retention (126). High endogenous TdR levels, such as found in rodents, can interfere with tracer retention by competing with FLT both at the level of nucleoside transporters as well as intracellular enzymes, resulting in low FLT retention despite proliferative tumors (127, 128). Moreover, some anti-cancer treatments may cause changes in circulating TdR (129). Likewise, high expression of TP in tumors has been shown to correlate with increased FLT accumulation in both preclinical models and patient biopsies (130, 131).

The primary determinant of cellular uptake of FLT is TK1 activity (132). TK1 is a cytosolic enzyme that catalyzes the transfer of a phosphate group from ATP to the 5' hydroxyl group of TdR to form TMP, and plays a key role in regulating intracellular TdR pools (133). Activity of TK1 is highly dependent on the growth state and phase of the cell cycle. The enzyme is up-regulated 10-fold during the S-phase of the cell cycle, and is low or absent in quiescent cells (134-136). Several studies across a wide range of cell lines and human xenografts have demonstrated a strong correlation between FLT retention and TK1 protein expression (137-140). In addition to protein levels, other factors related to TK1 activity, and therefore FLT uptake, have been elucidated. ATP is a required cofactor for the enzymatic activity of TK1, and kinetic analyses in glioma and fibrosarcoma have underscored the importance of ATP in FLT accumulation (141, 142).

Lastly, post-translational modification of TK1, specifically phosphorylation of serine residues, has also been shown to augment TK1 activity (143).

Imaging response to therapy with ^{18}F -FLT

Since its inception, ^{18}F -FLT has been used to examine the response of cancer to a variety of treatments such as chemotherapy, targeted agents, radiation, and endocrine treatment, among others. This review will focus on the use of FLT to monitor the effects of cytotoxic chemotherapy, which has undergone extensive research. Alkylating agents such as temozolamide and cyclophosphamide produce a decrease in ^{18}F -FLT uptake that is in line with decreases in Ki-67 in preclinical models of glioma and lymphoma (144, 145). Similarly, in patients with non-Hodgkin lymphoma treated with cyclophosphamide, hydroxydaunomycin, vincristine, and prednisone, ^{18}F -FLT was markedly decreased 7 days after the start of therapy (146). A decrease in ^{18}F -FLT uptake following treatment with the anthracycline doxorubicin has been found to predict response in preclinical models of lymphoma, lung cancer, and hepatoma (147-149). Furthermore, ^{18}F -FLT is now being investigated as a way to assess response in patients with acute myeloid leukemia being treated with a related compound, idarubicin (150). In addition, post-treatment reductions in ^{18}F -FLT retention have been shown to be predictive of response to cisplatin in patient-derived models of ovarian cancer (151).

Unlike the previous described treatments, which cause reductions in ^{18}F -FLT uptake as cells lose their proliferative capacity, agents that target the *de novo* TdR synthesis pathway, such as the TS-inhibitor 5-fluorouracil (5-FU), can lead to a transient rise in FLT uptake, termed the 'flare' phenomenon (152). As TMP levels drop due to TS inhibition, TdR salvage proteins, TK1 and hENT1, are upregulated, as cells attempt to

replenish TMP levels exogenously (126, 152, 153). This increase in TdR salvage leads to a window of 1-24 hours in which FLT uptake is increased until insufficient TMP results in arrest of DNA synthesis and cell death. This effect has been observed in response to nucleoside analogs: 5-FU and gemcitabine, as well as antifolates: methotrexate and pemetrexed (Pem) in preclinical models of glioma, esophageal, colon, and breast cancer (142, 152, 154-157). The flare has been explored as a marker for treatment response in a trial of colorectal cancer patients treated with 5-FU as well as a study of Pem in non-small cell lung cancer (NSCLC) patients. In both of these studies, the presence of a flare shortly after therapy did not correlate with response (158, 159). Of note, the results observed by Frings et al. may have been confounded by the use of steroids, which will be expounded upon later. As of now it remains unclear if the flare effect can be a useful tool for assessing response. It may simply be a way to indicate that the drugs are hitting their targets.

Limitations of ^{18}F -FLT PET

Despite its promise as a proliferation imaging agent, ^{18}F -FLT has a number of noteworthy limitations. High basal uptake in normal bone marrow and excretory organs (liver, kidneys, bladder) restrict the use of ^{18}F -FLT in cancers involving those regions (160). As discussed, ^{18}F -FLT uptake will underestimate cell proliferation in tumors that are heavily reliant on *de novo* TdR synthesis (121). Moreover, treatments that alter the balance between the *de novo* and salvage pathways such as TS-inhibiting agents, antifolates, or topoisomerase inhibitors can have drastic effects on tumor ^{18}F -FLT retention, which may not reflect changes in proliferation (142, 152, 155, 161). Finally, similar to what has been observed with FDG, inflammation can be a source of confusion when

imaging with ^{18}F -FLT. Previous work has illustrated that proliferating macrophages due to bacterial infection or atherosclerosis exhibit significant uptake of ^{18}F -FLT (162, 163). In trials examining FLT uptake in patients with head and neck cancers, high tracer uptake in proliferating lymphocytes within lymph nodes resulted in false-positive findings (164, 165).

Other fluoropyrimidine tracers

The success of FLT spurred the development of other fluoropyrimidine PET tracers. Like FLT, 1-(2'-deoxy-2'-fluoro- β -D-arabinofuranosyl) thymidine (FMAU) was developed as an anti-viral and anti-neoplastic compound due to cytotoxicity following its incorporation into DNA, but was later abandoned due to severe toxicity (166, 167). FMAU was later adapted to molecular imaging (160, 168). Like FLT, FMAU is resistant to TP-mediated cleavage due to the presence of fluorine on its ribose group. A key difference between the tracers, however, is that FMAU has an intact 3' hydroxyl group and can therefore incorporate into the DNA (Figure 1.1) (169). Furthermore, FMAU is a more potent substrate for thymidine kinase 2 (TK2), located in the mitochondria, than TK1 (167). Unlike TK1, TK2 is constitutively expressed, with low activity in both dividing and quiescent cells (170, 171). Accumulation of ^{18}F -FMAU is higher in tumors than most healthy tissues and preclinical studies have shown that its uptake is enhanced in response to conditions that produce an increase in mitochondrial mass such as oxidative, reductive, and energy stress (172, 173). In addition, low physiologic uptake of ^{18}F -FMAU by normal bone marrow may allow it to be useful in the detection and monitoring of bone marrow metastases (168). Further, the rapid clearance of ^{18}F -FMAU

from the blood in humans (90% cleared within 10 minutes), allows for improved imaging in the pelvis compared to ^{18}F -FLT and shortened imaging time (168, 174).

1-(2'-deoxy-2'-fluoro- β -D-arabinofuranosyl) uracil (FAU) is a nucleoside analog that functions as a prodrug form of FMAU (169). Following cellular uptake of FAU, it is phosphorylated to FAU monophosphate (FAU-MP) and then converted to FMAU monophosphate (FMAU-MP) via the action of TK1 and TS, respectively (175). FMAU-MP is then incorporated into DNA, resulting in cell death (176). Dependence on TS for activation was designed to target FAU against malignancies with high expression of this enzyme and to avoid the neurotoxicity that resulted in the discontinuation of clinical FMAU use (166, 177-179). High expression of TS is a major mechanism of resistance to chemotherapeutic agents such as 5-FU and capecitabine and has been associated with poor clinical outcome in breast and colorectal cancer (180-182). Furthermore, the structure of FAU allowed for its tissue distribution to be monitored using PET, and potentially serve as a technique for imaging the *de novo* TdR synthesis pathway (183, 184) (Figure 1.1). Early studies found that FAU caused significant growth inhibition when administered to cell models with high TS expression, and animal experiments showed incorporation of FAU into tumor DNA as FMAU (169, 179). However, the exploration of a FAU as a chemotherapeutic was later stopped when a patient developed fatal liver toxicity during a phase I clinical trial (185). However, a study of ^{18}F -labeled FAU in humans and dogs found higher uptake in tumors than normal tissue (177, 178). More recently, a pharmacokinetic modeling study demonstrated that the conversion of FAU to FMAU is greatly increased in tumors compared to normal tissues

(186). Therefore, its failures as a cancer treatment, FAU may have some utility as an imaging agent.

Glucocorticoids and their use in cancer

Glucocorticoids (GCs) are a class of steroid hormones that play a critical role in basal and stress-related homeostasis through their regulation of pathways involved in metabolism, cell proliferation and apoptosis, and inflammation (187-189). GCs comprise both endogenously produced cortisol, as well as a number of synthetic derivatives such as prednisone and dexamethasone (Dex). The actions of GCs are mediated by the glucocorticoid receptor (GR), a member of the nuclear receptor family of ligand-dependent transcription factors. Alternative splicing of the human GR gene yields two isoforms with distinct functions: GR α and GR β (190, 191). In the absence of hormone, GR α is located in the cytoplasm bound to a complex of chaperone proteins, including hsp90 (192). GC binding causes leads to the dissociation of GR α from its complex and subsequent translocation into the nucleus (193). In the nucleus, GR α homodimerizes and binds to Glucocorticoid Response Elements (GREs) where it has variable effects on the expression of target genes, depending on the specific promoter and GRE sequence (194). GR α can also exert GRE-independent effects on gene expression by interacting with transcription factors such as nuclear factor kappa-light-chain-enhancer of activated B cells (NF- κ B) and activator protein 1 (AP-1) (195, 196). Conversely, GR β resides in the nucleus, is unaffected by the presence of hormone, and is not transcriptionally active (197). Rather, GR β binds to GR α and prevents GR α -mediated transcriptional effects. Unlike GR α which is ubiquitously expressed, GR β is expressed highly in specific tissues such bronchiole epithelium, liver bile ducts, and the thymus (198). The

ratio of GR α : GR β in a given cell determines its sensitivity to GCs and contributes to the variability of their effects across different tissues (199).

GCs are standard-of-care treatments in several lymphoid malignancies including acute lymphoblastic leukemia, Hodgkin's and non-Hodgkin's lymphoma, and multiple myeloma (200-204). In these cell types GR signaling leads to apoptosis (205, 206). The precise mechanism of GC-mediated apoptosis remains unclear, but may be due to induction of pro-apoptotic members of the Bcl-2 family and/or inhibition of anti-apoptotic proteins (187, 207).

Unlike in cancers of hematopoietic cells, GCs do not typically cause apoptosis in solid tumors (208). However, GCs such as Dex have been found to exert an anti-proliferative effect in several cancer models through reversible G1 cell cycle arrest (209-211). Following the removal of Dex, cells reenter the cell cycle in a synchronized fashion, with an enrichment of cells in the S-phase after 24 to 48 hours (210, 212, 213). Growth inhibition by Dex occurs in only in tumors with high expression of GR and can be blocked by the GR antagonist RU-486 (214-216). High GR expression has been observed in many tumors such as breast, lung, renal, glioma, and melanoma, reflecting its wide distribution in healthy tissues (217, 218).

Given that many chemotherapeutic agents have been found to be most efficacious when applied to rapidly growing cells, and that radiation sensitivity varies by cell cycle, many studies have sought to examine the effect of Dex on the effectiveness on these cytotoxic treatments (219, 220). In both cell models and xenografts GC pretreatment has been demonstrated to reduce the therapeutic effect of commonly used agents such as including cisplatin, doxorubicin, methotrexate, and Pem (213, 221-224).

A large randomized trial in breast cancer patients found that the addition of low-dose prednisone to standard adjuvant chemotherapy resulted in no survival benefit and was associated with increased risk for bone relapses (225). Additionally, a retrospective study of teniposide in NSCLC patients with brain metastases found that patients who received GCs for peritumoral edema had a significantly lower response rate than patients who did not receive GCs (226). However, patients receiving GCs may have simply had more severe disease. Further research is likely required to determine if chemoprotective effects of GCs observed in cancer models extend into human disease.

For patients with solid tumors, GCs are most commonly used to provide symptomatic improvements such as relief of fever, weakness, and lethargy. GCs can also produce a feeling of mild euphoria and stimulation of appetite in critically ill patients (227, 228). In patients with brain tumors, daily Dex treatment is used to reduce edema that responsible for neurologic symptoms (229). GCs are also used to improve side effects associated with chemotherapy. Dex is routinely used to reduce chemotherapy-induced emesis (230). Pem, a standard therapy in advanced non-squamous NSCLC requires Dex prophylaxis to reduce the incidence and severity of a serious skin rash associated with its therapy (231).

In summary, there is a lot of evidence in the literature that GCs can have detrimental effects on many anticancer drugs used to treat solid tumors, and that these effects are mediated through GR. However, it is not advisable to completely abolish their use given that 1) they play a vital role in the supportive care of cancer patients and 2) not all tumors express GR at sufficient levels to elicit cell cycle arrest. A better option would be to explore the use of biomarkers to predict which patients would benefit from

GCs, and in which patients they should be avoided. In this dissertation I will explore the use of FLT-PET as such a biomarker.

I have the following specific aims:

- 1) Utilize FLT to detect Dex-mediated S-phase suppression in NSCLC cell lines, xenograft models, and in patients.
- 2) Examine a flare in TK1 activity following Pem treatment in NSCLC, and assess its utility as a marker for Dex suppression in NSCLC.
- 3) Explore the effects of capecitabine treatment on the uptake of fluoropyrimidine PET imaging agents.

CHAPTER 2 UTILIZING FLT UPTAKE TO MONITOR THE EFFECT OF DEXAMETHASONE ON NON-SMALL CELL LUNG CANCER

BACKGROUND

Lung cancer is the leading cause of cancer-related mortality in the United States, accounting for 27% of cancer deaths (4). NSCLC comprises 83% of lung cancers, and the majority of patients have advanced disease at the time of diagnosis (232). Several randomized clinical trials have shown that Pem, given as a monotherapy or in combination with a platinum-containing compound, is preferred chemotherapy for the treatment of advanced non-squamous NSCLC (233-236). Pem is a folate anti-metabolite that enters cells via the reduced folate carrier (RFC) and the proton-coupled folate transporter (PCFT), and causes cytotoxicity through inhibition of TS, as well as other enzymes involved in nucleotide biosynthesis including dihydrofolate reductase (DHFR) (237, 238).

Despite its relatively mild toxicity profile, a major adverse effect of Pem is the manifestation of a generalized, painful, pruritic skin rash (239). To protect against this rash, patients are administered 4 mg of Dex twice daily starting the day before therapy and continuing until the day after treatment (240). In addition, Dex is frequently used as an anti-emetic for patients receiving cisplatin or carboplatin (241). Dex is a synthetic GC that upon binding to GR α modulates genes involved in cell proliferation and apoptosis, as well as inflammation and the inflammatory response (242, 243). Recently, Dex, in a GR α -dependent fashion, has been found to cause reversible G1 cell cycle arrest in NSCLC cells, resulting in the protection of cells from Pem cytotoxicity (224).

Given that Pem is always accompanied by Dex pretreatment, chemotherapy with Pem may be contraindicated in subpopulation of tumors that are arrested when

exposed to the GC. It is therefore critical to develop a technique that can be used to ascertain the GR α level in patients who are candidates for Pem therapy. Analysis of biopsy specimens is likely inadequate for this task given the enormous clonal heterogeneity that has been observed within solid tumors and between metastatic foci (99, 100, 244). Furthermore, just the presence of GR α in a tumor may not indicate that the pathway is actually functional.

A rapid and non-invasive technique to functionally image the effect of Dex on NSCLC over a patient's entire cancer burden would be to monitor retention of ^{18}F -FLT. Developed for use with PET, radiolabeled FLT is taken up by tumor cells and trapped intracellularly via phosphorylation by the S-phase-specific enzyme TK1 (245). Changes in ^{18}F -FLT retention can therefore be used to monitor the effect of compounds such as Dex which alter cell cycle progression (108). Uptake of ^{18}F -FLT is reproducible and has been shown to correlate with the proliferative marker Ki-67 in NSCLC (119, 160, 246). Here we applied ^{18}F -FLT PET as a direct functional probe to measure Dex-mediated S-phase suppression in NSCLC. Additionally, we sought to use ^{18}F -FLT accumulation to monitor the effect of Pem *in vivo*. The basis for this was the observation that compounds that inhibit *de novo* TdR biosynthesis, such as Pem, elicit a transient increase in FLT uptake due to up-regulation of TdR salvage, termed the 'flare' phenomenon (154, 155). This effect may provide a way to visualize the interference of Dex with Pem activity *in vivo*.

MATERIALS AND METHODS

Cell culture and reagents

Non-squamous NSCLC cell lines A549, H1299, H358, H226, H460, H1650, and H292 were grown in RPMI 1640 medium (GE Life Sciences), supplemented with 10% fetal bovine serum (FBS) (Life Technologies, Carlsbad, CA), 1% penicillin and streptomycin and 2mM glutamine (GE Life Sciences) in a humidified incubator at 5% CO₂ and 37°C. H1299 cells over expressing GR α (H1299-GR α) were a generous gift from Dr. Manohar Ratnam at the Karmanos Cancer Institute; their development is described elsewhere (224). All Cell lines were authenticated using the PowerPlex(r) 16 System from Promega (Madison, WI) in the Applied Genomics Technology Center at Wayne State University. Sample collection and analyses are performed in the Biobanking and Correlative Sciences using ATCC and DSMZ reported karyotypes. The method requires a match of over 80% for a cell line to pass authentication and all the cell lines used had a 100% match (247). Charcoal-stripped FBS was purchased from Life Technologies to remove glucocorticoids. Dexamethasone used in cell studies was purchased from EMD Millipore (Billerica, MA) and Pemetrexed was obtained from LC Laboratories (Woburn, MA). Veterinary grade dexamethasone (Dexaject) was purchased from Bimeda (Llangefni, Wales, UK). PCR primers and TaqMan probes were either purchased from the Life Technologies inventory or custom synthesized by Integrated DNA Technologies (Coralville, IA). The anti-GR antibody (#12041) used in western blot and immunohistochemistry analysis was purchased from Cell Signaling Technology (Danvers MA).

³H-FLT uptake measurements

Cells were seeded 5 x 10⁵ cells/well in a 6-well plates in phenol-red-free medium supplemented with charcoal-stripped FBS. Treatments were initiated after the cells were

attached. After the pre-specified treatments, cells were transferred to media containing approximately 1600 Bq ^3H -FLT (95% pure by high performance liquid chromatography (HPLC)) obtained from Moravek Biochemicals (Brea, CA) and incubated for 1 hour. Media was then removed and cells were washed four times with ice cold phosphate-buffered saline (PBS) (Life Technologies) to remove radioactive media. After washing, cells were lysed by 1M KOH, mixed with 5 mL of Ultima Gold XR scintillation cocktail (PerkinElmer, Waltham, MA) and sample activity was measured by a Packard Tricarb 2910TR liquid scintillation analyzer (PerkinElmer, Waltham, MA). Activity of samples was normalized to cell number using a parallel experiment and cell counting via the trypan blue (Invitrogen, Carlsbad, CA) exclusion method. All experiments were performed in triplicates.

Establishment of NSCLC xenografts

The Wayne State University Institutional Animal Care and Use Committee approved all experimental procedures described herein. Subcutaneous tumor xenografts were established by implanting cubic fragments (~2 by 2 by 2 mm) of tumor tissue bilaterally into the axilla of 4-6 week old female SCID NCr mice purchased from Charles River Laboratories (Wilmington, MA) using a 12-gauge trocar. Mice were supplied water and food ad libitum. It is important to note that compared to humans, mice have 10-fold higher plasma levels of folates, predominantly levomefolic acid, which has been shown to reduce the activity of anti-folates such as Pem and raltitrexed (248, 249). In addition, there is a 10-fold higher level of TdR in murine plasma compared to human plasma, which represents a significant issue for the testing of TS inhibitors, such as PEM, in mice (250, 251). Circulating TdR can be taken up by cancer cells and

converted to TMP thereby rescuing TdR depletion caused by inhibition of TS (252). These two issues may complicate study of the anti-folate and TS inhibitor Pem in murine models. Feeding animals a folate-deficient diet has been shown to reduce endogenous folate levels and simulate drug toxicity observed in humans (253). Therefore, animals treated with Pem were placed on a low-folate diet (Harlan Teklad, Madison, WI) starting 10 days prior to treatment. Tumor measurements were made twice per week using calipers and tumor volumes were calculated by the formula, $V = (L \times W^2)/2$, where (L) is the longest diameter and width (W) is the shortest diameter. Animals were placed on study when tumors reached an average volume of 250 mm³.

MicroPET imaging

PET images were acquired using a Concorde Microsystems R4 scanner (Knoxville, TN). Animals were injected intravenously (iv) with approximately 9.5 MBq of ¹⁸F-FLT, synthesized as published (254). One hour following tracer injection, anesthesia was induced in mice with 3% and maintained 2% isofluorine for the duration of the experiment. Anesthetized mice were placed supine in the microPET scanner and positioned such that their tumors would near to the center of the field of view. During the 10-minute emission scan, animals' body temperature was maintained by a heating component under scanner bed. After their final scan, animals were euthanized while still under anesthesia via cervical dislocation, or if they had recovered from anesthesia, they were euthanized with CO₂ followed by cervical dislocation. Reconstructed images were evaluated with PMOD imaging software (Zurich, Switzerland) and tumor borders were defined with isocontours halfway between the minimum and maximum thresholds of the tumor. Tracer activity within these regions was corrected for decay and converted to

standardized uptake values (SUVs), using the formula $SUV = [\text{Radioactivity concentration in Tumor (kBq/cc)} / \text{Injected Dose (kBq)} / \text{Body Weight (g)}]$. Data is expressed in terms of SUV_{max} , which reflects the activity of the hottest pixel within the tumor.

Measurement of Dex levels in animal blood

Whole blood was collected from animals treated with Dex at pre-determined intervals via cardiac puncture. Serum was collected by allowing whole blood to clot at room temperature for 30 minutes, followed by refrigerated (4°C) centrifugation at 10,000 x g for 15 minutes to remove the clot. The resultant serum samples were stored at -20°C. Serum Dex concentration was then measured with LCMS/MS analysis following published protocols (255).

Tissue preparation and IHC

Animal tumors were removed and fixed in 10% neutral-buffered formalin (Fisher Scientific, Pittsburgh, PA) at room temperature for 48 hours. Specimens were then dehydrated with ethanol and embedded into paraffin blocks. Blocks were divided into 5 µM sections using a microtome and transferred onto glass slides. For IHC, paraffin was removed from tissue sections and antigens were retrieved by heating-induced epitope retrieval. Sections were incubated for 1 hour at room temperature with 10% goat serum in PBS to decrease non-specific binding and incubated overnight at 4°C with rabbit anti-GR (1:400). Samples were counterstained with Meyer's hematoxylin (Lab Vision, Fremont, CA).

Patient imaging

Four patients recently diagnosed with advanced non-squamous NSCLC were enrolled at the Karmanos Cancer Center. Patients were selected because they were scheduled to receive Dex alongside chemotherapy with Pem or docetaxel. Patients were imaged with ^{18}F -FLT PET at baseline and after treatment with oral Dex (4 mg twice daily) for 24 hours. ^{18}F -FLT was synthesized as described previously, and injected iv into patients (range: 167-265 MBq; mean: 226 MBq) over 60 seconds. Following an incubation period of 1 hour, static, whole body PET and CT images were collected using a GE Discovery STE PET/CT scanner (GE Medical Systems, Milwaukee, WI). Reconstructed images were viewed using Osirix Imaging Software (Geneva, Switzerland). Tumor SUV_{max} values were obtained by drawing volumes of interest over the tumor plane with the most active pixel and the two adjacent planes. In patients with multiple lesions, all evaluable (> 2 cm) lesions were assessed using this technique. The protocol for this study was reviewed and approved by the institutional review board at Wayne State University. All patients signed a written informed consent prior to their enrollment.

Statistical considerations

All statistical tests were conducted using GraphPad Prism version 6 (GraphPad Software, La Jolla, California, USA). For cellular tracer uptake studies, one-way ANOVA analysis was used. For animal studies we utilized paired sample ANOVA analysis adjusting for unequal sample size, when appropriate.

RESULTS

Changes in ^3H -FLT uptake reflect sensitivity to Dex

As discussed, the level of expression of GR α was found to be the major factor in determining whether cells would be protected from Pem following Dex pretreatment. To determine whether Dex sensitivity is associated with changes in FLT uptake, several NSCLC cell lines with varying expression of GR α were tested, including A549, H292, H226, H358, H460, H1650, H1299, and the recombinant cell line H1299-GR α (Figure 2.1). Cells were plated in glucocorticoid-depleted media, and treated with Dex (100 nM), which corresponds to the peak plasma dose of Dex in humans following a single dose 4 mg oral Dex (256). In cells with the highest relative GR α expression there was a significant reduction in ³H-FLT accumulation after 24 h Dex (Figure 2.2). ³H-FLT was further decreased after 48 h, in-line with observed suppression of the S-phase fraction of cells ($P < 0.01$).

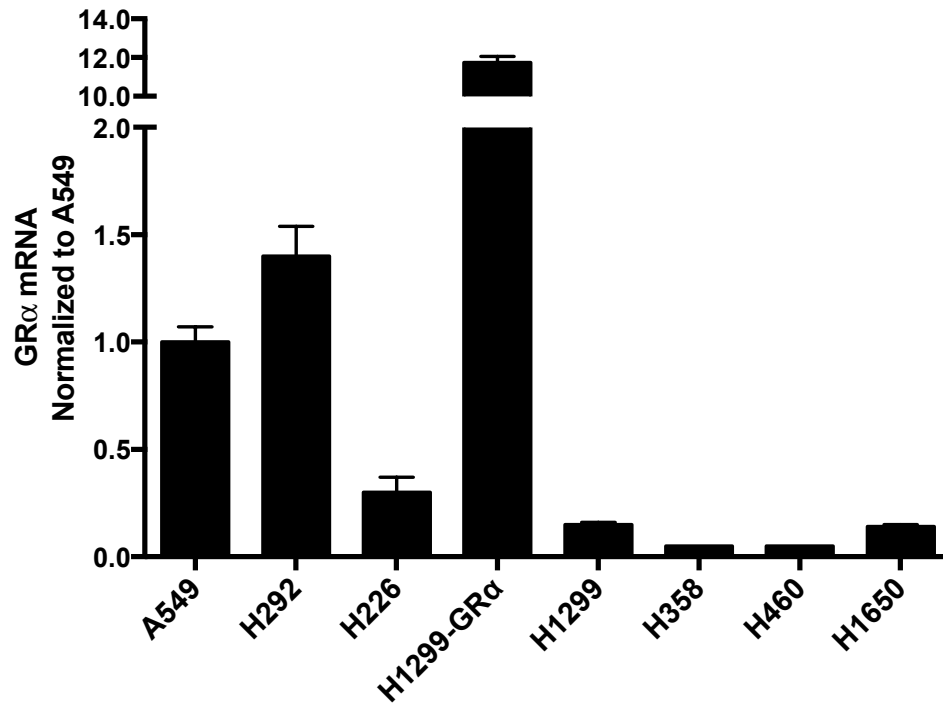
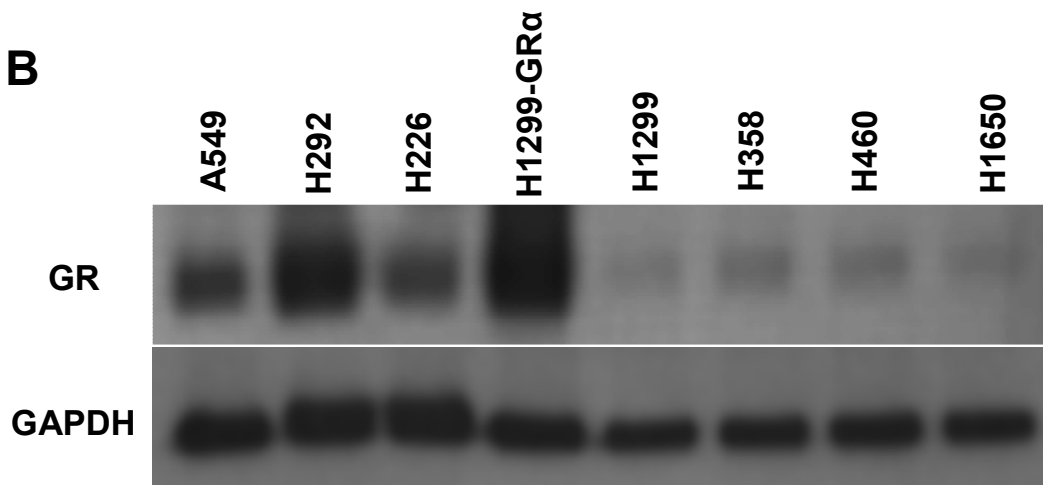
A**B**

Figure 2.1: GR expression in NSCLC cell lines. (A) GR α mRNA measured by RT-PCR. Error bars represent standard deviation between biological triplicate samples (B) Western blot showing total GR protein expression.

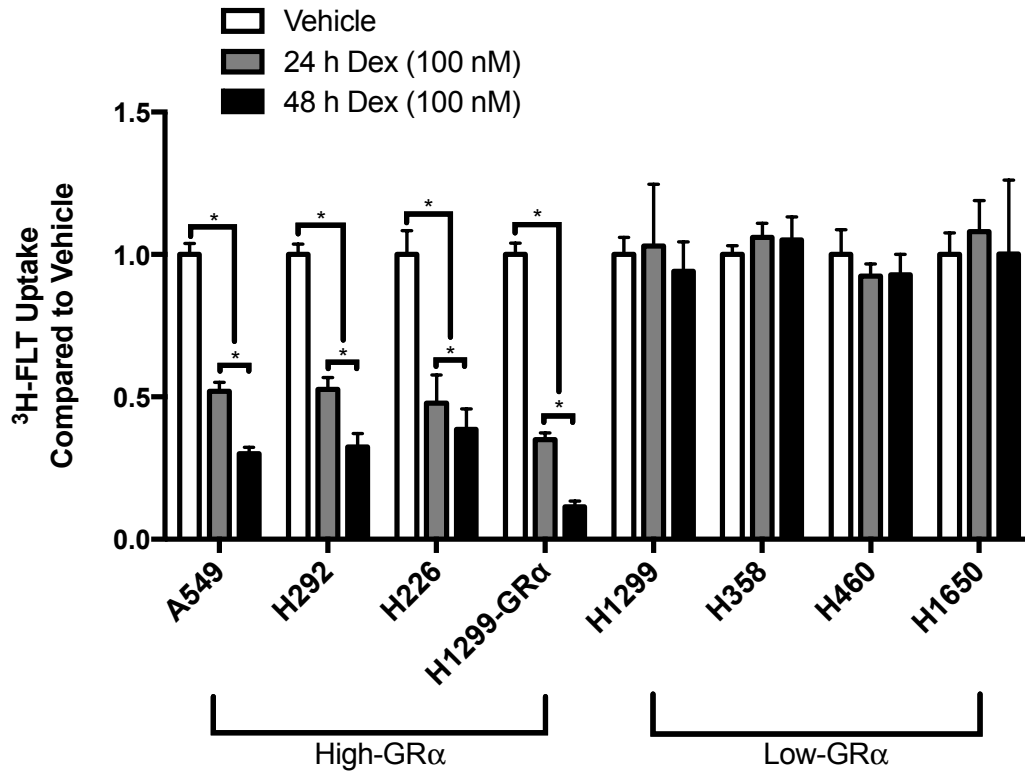


Figure 2.2: Effect of Dex on ^3H -FLT retention in NSCLC cell lines: NSCLC cell lines were grown in glucocorticoid-depleted media and treated with Dex (100 nM) or vehicle (ethanol) for 24 or 48 hours. Cells were then transferred to media containing ^3H -FLT and incubated for 1 hour. After washing, cells were lysed by KOH and the activity of samples was measured with a liquid scintillation counter and normalized to vehicle. Cell lines with the highest relative levels of GR α exhibited significant reductions in ^3H -FLT uptake after Dex treatment. In contrast, tracer uptake low-GR α expressing cells was unchanged by Dex. $P < 0.01$

Dex reversibly decreases ¹⁸F-FLT retention in human xenografts

To determine whether ¹⁸F-FLT PET can detect Dex sensitivity *in vivo*, SCID mice were implanted bilaterally with A549 tumors and were treated and imaged according to the protocol shown in Figure 2.3. Dex dosing in animals was scheduled to simulate the dosing regimen used clinically, and serum Dex levels were verified using LCMS/MS (Table 2.1). A dosing system of 15 mg/kg, twice daily, intraperitoneally (ip) was found to produce steady state serum concentrations within the pharmacological effective range of Dex (~37 nM 12 hours after the 3rd dose) (257). SUV_{max} in A549 tumors decreased by an average of 63.1% following 24 h Dex (Figure 2.4). 72 h post treatment, tumors regained their proliferative capacity and SUV_{max} values were in-line with control tumors, indicating the reversibility of Dex-mediated cell cycle arrest $P < 0.01$.

To further establish the ability of ¹⁸F-FLT to image the anti-proliferative effect of Dex, we imaged mice bearing low-GR α H1299 tumors as well as H1299 tumors in which GR α has been lentivirally transduced. Similar to animals with A549 tumors, mice bearing H1299-GR α exhibited post-treatment reductions in tumor SUV_{max} that rebounded after 72 h Dex withdrawal (Figure 2.4). Interestingly, in H1299 tumors, which express low levels of GR α and were unaffected by Dex in cell culture, we observed a mean decrease of 20.8% in FLT accumulation. Harvested tumors revealed that although GR α mRNA levels remain lower in H1299 tumors than the other xenograft models used herein, H1299 tumors stained positive for GR (Figure 2.5). This result is likely due to greater cellular stress (e.g. hypoxia) in tumor cells compared to H1299 cells grown in culture leading to an upregulation of GR (258).

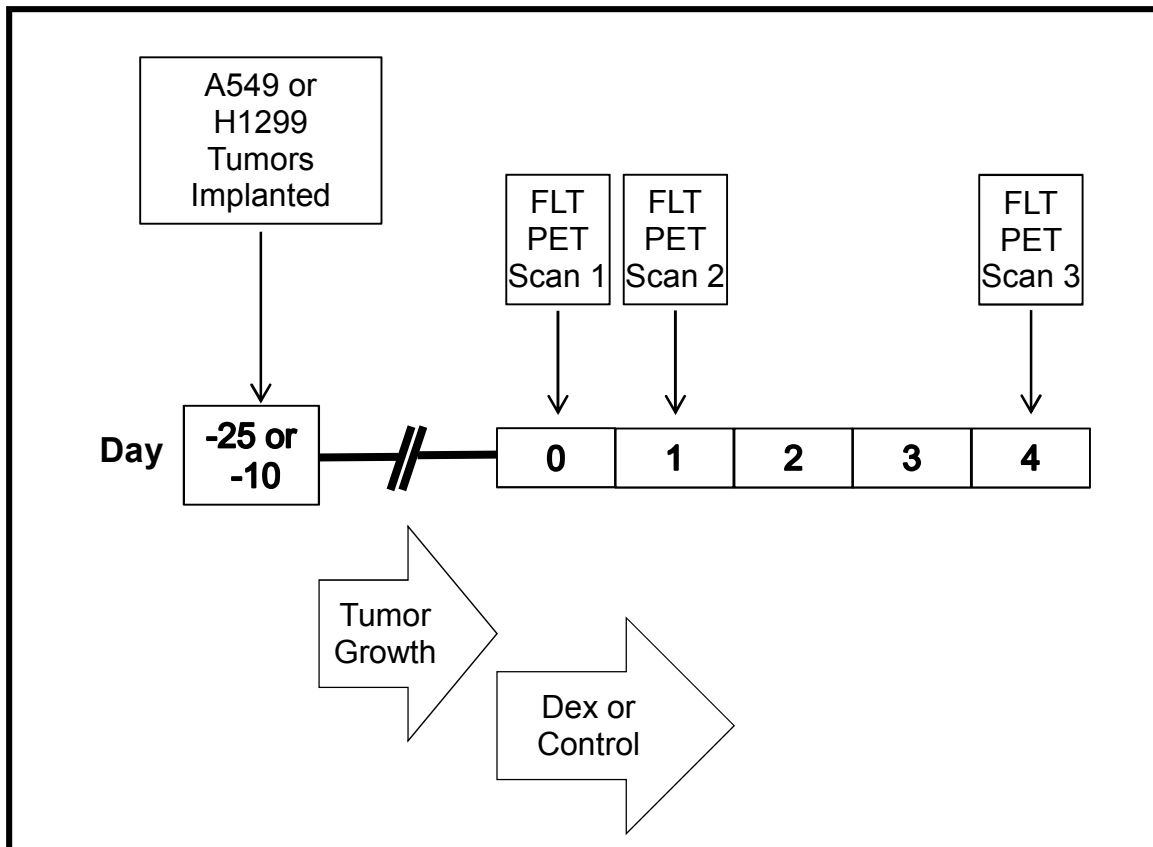


Figure 2.3: Dex treatment and animal imaging protocol. 4-6 week-old female SCID mice were implanted with A549 or H1299 xenografts via trocar. After a period of tumor growth animals were imaged at baseline (Scan 1), after 24 h of treatment with Dex (15 mg/kg twice daily, ip) or control (Scan 2), and again 72 h after the final treatment (Scan 3) to assess reversibility.

Sampling Time (Hr)	Serum Dex Concentration (nM)
24 (pre-dose)	22
24 (pre-dose)	28
26	4970
26	8140
36	61
36	14
48	0
48	0

Table 2.1: Measurement of serum Dex at various time points. To validate our Dex dosing regimen, mice were treated (15 mg/kg ip, twice daily) for 24 h (3 doses total). Blood samples were collected at 24 hours (pre-dose), 26 h, 36 h, and 48 h. Two mice were used for each time point. Serum Dex spiked 2 h post treatment and settled to an average of 38 nM by 36 h. Dex levels were undetectable 24 h after the final dose.

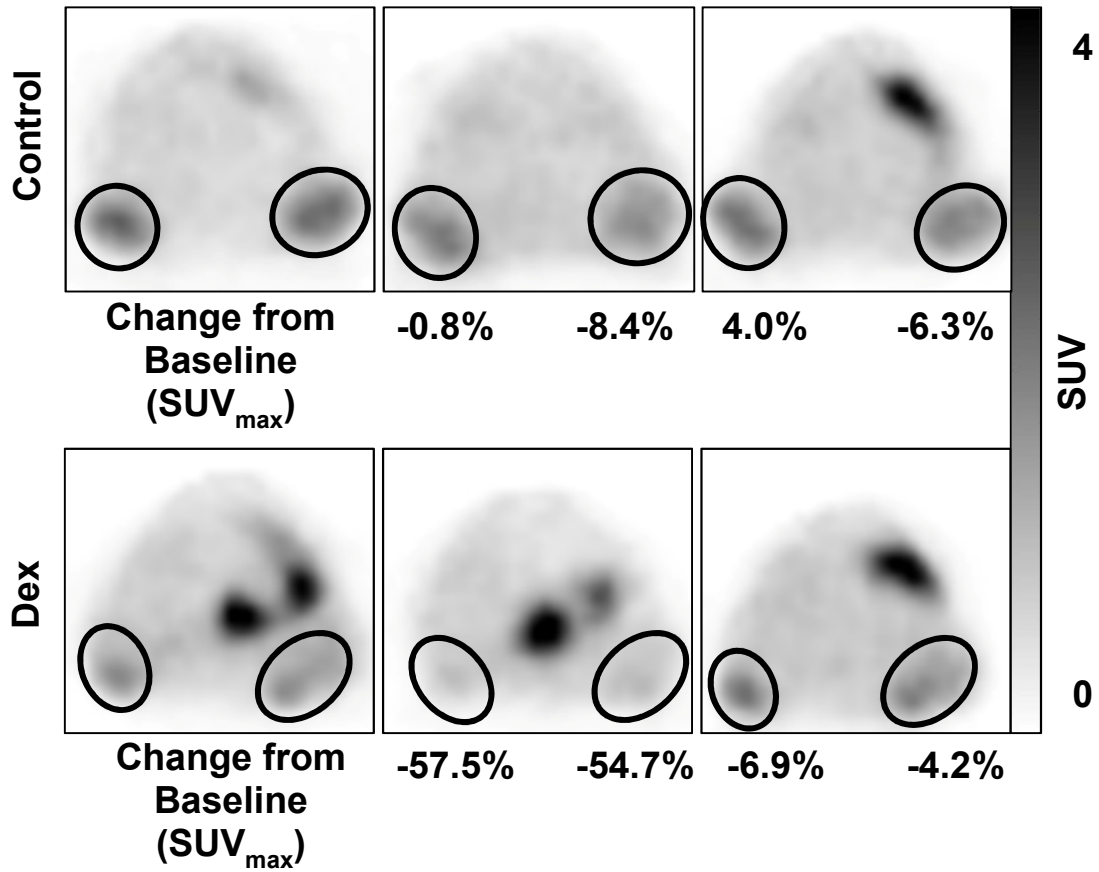


Figure 2.4A: Representative ^{18}F -FLT PET images of mice with A549 xenografts. In control animals (top panel) tumors exhibited negligible change in ^{18}F -FLT uptake between the three scans. In mice treated with Dex for 24 h (bottom panel), tumor ^{18}F -FLT retention decreased by 57.5 and 54.7. 72 h after the final dose of Dex, tumors returned to baseline levels of tracer uptake.

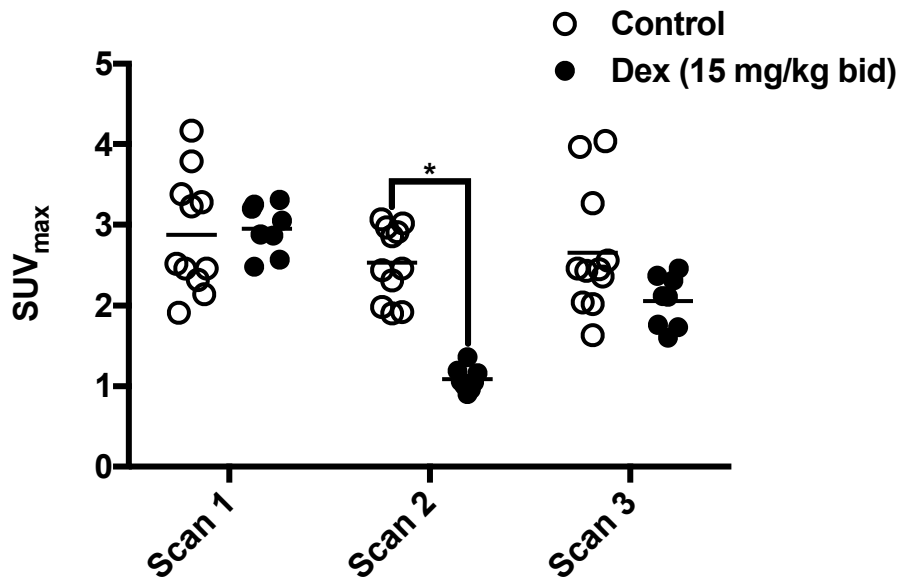


Figure 2.4B: ^{18}F -FLT uptake in high-GR α A549 xenografts. SUVmax values of tumors treated with Dex (15 mg/kg bid, ip) (n = 9) or control (saline) (n = 11) at baseline, after 24 h treatment, and 72 h post-treatment. After 24 h Dex tumor ^{18}F -FLT retention declined by an average of 63.1%. 72 h after the final dose of Dex, however, tumors return to control levels of tracer uptake. *P < 0.01

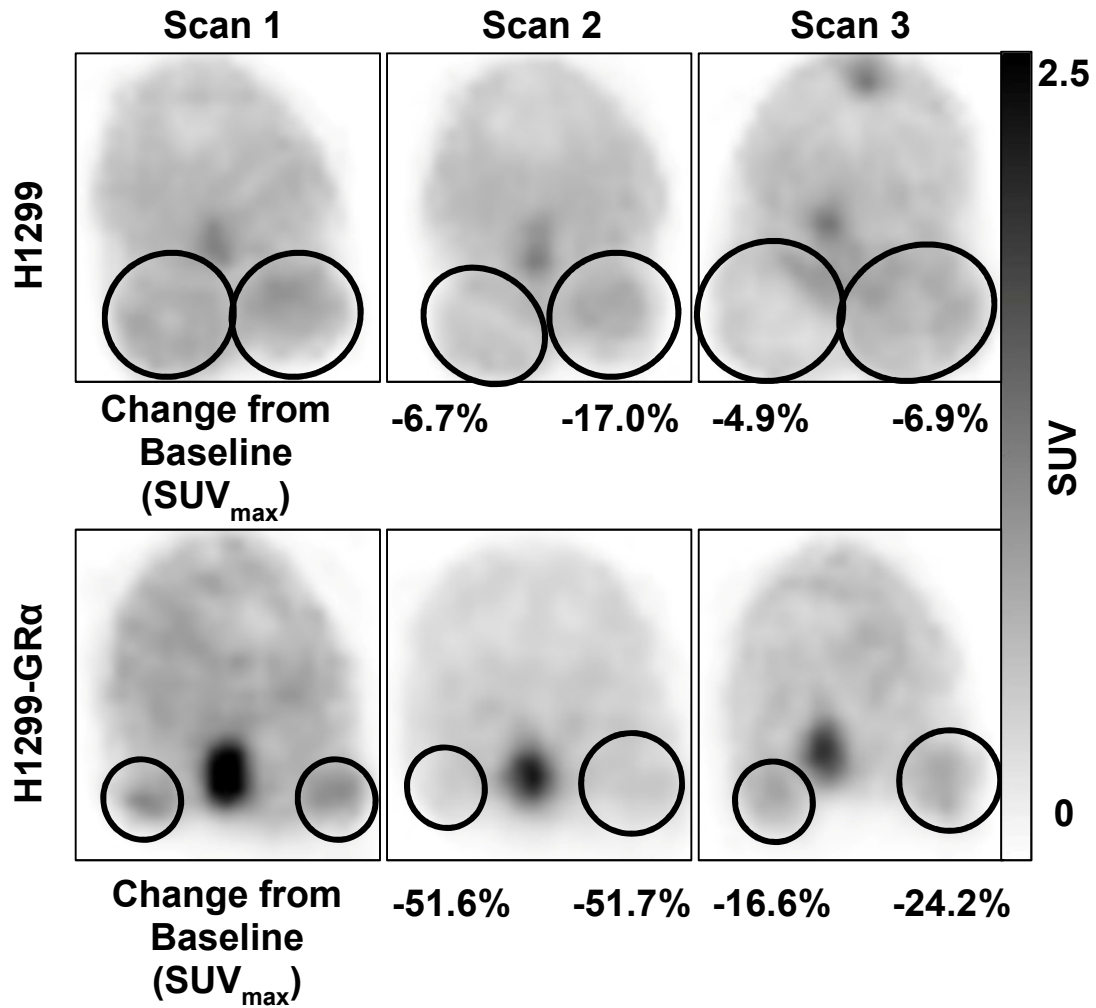


Figure 2.4C: ^{18}F -FLT PET images of mice with H1299 xenografts. Animals were implanted bilaterally with either H1299 or H1299-GR α tumors. In animals with low-GR α H1299 tumors (top panel) ^{18}F -FLT uptake decreased by 6.7% and 17.0% after 24 h Dex. In H1299-GR α tumors, ^{18}F -FLT uptake decreased by 51.6% and 51.7%.

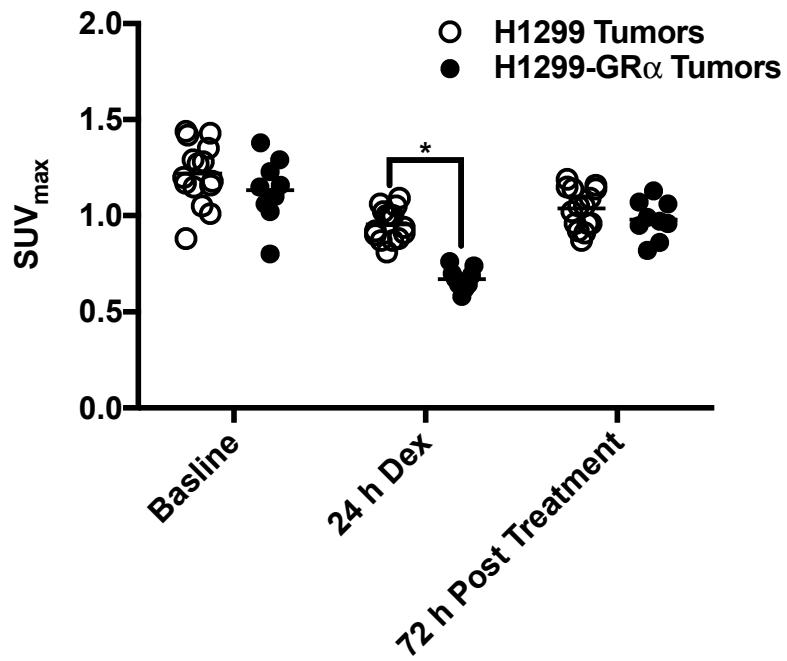


Figure 2.4D: ^{18}F -FLT uptake in H1299 xenografts. Dot-plot comparing SUV_{max} values of H1299 (n = 15) tumors with H1299-GR α (n = 9) following 24 h Dex (15 mg/kg bid, ip) treatment. ^{18}F -FLT uptake in H1299 tumors decreased by 20.8% versus in 41.3% H1299-GR α . Effects of Dex reversed 72 h after the final Dex treatment. P < 0.01.

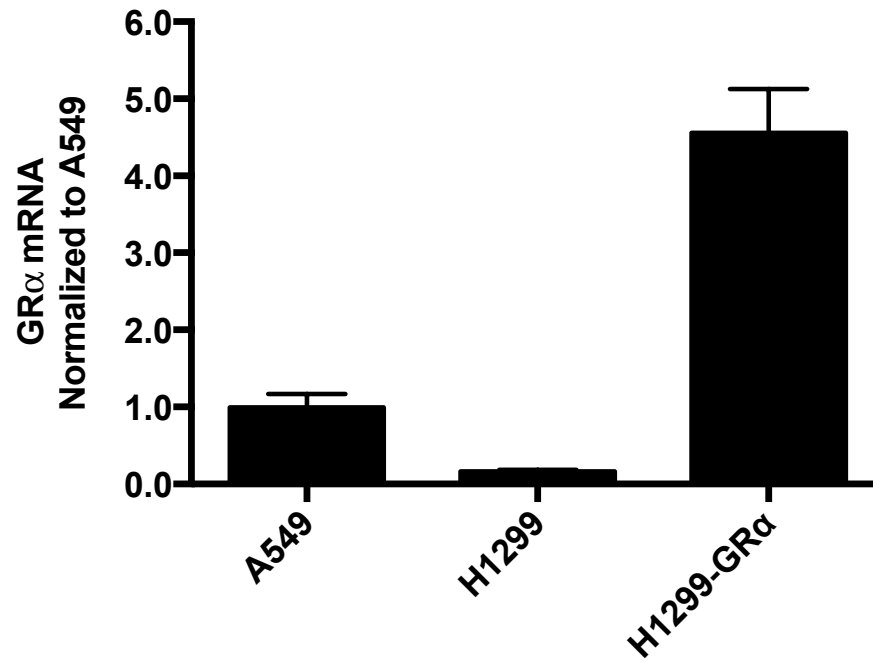


Figure 2.5A: GR α mRNA in human xenografts. Tumors were harvested and GR α mRNA was measured by RT-PCR. Error bars represent standard deviation between biological triplicate samples.

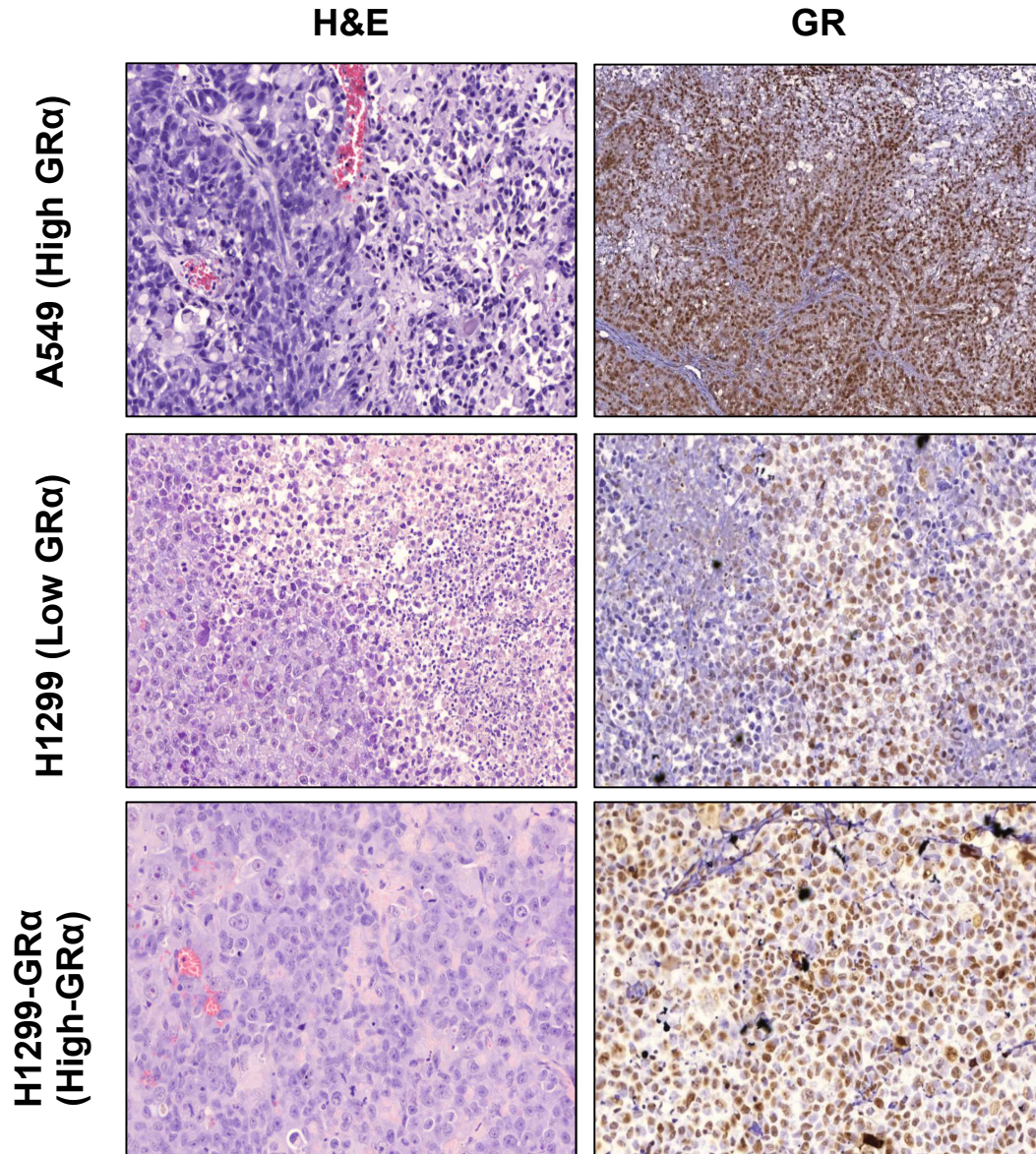


Figure 2.5B: GR staining in human xenografts. Representative pictures of tumors stained with hematoxylin and eosin (left) or an anti-GR antibody.

¹⁸F-FLT PET visualizes interlesion heterogeneity in Dex sensitivity between metastases in human tumors

To determine whether our findings in NSCLC cell lines and xenografts extend to human disease, we have extended our work into four patients with advanced NSCLC. Patients were imaged at baseline and again after 24 h of oral Dex treatment (4 mg bid) as is standard practice in patients receiving Pem chemotherapy. After 24 h Dex, tumors in patients #1 and #3 demonstrated marked reductions in tumor SUV_{max} (-64.7% and -54.3%, respectively). Conversely, patients #2 and #4 were largely unaffected by Dex treatment, highlighting variability in GR α expression in between individual cancers (Table 2.2). Furthermore, we observed marked heterogeneity within individual patients, as the lesions of patient #1 showed variable change in ¹⁸F-FLT uptake after Dex (Figure 2.6). This finding demonstrates the value of imaging in this setting, as this may have gone unnoticed with a purely biopsy-based approach.

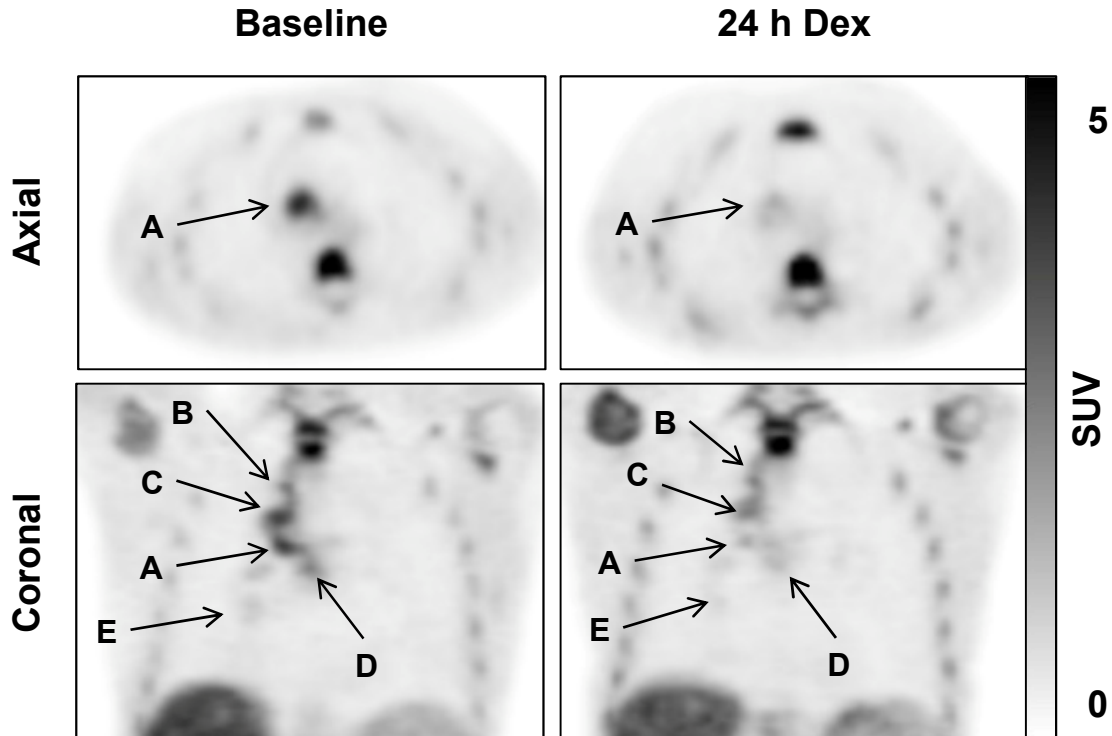


Figure 2.6: Interlesion heterogeneity in a NSCLC patient. ^{18}F -FLT PET images from a patient with NSCLC at baseline (left) and after 24 h Dex (4 mg twice daily, left). In the lymph node metastasis indicated 'A', ^{18}F -FLT uptake decreased by 64.7% after 24 h Dex. However, as shown in the coronal reconstructions in the left panels, change in ^{18}F -FLT retention is highly variable between different nodal metastases. Tracer retention in lesions indicated by 'B', 'C', 'D', and 'E' decreased by 13.7%, 33.1%, 18.1%, and 34.6% respectively.

Patient	Lesion	Baseline (SUV _{max})	24 h Dex (SUV _{max})	% Change from Baseline
1	Primary Lesion	3.60	2.07	-42.6
	Lymph Node A	4.02	1.42	-64.7
	Lymph Node B	3.89	3.36	-13.7
	Lymph Node C	3.79	2.54	-33.1
	Lymph Node D	3.32	2.72	-18.1
	Lymph Node E	2.34	1.53	-34.4
2	Primary Lesion	8.42	7.22	-14.3
	Lymph Node A	5.74	4.60	-19.9
	Lymph Node B	5.18	5.04	-2.80
3	Primary Lesion	3.26	2.07	-36.4
	Lymph Node A	2.36	1.77	-25.1
	Lymph Node B	1.64	0.75	-54.3
	Lymph Node C	1.49	0.85	-42.8
4	Tumor A	2.08	1.85	-11.4
	Tumor B	4.00	3.43	-14.3
	Lymph Node A	6.13	6.83	11.5
	Lymph Node B	4.90	4.07	-17.0
	Lymph Node C	3.48	1.93	-44.6

Table 2.2: Change in tumor ¹⁸F-FLT uptake in NSCLC patients after Dex. Patient #1 and #3 displayed notable changes in ¹⁸F-FLT retention 24 h after Dex treatment, with differential changes between tumor lesions. In patients #2 and #4, changes in ¹⁸F-FLT uptake were less pronounced, highlighting the variability in sensitivity to Dex between patients. GR α expression is currently being assessed using IHC on fixed biopsy samples.

Dex abolishes Pem-mediated flare in ³H-FLT uptake in NSCLC cell lines

As mentioned, compounds that interfere with *de novo* TdR biosynthesis, such as Pem, can lead to a temporary upregulation in TdR salvage, and therefore FLT accumulation, as cells seek to replenish intracellular TdR exogenously. Exploiting this phenomenon may provide a method to monitor Pem activity *in vivo*. To test this idea, we measured ³H-FLT uptake in NSCLC cells following 4 h Pem (5 μM) treatment (Figure 2.7). ³H-FLT accumulation significantly increased in all cell lines (P < 0.01). However, 24 h pretreatment with Dex (100 nM) abrogated this effect in Dex-sensitive cell lines.

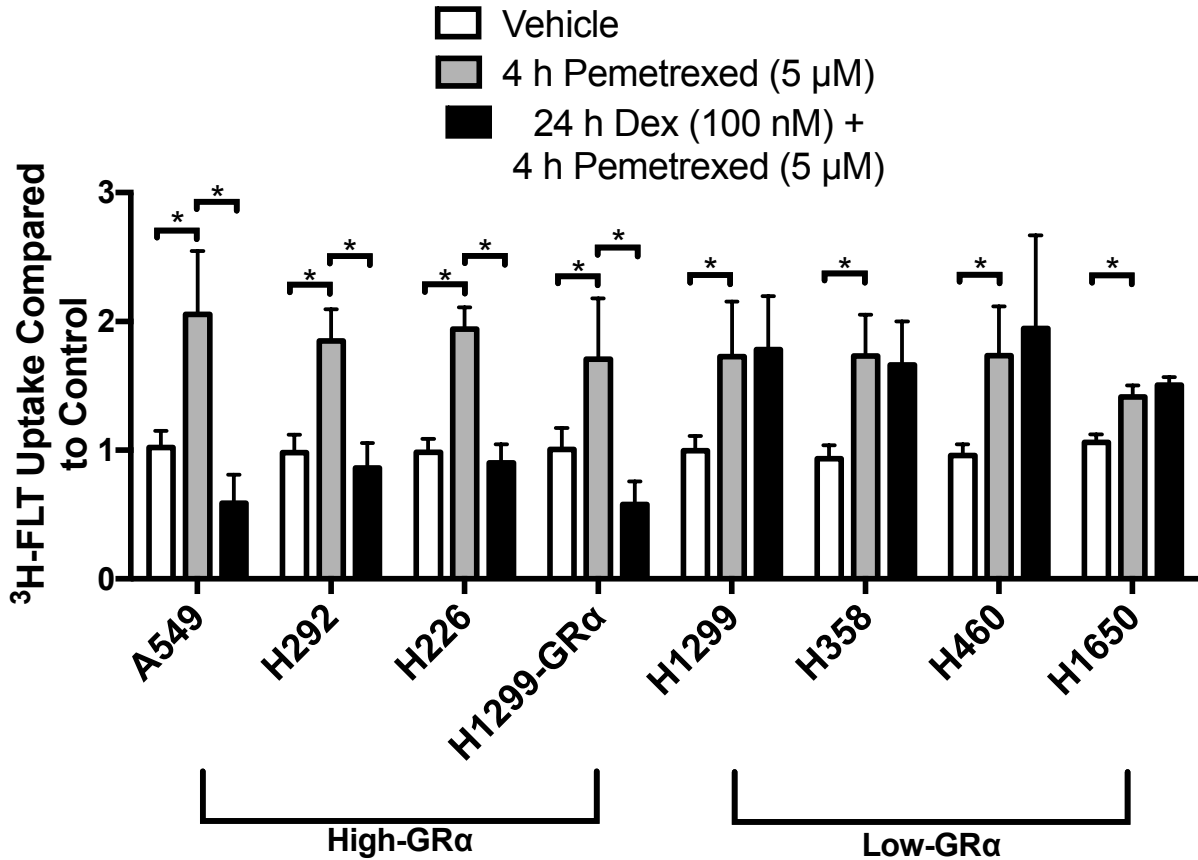


Figure 2.7: Effect of Dex and Pem on ^3H -FLT retention in NSCLC cell lines. NSCLC cells were grown in glucocorticoid-depleted media, treated 5 μM Pem with or without pretreatment with 100 nM Dex for 24 h. Cells were then transferred to media containing ^3H -FLT and incubated for 1 h. After washing, cells were lysed by KOH and the activity of samples was measured via liquid scintillation. All cell lines produced a significant flare after 4 h Pem treatment. When cells were pretreated with 24 h Dex, the flare was abolished in cells with high GR α expression (A549, H292, H226, recombinant cell line H1299-GR α). * $P < 0.01$

¹⁸F-FLT visualizes Dex interference with Pem activity

To evaluate the flare effect *in vivo*, we utilized the same xenograft models as earlier experiments. Animals were imaged at baseline and again 4 h after receiving Pem (10 mg/kg) with or without pretreatment with Dex for 24 h. Mice were placed on a folate-deficient diet to decrease serum folates to levels closer to humans simulate Pem efficacy observed in humans (253). As was observed in cell culture, ³H-FLT uptake increased from baseline after 4 h Pem (mean change in SUV_{max} of 48.9%), but this effect was abolished if animals received Dex pretreatment (mean change in SUV_{max} of -44.5%) (Figure 2.8) P < 0.01.

Following 4 h Pem, H1299 tumors exhibited a greater flare from baseline than A549 xenografts: SUV_{max} in H1299 and H1299-GR α tumors increased by 107.3% and 68.7%, respectively. If animals were pretreated with Dex, the flare response was completely eradicated H1299-GR α , and the change from baseline resembled that of animals treated with Dex alone. H1299 tumors still exhibited a significant flare from baseline (% change in SUV_{max}: 32.9%), but it was smaller than that produced by Pem alone, likely due to GR up-regulation, as seen before P < 0.01.

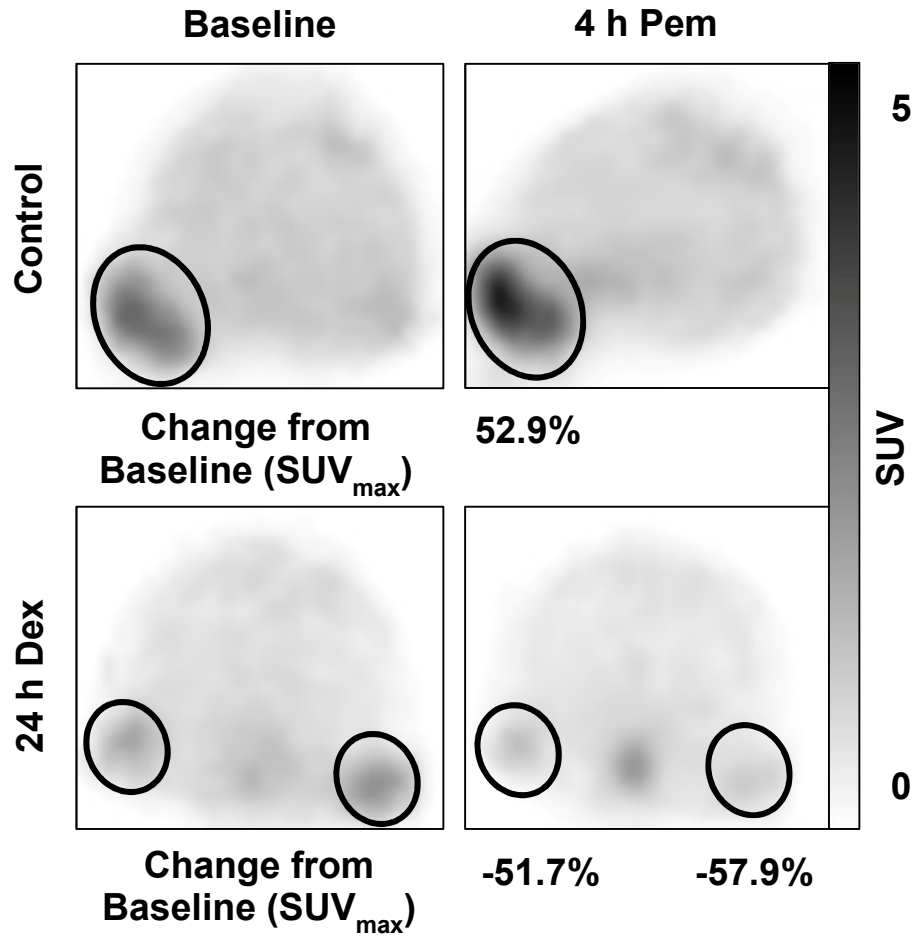


Figure 2.8A: Effect of Pem on ^{18}F -FLT uptake in A549 xenografts. Mice were implanted with high-GR α A549 tumors and imaged at baseline and 4 h after injection with Pem (10 mg/kg, iv), with or without Dex pretreatment (15 mg/kg bid, ip) for 24 h. Representative images of a mouse bearing A549 tumors. In the top panel, tumor SUV_{max} increased by 52.9% after 4 h Pem. In the bottom panel, the flare response was completely abrogated, with tumor SUV_{max} decreasing by an average of 52.9%.

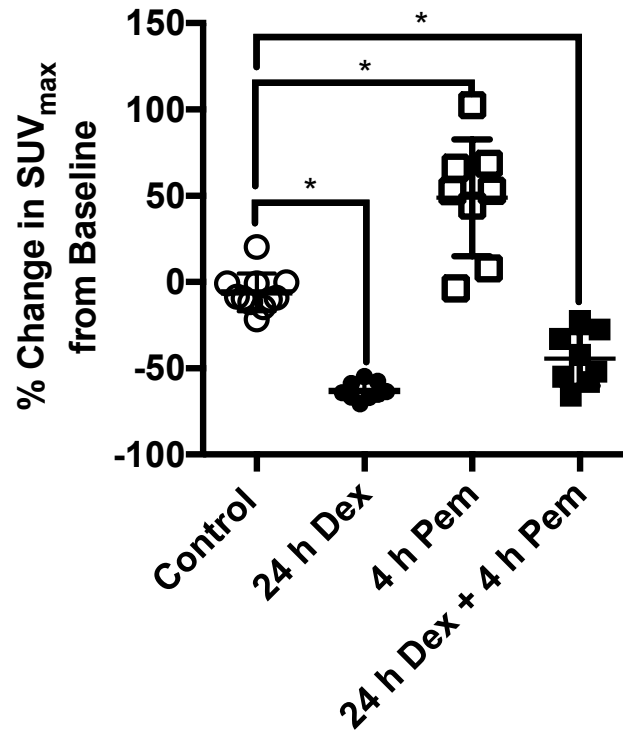


Figure 2.8B: Summary of the effect of Dex and Pem treatments on ^{18}F -FLT retention in A549 tumors. SUV_{max} in control animals (n = 11 tumors) decreases by an average of 6.0% after 24 h. Following 24 h Dex (15 mg/kg bid, ip) (n = 9 tumors), tumor SUV decreases by 63.1%. 4 h Pem (10 mg/kg, iv) (n = 8 tumors) produces a mean increase of 48.9% in tumor ^{18}F -FLT uptake, but this effect is abolished when animals are pretreated with Dex for 24 h (average change: -44.5%, n = 8 tumors). *P < 0.01.

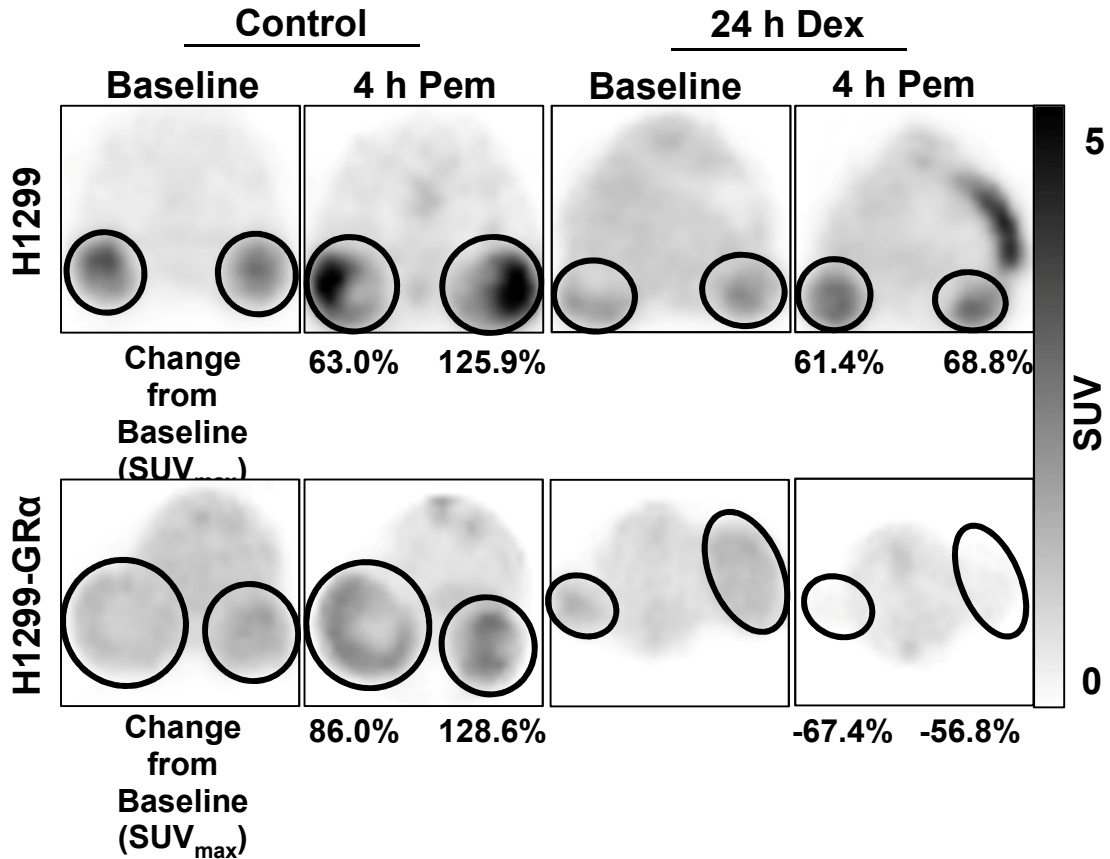


Figure 2.9A: Effect of Pem on ^{18}F -FLT uptake in H1299 xenografts. Mice were implanted with H1299 (top) or H1299-GR α (bottom) tumors and imaged at baseline and 4 h after injection with Pem (10 mg/kg, iv), with or without Dex pretreatment (15 mg/kg bid, ip) for 24 h. Representative images from one animal with each condition are displayed. In mice bearing H1299 xenografts, there was a marked increase in ^{18}F -FLT uptake after Pem with or without Dex pretreatment. Mice with H1299-GR α also demonstrated a sharp increase in tumor ^{18}F -FLT uptake after Pem, but this effect was abolished if animals were pretreated with Dex for 24 h.

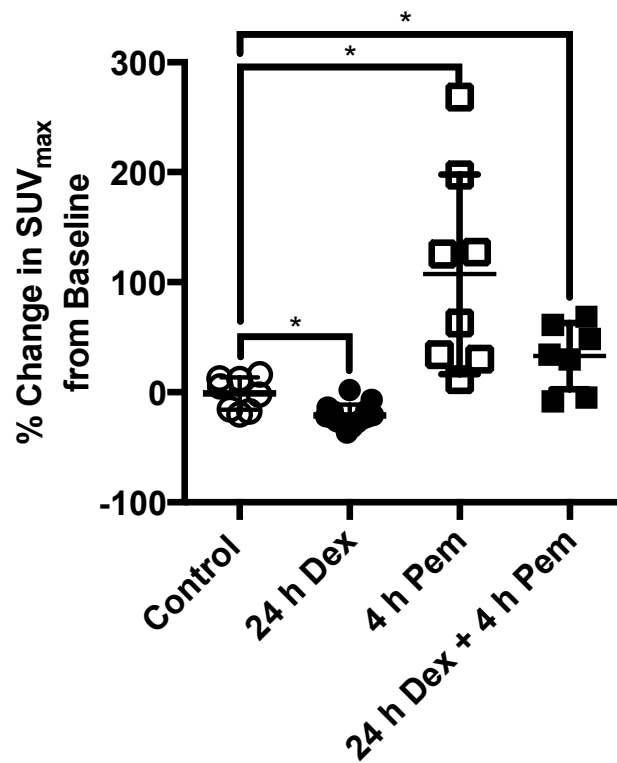


Figure 2.9B: Summary of the effect of Dex and Pem treatments on ^{18}F -FLT retention in H1299 tumors. SUV_{max} in control animals (n = 8 tumors) decreases by an average of 1.0% after 24 h. Following 24 h Dex (15 mg/kg bid, ip) (n = 15 tumors), tumor SUV decreases by 20.1%. 4 h Pem (10 mg/kg, iv) (n = 8 tumors) produces a mean increase of 107.3% in tumor ^{18}F -FLT uptake. This flare is reduced in magnitude when animals are pretreated with Dex (average change: 32.9%, n = 7 tumors), but still present. *P < 0.01.

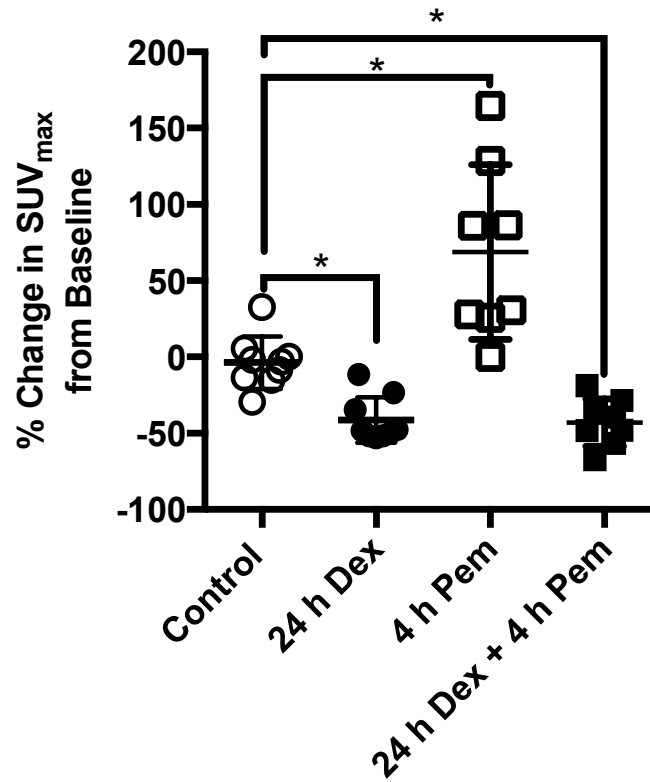


Figure 2.8C: Summary of the effect of Dex and Pem treatments on ^{18}F -FLT retention in H1299-GR α tumors. SUV_{max} in control animals (n = 9 tumors) decreases by an average of 3.7% after 24 h. Following 24 h Dex (15 mg/kg bid, ip) (n = 9 tumors), tumor SUV decreases by 41.3%. 4 h Pem (10 mg/kg, iv) (n = 8 tumors) produces a mean increase of 68.7% in tumor ^{18}F -FLT uptake, but this effect is abolished when animals are pretreated with Dex for 24 h (average change: -42.9%, n = 8 tumors). *P < 0.01.

DISCUSSION

Although widely used, Pem has proved to have a modest and variable effect in patients, with a median increase in progression-free survival of 5.3 months in the front-line setting when combined with cisplatin, and only 3.3 months when used as a monotherapy in patients unable to tolerate platinum-based chemotherapy (236, 259). Furthermore, the 5-year survival for metastatic NSCLC remains dismal, at less than 4% (260). Given this paradigm, it is critical to identify factors that can be used to predict and optimize the clinical benefit of Pem in order to maximize efficacy and spare non-responders the toxicity of ineffective chemotherapy. To that end, several studies have observed an association between low tumor expression of TS and better outcomes in patients treated with Pem (261). However, this has not been shown to be a powerful independent predictor of patient response to Pem, and is not used clinically (262).

A recent study by Patki et al. found that in a subset of NSCLC cell models, Dex reversibly inhibits entry of cells into the S-phase of the cell cycle resulting in the decreased expression of Pem targets TS and DHFR, as well as its membrane transporters: RFC and PCFT (224). Analysis of GR α in NSCLC biopsy specimens has indicated that there is an approximately equal distribution of tumors with high and low GR α expression (263). It is possible that the protective effect of Dex, combined with differential tumor GR α expression may explain, in part, the variable efficacy of Pem in clinical practice.

Here, we explored the use of FLT retention as a direct functional probe to monitor Dex-mediated S-phase suppression in several models of NSCLC. Studies in NSCLC cell lines indicated that treatment with Dex for 24 h produced a significant

reduction in ^3H -FLT uptake in cell lines with relatively high GR α expression. This result was translatable to animal studies, where implanted with high-GR α A549 tumors demonstrated an average change of -63.1% in SUVmax after 24 h Dex treatment. Furthermore, when imaging isogenic H1299 and H1299-GR α tumors, we found that the magnitude of change in ^{18}F -FLT retention in response to Dex is correlated to the expression level of GR α . In patients with advanced NSCLC, the changes were much more variable, 2/4 patients showing some response to Dex. Furthermore, ^{18}F -FLT PET was able to detect heterogeneity in Dex sensitivity between lesions within individual patients. The ability to simultaneously evaluate all tumor foci in patients is a major advantage of imaging compared to tissue analysis, given that NSCLC patients receiving chemotherapy have advanced disease.

In addition, we sought to use FLT accumulation to monitor Pem activity through its inhibitory effect on TS, and subsequent increase in FLT accumulation. To that end, we found that 4 h Pem treatment produced a significant increase in ^3H -FLT retention compared to control. This effect was found to be eradicated in high GR α -expressing cells if they were pretreated with Dex. This finding was corroborated with animal imaging. Mice bearing A549 and H1299-GR α tumors exhibited a significant flare from baseline after Pem treatment which was abolished if animals received Dex prior to chemotherapy. Conversely, low-GR α H1299 tumors produced a flare regardless of Dex treatment. Taken together, these data suggest that the presence of a flare in response to Pem may be indicative of the activity of the drug, and may be useful as an early marker for assessing response to therapy. A recent study in NSCLC patients treated with PEM attempted to correlate a flare in ^{18}F -FLT uptake with drug efficacy. The

authors found that only 2/11 exhibited a flare, with the remaining individuals demonstrating either reduced or no change in tumor ^{18}F -FLT uptake after Pem. Furthermore, the flare did not correlate with response to therapy (158). However, given that all patients on study received Dex prior to their treatment, this result is likely due to Dex-mediated suppression of TK1, which counteracts the compensatory rise in TdR salvage due to TS inhibition.

Ultimately, the imaging approach used here could allow for the stratification of patient tumors by Dex sensitivity, and patients with sensitive cancers could be given a treatment regimen that does not require Dex prophylaxis. Alternatively, it may facilitate adjustment of the Dex treatment schedule so that the interference with therapy could be minimized while still preventing adverse events. In the bigger picture, numerous preclinical studies have found that GCs reduce the therapeutic effect of commonly used anti-neoplastic agents such as including cisplatin, doxorubicin, and gemcitabine, among others (219). ^{18}F -FLT PET may facilitate examination of other chemotherapeutic agents, many of which are accompanied with GCs as part of supportive care.

CHAPTER 3 EFFECT OF CAPECITABINE TREATMENT ON THE UPTAKE OF THYMIDINE ANALOGS USING EXPLORATORY PET IMAGING AGENTS: FAU, FMAU, AND FLT

BACKGROUND

Capecitabine is a carbamate prodrug form of 5-FU, approved for the treatment of metastatic colorectal and breast cancers, and can be used as monotherapy or in combination with other cytotoxic and targeted agents (264, 265). Conversion to 5-FU is accomplished via the action of three enzymes: carboxylesterase, cytidine deaminase, and TP, the latter of which is found at higher concentrations in tumor cells than normal, healthy tissue (266, 267). Following conversion to 5-FU, anti-tumor activity is achieved via inhibition of TS and incorporation of 5-FU into RNA and DNA (267, 268). Despite its widespread use, additional research is needed to explore its mechanisms of cytotoxicity, activation, metabolism, and to develop methods to monitor efficacy.

Due to its effects on TdR synthesis and incorporation pathways, capecitabine may alter the uptake and retention of TdR analogs used with PET imaging and this could provide a method for assessing response and understanding drug pharmacodynamics. In part, this is due to increased expression of TK1 in the pyrimidine salvage pathway, which is involved in the uptake and utilization of TdR from the plasma through phosphorylation. Increased TK1 expression in tumors has been imaged with ^{11}C -TdR and TdR analogs such as FLT (137, 160, 269). FLT has been used to monitor cell proliferation (119, 270), since after uptake by tumor nucleoside transporters, FLT is phosphorylated by TK1, causing it to be trapped intracellularly (108, 118). Because FLT is minimally incorporated into DNA structure due to the lack of a 3' hydroxyl, its retention principally reflects intracellular TK1 activity (115, 132, 271). Uptake of FLT is

reproducible and has been shown to be correlated with the proliferative marker Ki-67 in several neoplasms (119, 160, 246).

FMAU is another analog of TdR that was originally introduced as an anti-viral and anti-neoplastic compound due to cytotoxicity following its incorporation into DNA (166, 167). More recently, FMAU has been adapted to molecular imaging (160, 168). After entering the cell, FMAU is phosphorylated by mitochondrial TK2, and its uptake has found to be increased in response to conditions that cause an increase in mitochondrial mass, such as oxidative, reductive, and energy stress (167, 172, 173). Unlike FLT, which accumulates in highly proliferative tissues, FMAU is not retained in normal bone marrow, which may allow it to be useful in the detection and monitoring of bone marrow metastases. Additionally, FMAU is cleared rapidly from the blood, allowing for a short imaging time and simplified kinetic analysis.

FAU is a uracil analog that has been considered for cancer treatment due to its inhibitory effect on cell proliferation (169, 175, 176). After cells take up FAU, it is converted to FAU-MP and then to FMAU-MP via the action of TK1 and TS, respectively. Dependence on TS for activation may increase the specificity of FAU towards tumors with high expression of this enzyme, such as breast and colorectal cancers (177-179). Indeed, a recent pharmacokinetic modeling study found that conversion of FAU to FMAU is greatly increased in tumors compared to normal tissues (186). Moreover, increased TS expression has been found to be associated with poor therapeutic response in colorectal cancer, and therefore, high uptake of FAU may be a negative prognostic indicator in a subset of patients. Given the differences in metabolism for each of the tracers, the effects of capecitabine were expected to vary.

The purpose of this study was to gauge the retention and usefulness of radiolabeled fluoropyrimidines FLT, FAU, and FMAU in the evaluation of patients with breast and gastrointestinal cancers who received capecitabine. The primary objective was to monitor changes in tracer uptake as measured by mean standardized uptake value (SUV_{mean}) along with kinetic parameters. These parameters may provide an approximation of the physiological effect of capecitabine on tumors.

MATERIALS AND METHODS

Radiochemistry and Patient Imaging

PET tracers were synthesized as previously published and patients were injected intravenously with FLT (range, 347-389 MBq; mean 372 MBq), FAU (range, 211-396 MBq; mean 346 MBq), or FMAU (range, 191-388 MBq; mean 339 MBq) over 60s as described (174, 254, 272). All subjects underwent dynamic PET with a series of timed images (4x20s, 4x40s, 4x60s, and 4x180s). In patients injected with FLT and FAU, but not FMAU, an additional series of images was collected (8x300s). PET was conducted with a 15-cm field of view over the area of the tumors (neck, thorax, or abdomen) followed by a whole body image using an Exact/HR tomograph (Siemens Medical Solutions, Malvern, Pennsylvania, USA).

Fifteen patients with solid tumors were imaged, five with each of the ^{18}F -labeled PET tracers. Patient accrual alternated between the three agents based primarily on tracer availability. Tumor types were breast, colorectal, gastric, and esophageal cancers. Patients had not received therapy for at least 4 weeks prior to the first PET scan, and had not been previously treated with 5-FU, capecitabine or other fluorop

ymidines. Six of the fifteen patients studied received capecitabine alone. Other patients were placed on standard regimens, which utilized radiotherapy and oxaliplatin as well as targeted agents such as lapatinib, bevacizumab, and trastuzumab (Table 3.1). When capecitabine was combined with other treatments they were started after the third dose of capecitabine and after completion of the final PET scan. Patients underwent imaging within one week before therapy, and again one day after the start of therapy, after receiving three doses of capecitabine.

Patient images were analyzed with PMOD (Zurich, Switzerland) software and regions of interest (ROIs) were defined in a semi-automated fashion as published (168). ROIs were chosen in the three adjacent planes with the highest activity, using isocontours halfway between the minimum and maximum thresholds of the tumor. Tracer uptake was measured by standardized uptake value (SUV). Mean SUVs (SUV_{mean}) were calculated on whole ROIs, and maximum SUVs (SUV_{max}) were measured as the pixels with the most activity in the same ROIs.

Kinetic Analysis

Kinetic modeling was conducted using PMOD (Zurich, Switzerland) software as has been published previously (117). In short, FLT and FAU time-activity curves were fitted using a 3-compartment model, which produced rate constants K_1 , k_2 , and k_3 . K_1 (mL/g/min) represents the unidirectional transport of tracer from blood into tissue, k_2 (min^{-1}) represents the reverse transport, and k_3 (min^{-1}) characterizes phosphorylation and intracellular trapping via TK1 activity. The flux values for FLT and FAU were then calculated as $K_1 \times k_3 / (k_2 + k_3)$. Tumor uptake values and blood tissue kinetics were

interpreted with respect to the blood activity level, obtained from measurements of tracer activity within great vessels.

For FMAU kinetic analysis, we utilized tumor retention ratio (TRR), which has been shown to correlate strongly with compartmental-K. TRR was obtained by dividing the tumor FMAU activity—obtained in an image from 5 to 11 min post-injection—area under the curve (AUC) by of FMAU blood activity AUC. AUC values were calculated using GraphPad Prism version 6 (GraphPad Software, La Jolla, California, USA), which measures AUC using the trapezoid method. To reduce image noise, the first 5 minutes were omitted. Furthermore, we have previously shown that in FMAU blood activity decreases sharply in the first 11 minutes after injection, and that images taken within the 5-11 window are comparable to images from 50-60 minutes (168).

Statistical Considerations

The relationship of one PET parameter to another was measured using linear regression models, and the goodness of fit of these models was assessed using the r^2 value. Regression models were fit and assessed using GraphPad Prism version 6 (GraphPad Software, La Jolla, California, USA).

Table 3.1: Patient Characteristics

Patient No.	Age	Sex	Tumor Type	Other Therapy with Capecitabine	Tracer
1	47	F	Breast	Lapatinib	
2	65	F	Breast	None	
3	62	F	Esophageal	Radiation, Irinotecan	FLT
4	62	F	Colorectal	Bevacizumab, Oxaliplatin, Radiation	
5	56	F	Colorectal	Oxaliplatin	
6	63	F	Breast	None	
7	52	F	Breast	Lapatinib	
8	46	F	Breast	Lapatinib	FMAU
9	73	F	Breast	None	
10	63	F	Breast	None	
11	64	F	Breast	None	
12	62	F	Colorectal	Oxaliplatin, Bevacizumab	
13	53	F	Gastric	None	
14	49	M	Colorectal	Oxaliplatin, Radiation	FAU
15	37	M	Esophageal	Oxaliplatin, Trastuzumab	

RESULTS

FLT-PET imaging

Five patients (median age: 62) with breast, esophageal, and colorectal carcinomas were imaged with ^{18}F -FLT-PET at baseline, and then following capecitabine therapy. In addition to capecitabine, 4/5 patients underwent other anti-neoplastic therapy including: oxaliplatin, irinotecan, bevacizumab, lapatinib, and radiation after the second scan (Table 3.1). Variable changes in tumor activity were observed post-treatment (Table 3.2). Patient 3 exhibited the largest change in SUV_{mean} , with an increase of 172.3% from baseline (Figure 3.1). Patient 4 also had a marked change in tracer retention, with a SUV increase of 89.9% after capecitabine. The other three patients imaged had more modest changes in tumor SUV, ranging from an increase of 19.4% to a decline of 25.4%. Although the primary endpoint was tracer uptake as measured by SUV_{mean} , the changes observed correlated with changes in SUV_{max} ($r^2 = 0.98$, $P = 0.0014$). Although differences in tracer flux, calculated from compartmental-K, trended with changes in tumor SUV (Table 2), flux and SUV_{mean} were not correlated ($r^2 = 0.57$, $P = 0.1404$).

Table 3.2: Tumor Retention in Patients Imaged with FLT

Patient No.	Tumor SUV_{mean}			Tracer Flux into Tumor (cc/min)		
	Baseline	Post-Treatment	% Change	Baseline	Post-Treatment	% Change
1	1.97	1.58	-19.8	0.0271	0.0211	-22.1
2	1.96	2.34	19.4	0.0314	0.0526	67.5
3	4.7	12.8	172.3	0.0217	0.0796	266.8
4	2.27	4.31	89.9	0.0187	0.109	482.9
5	1.34	1	-25.4	0.0267	0.0213	-20.2

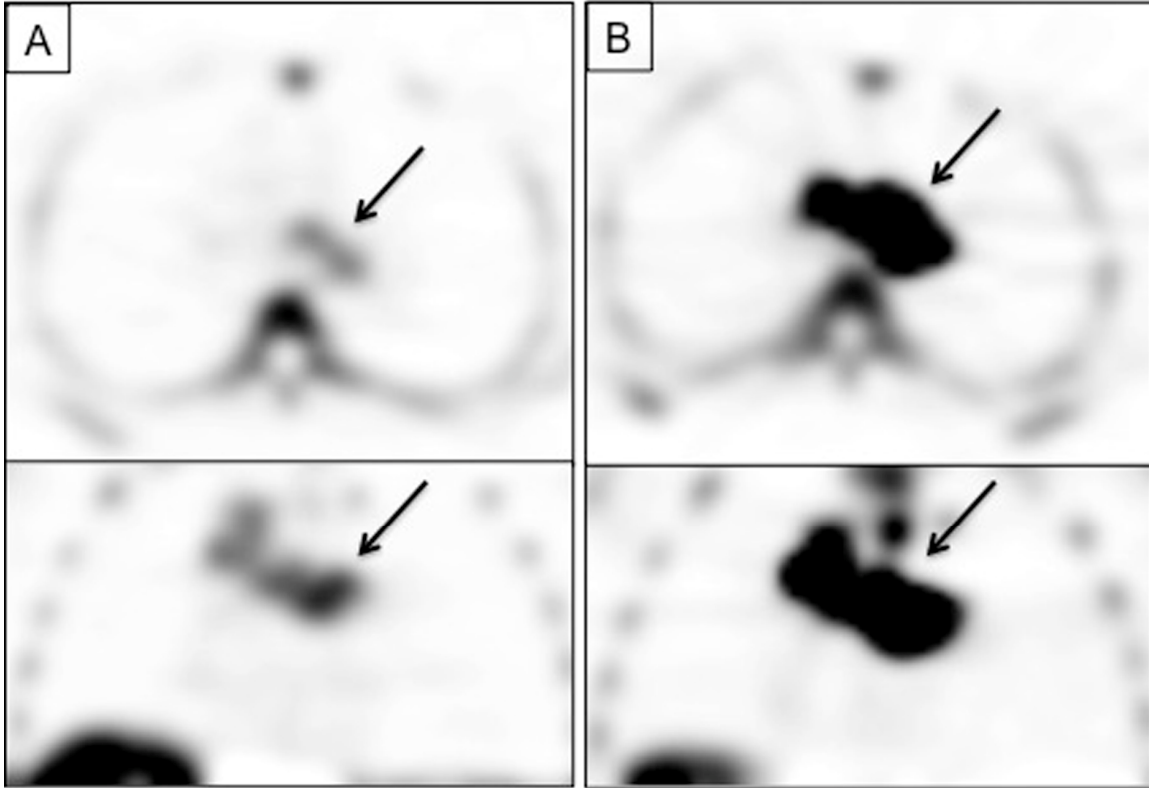


Figure 3.1: Tumor FLT Uptake in Patient 3. Axial (top) and coronal (bottom) FLT Images of a mediastinal metastasis (arrow) in a patient with esophageal cancer at baseline (A) and after 1 day of capecitabine therapy (B). Tumor SUV_{mean} increased from 4.70 to 12.80.

FMAU-PET imaging

Five patients with breast cancer (median age: 63) were imaged with FMAU-PET at baseline and following capecitabine treatment. Two patients received lapatinib after the start of capecitabine (Table 3.1). Although tumor activity was consistently high in patients imaged with ^{18}F -FMAU (median SUV_{mean} at baseline: 2.58), there was non-specific tracer uptake throughout the lungs, which gave images a ‘grainy’ appearance (Figure 3.2). SUV_{mean} values ranged from an increase in 23.1% to a decline of 24.4% with an average change of 0.2% (Table 3.3). SUV_{mean} correlated strongly with SUV_{max} measurements ($r^2 = 0.95$, $P = 0.005$). As mentioned, TRR was used for kinetic analysis in lieu of compartmental-K in patients imaged with FMAU because the rapid clearance of FMAU prevents the establishment of equilibrium between tissue compartments (168). Similarly to what was observed in patients imaged with FLT, differences in SUV_{mean} and TRR after treatment trended in the same direction, but were not well correlated ($r^2 = 0.65$, $P = 0.098$).

Table 3.3: Tumor Uptake in Patients Imaged with FMAU

Patient No.	Tumor SUV_{mean}			Tumor Retention Ratio		
	Baseline	Post-Treatment	% Change	Baseline	Post-Treatment	% Change
6	4.64	5.06	9.1	3.01	3.47	15.3
7	3.76	4.63	23.1	3.56	3.9	9.6
8	1.97	2.11	7.1	2.18	2.74	25.7
9	2.58	1.95	-24.4	2.03	1.65	-18.9
10	2.14	1.84	-14	1.22	0.96	-21.3

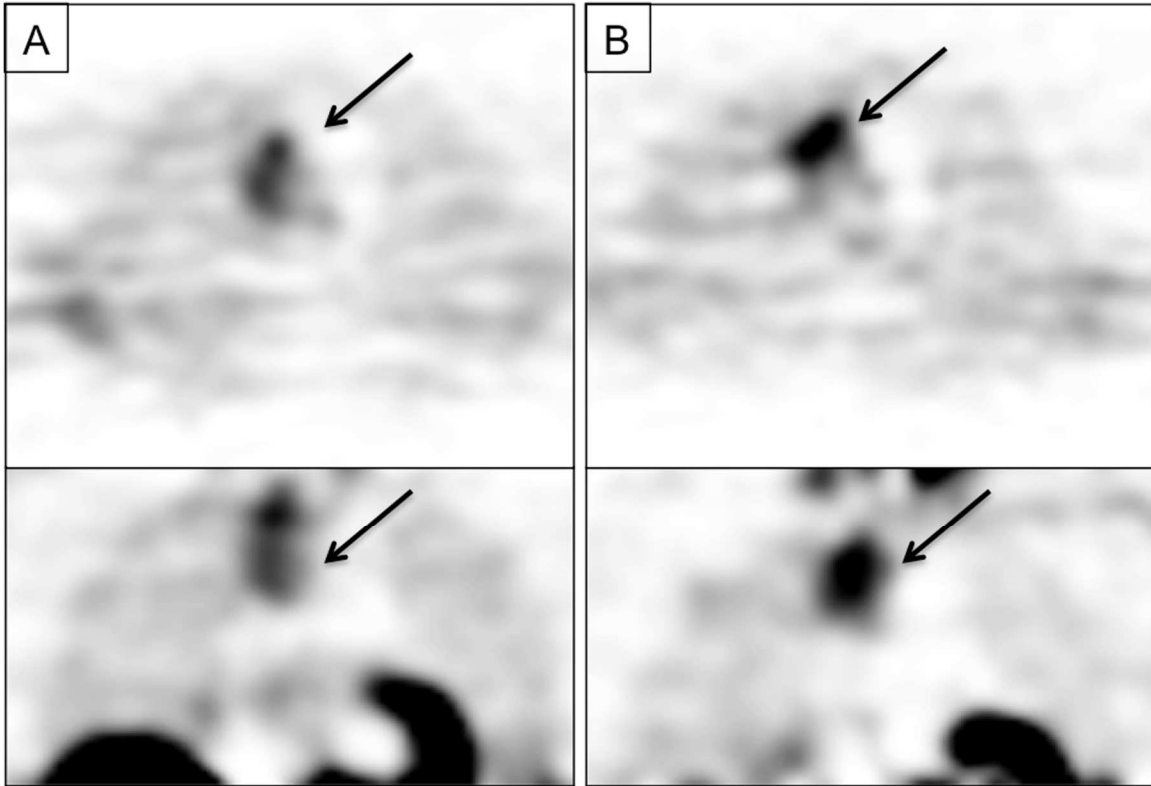


Figure 3.2: Tumor FMAU Uptake in Patient 7. Axial (top) and coronal (bottom) FMAU Images of a lung metastasis (arrow) in a patient with breast cancer at baseline (A) and after 1 day of capecitabine therapy (B). Tumor SUV_{mean} increased from 3.76 to 4.63.

FAU-PET Imaging

Five patients (median age: 53) with breast, gastric, colorectal, and esophageal junction tumors underwent ^{18}F -FAU-PET scans before and after capecitabine treatment. Two patients were on no other therapies, and the remaining three also received chemotherapy with either an antibody or radiation (Table 3.1). The majority of the patients showed little change in tracer uptake post-treatment (average change -10.2%) (Table 3.4). Only patient 15 displayed a notable change in FAU retention, with a decline of 40.3% after capecitabine (Figure 3.3). Like the previous tracers, FAU retention was high in the kidneys and liver, but greater non-specific tissue uptake was observed compared to patients imaged with FLT and FMAU. In addition, of the tracers studied, FAU had the lowest tumor activity. As with FLT, changes in SUV_{mean} measurements correlated strongly with changes in SUV_{max} ($r^2 = 0.98$, $P = 0.001$). Tracer flux was calculated for 4/5 patients, with patient 11 being not evaluable due to lack of dynamic imaging. As with the previous two tracers studied herein, in patients imaged with FAU, tracer flux and SUV_{mean} were not significantly correlated ($r^2 = 0.72$, $P = 0.1534$). Furthermore, mean pretreatment FAU flux values were far lower than what was observed with FLT (0.00059 cc/min versus 0.0251 cc/min), further underscoring the low tumor retention of FAU in this patient cohort.

Table 3.4: Tumor Retention in Patients Imaged with FAU

Patient No.	Tumor SUVmean			Tracer Flux into Tumor (cc/min)		
	Baseline	Post-Treatment	% Change	Baseline	Post-Treatment	% Change
11	1.03	1.06	2.9	No Dynamic Images		
12	1.05	0.87	-17.1	0.0032	0.0019	-40.6
13	2.57	2.15	-16.3	0.0058	0.0055	-5.2
14	1.82	2.17	19.2	0.0108	0.0158	46.3
15	3.47	2.07	-40.3	0.0039	0.0029	-25.6

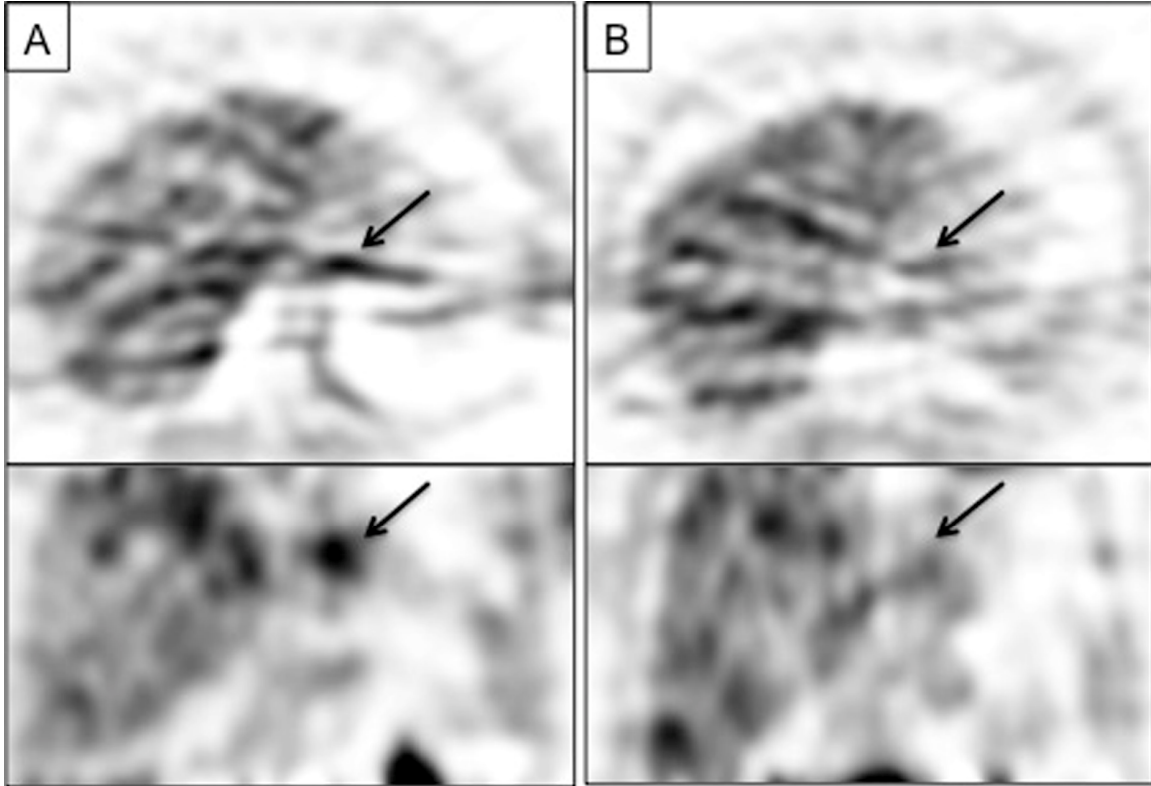


Figure 3.3: Tumor FAU Uptake in Patient 15. Axial (top) and coronal (bottom) FAU Images of an esophageal tumor (arrow) at baseline (A) and after 1 day of capecitabine therapy (B). Tumor SUV_{mean} decreased from 3.47 to 2.12.

DISCUSSION

Although several radiolabeled molecules have been developed for use with PET, FDG remains the principal approved compound for the detection and staging of cancer. Although FDG uptake correlates with general tumor metabolism, this may not accurately describe the proliferative capacity of cancers, which is a major consideration for treatment and prognosis. Further, because many chemotherapeutics used today function by impairing cellular proliferation, it is desirable to develop imaging modalities to monitor these pathways. Accordingly, we sought to examine the effect of capecitabine, a frequently used anti-neoplastic compound, on the uptake and retention of three nucleoside analogs. The goal of this study was to gain an increased understanding of the effect of capecitabine on tumor TdR metabolism, and to assess the usefulness of these tracers in the setting of cancer treatment.

A previous study in 9 non-small cell lung cancer patients found the error of FLT-PET to approximately 20% (246). More recently, a multi-center trial examining the repeatability of FDG-PET in untreated patients found tumor SUV to vary between a decrease of 30% to an increase of 40% (273). Although, there have been no studies examining the repeatability of FMAU and FAU imaging, tumor uptake of these tracers is lower than FDG, and thus, one would not expect improved reproducibility.

Patients imaged with FLT had a variable change in uptake after treatment, with two patients displaying a substantial increase in tumor retention (89.9 and 172.3%). Since FLT uptake reflects cellular TK1, the large increase in SUV_{mean} indicates an upregulation of TK1 activity following capecitabine. This may be caused by the inhibitory effect of 5-FU on TS (152). As TdR levels drop due to TS inhibition, there is an increase

in TK1 activity as cells attempt to replenish TdR exogenously. This increase leads to a window of 1-24 hours in which FLT uptake is significantly increased, and has been termed the 'flare' phenomenon (154, 157). Conversely, the absence of change in FLT retention in the remaining three patients may suggest that capecitabine was unable to effectively block TS. This could be due to upregulation of intracellular TS levels leading to drug resistance, or inefficient conversion of capecitabine to 5-FU (274).

Subjects imaged with FMAU demonstrated little change in tracer retention after treatment. The average change in tumor SUV_{mean} was 0.18% (range -24.4 to 23.1) (Table 3.3). Previous studies have shown increases in FMAU retention in response to oxidative, reductive, and energy stresses due to upregulation of mitochondrial TK2 levels (245). Furthermore, it has been shown that anti-cancer agents can lead to an increase in mitochondrial mass during apoptosis (275, 276). Interestingly, patients imaged with FMAU had the highest baseline tumor uptake: 2.58 versus 2.45 in patients scanned with FLT and 1.99 patients scanned with FAU. These findings suggest that while tumor cells are under a high basal level of cellular stress, this is not increased significantly by short-term capecitabine treatment.

Similar to patients imaged with FMAU, patients scanned with FAU demonstrated little change in tracer retention after capecitabine (Table 3.4), with an average change in SUV_{mean} of -10.2%. No difference in measurement may be due to several factors, including elevated tumor TS. As discussed, high tumor TS is a common mechanism of treatment resistance in breast and colorectal cancers (182). In this case TS will continue to convert FAU-P to FMAU-P, with treatment having a negligible effect on this process. One patient demonstrated a decrease of 40.3% in tumor SUV_{mean} from baseline in

response to capecitabine. This may be evidence of inhibition of TS by capecitabine, given that TS required for retention of FAU (175). This may signal some prognostic value to FAU-PET. It is worth noting, however, that FAU produced the lowest SUVs among the three tracers studied, suggesting a low level of tumor specificity.

Despite small cohorts, differences in the imaging properties for these probes were found in response to capecitabine, a commonly used chemotherapeutic. These findings may have great implications regarding the cellular pathways within various tumors, and may prove useful in the generation of treatment biomarkers in the future. Unfortunately, the majority of the patients enrolled in this study were administered other treatments in addition to capecitabine, and therefore we are unable to make any determinations regarding patient response to therapy. Further studies are warranted to determine if the effects observed herein have prognostic significance.

CHAPTER 4 SUMMARY

Imaging is an essential element in modern oncologic practice. It provides invaluable information needed for the diagnosis and staging of cancer, as well as for the optimization of treatment. Although anatomic imaging is the most prevalent form used in oncology and is the basis for RECIST, its limitations have led to the development of specialized probes and an expanded role for PET. PET allows for the *in vivo* assessment of the molecular pathways in cancer and therefore, a greater understanding of tumor physiology. While PET is still typically used with FDG to assess tumor metabolism, newer tracers can be used to visualize a variety of cellular processes.

Aberrant cellular proliferation is a defining characteristic of cancer. Initial methods for assessing proliferation in patient cancers involved measurements conducted on patient biopsy samples. However, logistical issues associated with biopsy collection and the complex, heterogeneous nature of human malignancies have led to the development of imaging agents to monitor tumor proliferation. The most successful proliferation tracer to date has been FLT, which tracks proliferation through monitoring of the TdR salvage pathway. Cellular retention of FLT is mediated by the action of the highly S-phase-specific enzyme TK1, and FLT has been used to image the response of numerous anti-neoplastic treatments. Here, we sought to use FLT-PET to image the potential anti-proliferative effect of GCs.

GCs are frequently used in the management of cancer, either as direct anti-neoplastic therapy or for supportive care. However, a number of studies have shown that GCs such as Dex, through the action GR α , can produce cell cycle arrest in solid tumors, leading to chemotherapy resistance. This has prompted many to ask whether the use of GCs should be scaled back, despite their obvious value for the palliative care

of cancer patients. This question is especially pertinent in the setting of Pem treatment, in which all patients are administered Dex alongside their chemotherapy.

To address this issue, we utilized FLT for the detection of Dex-mediated S-phase suppression using different models of NSCLC. In cell lines and human xenografts with high relative expression of GR α , a reversible decrease in FLT retention was observed following 24 h of Dex treatment, indicating that FLT accumulation can be used as a method for detecting Dex sensitivity. In NSCLC patients imaged with FLT, tracer retention was variable after 24 h Dex, with differences from patient-to-patient and between lesions within an individual. Taken together, these data suggest that the susceptibility to Dex-mediated cell cycle arrest is heterogeneous in patient disease, but that it can be detected using FLT-PET.

In addition, we examined the FLT flare phenomenon, whereby TdR salvage is upregulated in response to inhibition of *de novo* TdR biosynthesis, in the context of Pem treatment. We found that while all cells produced a significant flare following Pem, this was abolished in high-GR α cells and human xenografts when chemotherapy was accompanied by Dex treatment. This adds support to the data indicating that Dex interferes with the activity of Pem, and demonstrates that this phenomenon can be monitored using FLT-PET. The flare effect is variable, however, as was shown in our studies conducted in patients with gastrointestinal and breast cancers treated with capecitabine. The flare was present in only 2/5 patients after chemotherapy.

In addition, we explored the use of other fluoropyrimidine PET tracers: FMAU and FAU, which unlike FLT, can incorporate into DNA. FMAU is a TdR analog that is a substrate for TK2 and its uptake is reflective of cellular mitochondrial mass, which is

increased by cellular stress. FAU is a suicide prodrug of FMAU that requires TS, which is upregulated in many cancers, for activation. Although we observed a change from baseline in some patients imaged with FLT, tracer accumulation was largely unaffected in patients imaged with FMAU and FAU after capecitabine treatment, highlighting the differences in imaging properties between the agents.

In conclusion, FLT continues to be a promising agent for imaging cellular proliferation, and this work presents a new potential application for the use of FLT-PET: the prediction of GC sensitivity in solid tumors. Further studies are likely needed to determine if the presence of a flare has value in assessing response to chemotherapy.

REFERENCES

1. Lengauer C, Kinzler KW, Vogelstein B. Genetic instabilities in human cancers. *Nature*. 1998;396(6712):643-9. doi: 10.1038/25292. PubMed PMID: 9872311.
2. Nowell PC. Tumor progression: a brief historical perspective. *Semin Cancer Biol*. 2002;12(4):261-6. PubMed PMID: 12147207.
3. Xu J, Murphy SL, Kochanek KD, Bastian BA. Deaths: Final Data for 2013. *National vital statistics reports : from the Centers for Disease Control and Prevention, National Center for Health Statistics, National Vital Statistics System*. 2016;64(2):1-119. PubMed PMID: 26905861.
4. Siegel RL, Miller KD, Jemal A. Cancer statistics, 2016. *CA: a cancer journal for clinicians*. 2016;66(1):7-30. doi: 10.3322/caac.21332. PubMed PMID: 26742998.
5. Byers T. Two decades of declining cancer mortality: progress with disparity. *Annual review of public health*. 2010;31:121-32. doi: 10.1146/annurev.publhealth.121208.131047. PubMed PMID: 20070204.
6. Edwards BK, Noone AM, Mariotto AB, Simard EP, Boscoe FP, Henley SJ, Jemal A, Cho H, Anderson RN, Kohler BA, Ehemann CR, Ward EM. Annual Report to the Nation on the status of cancer, 1975-2010, featuring prevalence of comorbidity and impact on survival among persons with lung, colorectal, breast, or prostate cancer. *Cancer*. 2014;120(9):1290-314. doi: 10.1002/cncr.28509. PubMed PMID: 24343171; PMCID: 3999205.
7. Weissleder R, Pittet MJ. Imaging in the era of molecular oncology. *Nature*. 2008;452(7187):580-9. doi: 10.1038/nature06917. PubMed PMID: 18385732; PMCID: 2708079.

8. Brindle K. New approaches for imaging tumour responses to treatment. *Nat Rev Cancer*. 2008;8(2):94-107. doi: 10.1038/nrc2289. PubMed PMID: 18202697.
9. Hussain T, Nguyen QT. Molecular imaging for cancer diagnosis and surgery. *Advanced drug delivery reviews*. 2014;66:90-100. doi: 10.1016/j.addr.2013.09.007. PubMed PMID: 24064465; PMCID: 4464660.
10. Silvestri GA, Gonzalez AV, Jantz MA, Margolis ML, Gould MK, Tanoue LT, Harris LJ, Detterbeck FC. Methods for staging non-small cell lung cancer: Diagnosis and management of lung cancer, 3rd ed: American College of Chest Physicians evidence-based clinical practice guidelines. *Chest*. 2013;143(5 Suppl):e211S-50S. doi: 10.1378/chest.12-2355. PubMed PMID: 23649440.
11. Eisenhauer EA, Therasse P, Bogaerts J, Schwartz LH, Sargent D, Ford R, Dancey J, Arbuck S, Gwyther S, Mooney M, Rubinstein L, Shankar L, Dodd L, Kaplan R, Lacombe D, Verweij J. New response evaluation criteria in solid tumours: revised RECIST guideline (version 1.1). *Eur J Cancer*. 2009;45(2):228-47. doi: 10.1016/j.ejca.2008.10.026. PubMed PMID: 19097774.
12. Skehan P. On the normality of growth dynamics of neoplasms in vivo: a data base analysis. *Growth*. 1986;50(4):496-515. PubMed PMID: 3596327.
13. Kircher MF, Willmann JK. Molecular body imaging: MR imaging, CT, and US. part I. principles. *Radiology*. 2012;263(3):633-43. doi: 10.1148/radiol.12102394. PubMed PMID: 22623690; PMCID: 3359513.
14. Hoffman JM, Gambhir SS. Molecular imaging: the vision and opportunity for radiology in the future. *Radiology*. 2007;244(1):39-47. doi: 10.1148/radiol.2441060773. PubMed PMID: 17507723.

15. Warburg O, Wind F, Negelein E. The Metabolism of Tumors in the Body. *J Gen Physiol.* 1927;8(6):519-30. PubMed PMID: 19872213; PMCID: PMC2140820.
16. Kelloff GJ, Hoffman JM, Johnson B, Scher HI, Siegel BA, Cheng EY, Cheson BD, O'Shaughnessy J, Guyton KZ, Mankoff DA, Shankar L, Larson SM, Sigman CC, Schilsky RL, Sullivan DC. Progress and promise of FDG-PET imaging for cancer patient management and oncologic drug development. *Clin Cancer Res.* 2005;11(8):2785-808. doi: 10.1158/1078-0432.CCR-04-2626. PubMed PMID: 15837727.
17. Kubota K, Matsuzawa T, Fujiwara T, Ito M, Hatazawa J, Ishiwata K, Iwata R, Ido T. Differential diagnosis of lung tumor with positron emission tomography: a prospective study. *J Nucl Med.* 1990;31(12):1927-32. PubMed PMID: 2266388.
18. Gupta NC, Frank AR, Dewan NA, Redepenning LS, Rothberg ML, Mailliard JA, Phalen JJ, Sunderland JJ, Frick MP. Solitary pulmonary nodules: detection of malignancy with PET with 2-[F-18]-fluoro-2-deoxy-D-glucose. *Radiology.* 1992;184(2):441-4. doi: 10.1148/radiology.184.2.1620844. PubMed PMID: 1620844.
19. Hoh CK, Hawkins RA, Glaspy JA, Dahlbom M, Tse NY, Hoffman EJ, Schiepers C, Choi Y, Rege S, Nitzsche E, et al. Cancer detection with whole-body PET using 2-[18F]fluoro-2-deoxy-D-glucose. *Journal of computer assisted tomography.* 1993;17(4):582-9. PubMed PMID: 8331230.
20. Gambhir SS. Molecular imaging of cancer with positron emission tomography. *Nat Rev Cancer.* 2002;2(9):683-93. doi: 10.1038/nrc882. PubMed PMID: 12209157.
21. Kohl G. The evolution and state-of-the-art principles of multislice computed tomography. *Proc Am Thorac Soc.* 2005;2(6):470-6, 99-500. doi: 10.1513/pats.200508-086DS. PubMed PMID: 16352750.

22. Ambrose J. Computerized transverse axial scanning (tomography). 2. Clinical application. *Br J Radiol.* 1973;46(552):1023-47. doi: 10.1259/0007-1285-46-552-1023. PubMed PMID: 4757353.
23. Hounsfield GN. Computerized transverse axial scanning (tomography). 1. Description of system. *Br J Radiol.* 1973;46(552):1016-22. doi: 10.1259/0007-1285-46-552-1016. PubMed PMID: 4757352.
24. Black WC, Gareen IF, Soneji SS, Sicks JD, Keeler EB, Aberle DR, Naeim A, Church TR, Silvestri GA, Gorelick J, Gatsonis C, National Lung Screening Trial Research T. Cost-effectiveness of CT screening in the National Lung Screening Trial. *N Engl J Med.* 2014;371(19):1793-802. doi: 10.1056/NEJMoa1312547. PubMed PMID: 25372087; PMCID: PMC4335305.
25. Detterbeck FC, Mazzone PJ, Naidich DP, Bach PB. Screening for lung cancer: Diagnosis and management of lung cancer, 3rd ed: American College of Chest Physicians evidence-based clinical practice guidelines. *Chest.* 2013;143(5 Suppl):e78S-92S. doi: 10.1378/chest.12-2350. PubMed PMID: 23649455; PMCID: PMC3749713.
26. Jaklitsch MT, Jacobson FL, Austin JH, Field JK, Jett JR, Keshavjee S, MacMahon H, Mulshine JL, Munden RF, Salgia R, Strauss GM, Swanson SJ, Travis WD, Sugarbaker DJ. The American Association for Thoracic Surgery guidelines for lung cancer screening using low-dose computed tomography scans for lung cancer survivors and other high-risk groups. *J Thorac Cardiovasc Surg.* 2012;144(1):33-8. doi: 10.1016/j.jtcvs.2012.05.060. PubMed PMID: 22710039.

27. Wood DE. National Comprehensive Cancer Network (NCCN) Clinical Practice Guidelines for Lung Cancer Screening. *Thorac Surg Clin*. 2015;25(2):185-97. doi: 10.1016/j.thorsurg.2014.12.003. PubMed PMID: 25901562.
28. Aberle DR, DeMello S, Berg CD, Black WC, Brewer B, Church TR, Clingan KL, Duan F, Fagerstrom RM, Gareen IF, Gatsonis CA, Gierada DS, Jain A, Jones GC, Mahon I, Marcus PM, Rathmell JM, Sicks J, National Lung Screening Trial Research T. Results of the two incidence screenings in the National Lung Screening Trial. *N Engl J Med*. 2013;369(10):920-31. doi: 10.1056/NEJMoa1208962. PubMed PMID: 24004119; PMCID: PMC4307922.
29. National Lung Screening Trial Research T, Aberle DR, Adams AM, Berg CD, Black WC, Clapp JD, Fagerstrom RM, Gareen IF, Gatsonis C, Marcus PM, Sicks JD. Reduced lung-cancer mortality with low-dose computed tomographic screening. *N Engl J Med*. 2011;365(5):395-409. doi: 10.1056/NEJMoa1102873. PubMed PMID: 21714641; PMCID: PMC4356534.
30. Rabi I, Zacharias J, Millman S, Kusch P. A New Method of Measuring Nuclear Magnetic Moment. *Physical Review*. 1938;53:318.
31. Purcell E, Torrey H, Pound R. Resonance absorption by nuclear magnetic moments in a solid. *Physical Review*. 1946;69:37.
32. Bloembergen N, Purcell E, Pound R. Relaxation Effects in Nuclear Magnetic Resonance Absorption. *Physical Review*. 1948;73:679-712.
33. Lauterbur PC. Image formation by induced local interactions: examples employing nuclear magnetic resonance. *Nature*. 1973;242:190-1.

34. Damadian R. Tumor detection by nuclear magnetic resonance. *Science*. 1971;171(3976):1151-3. PubMed PMID: 5544870.
35. Kriege M, Brekelmans CT, Boetes C, Besnard PE, Zonderland HM, Obdeijn IM, Manoliu RA, Kok T, Peterse H, Tilanus-Linthorst MM, Muller SH, Meijer S, Oosterwijk JC, Beex LV, Tollenaar RA, de Koning HJ, Rutgers EJ, Klijn JG, Magnetic Resonance Imaging Screening Study G. Efficacy of MRI and mammography for breast-cancer screening in women with a familial or genetic predisposition. *N Engl J Med*. 2004;351(5):427-37. doi: 10.1056/NEJMoa031759. PubMed PMID: 15282350.
36. Kuhl CK, Schrading S, Leutner CC, Morakkabati-Spitz N, Wardelmann E, Fimmers R, Kuhn W, Schild HH. Mammography, breast ultrasound, and magnetic resonance imaging for surveillance of women at high familial risk for breast cancer. *J Clin Oncol*. 2005;23(33):8469-76. doi: 10.1200/JCO.2004.00.4960. PubMed PMID: 16293877.
37. Leach MO, Boggis CR, Dixon AK, Easton DF, Eeles RA, Evans DG, Gilbert FJ, Griebisch I, Hoff RJ, Kessar P, Lakhani SR, Moss SM, Nerurkar A, Padhani AR, Pointon LJ, Thompson D, Warren RM, group Ms. Screening with magnetic resonance imaging and mammography of a UK population at high familial risk of breast cancer: a prospective multicentre cohort study (MARIBS). *Lancet*. 2005;365(9473):1769-78. doi: 10.1016/S0140-6736(05)66481-1. PubMed PMID: 15910949.
38. Vargas HA, Akin O, Franiel T, Mazaheri Y, Zheng J, Moskowitz C, Udo K, Eastham J, Hricak H. Diffusion-weighted endorectal MR imaging at 3 T for prostate cancer: tumor detection and assessment of aggressiveness. *Radiology*.

2011;259(3):775-84. doi: 10.1148/radiol.11102066. PubMed PMID: 21436085; PMCID: PMC3099046.

39. Lin SP, Brown JJ. MR contrast agents: physical and pharmacologic basics. *J Magn Reson Imaging*. 2007;25(5):884-99. doi: 10.1002/jmri.20955. PubMed PMID: 17457803.

40. Thorek DL, Chen AK, Czupryna J, Tsourkas A. Superparamagnetic iron oxide nanoparticle probes for molecular imaging. *Ann Biomed Eng*. 2006;34(1):23-38. doi: 10.1007/s10439-005-9002-7. PubMed PMID: 16496086.

41. Islam T, Josephson L. Current state and future applications of active targeting in malignancies using superparamagnetic iron oxide nanoparticles. *Cancer Biomark*. 2009;5(2):99-107. doi: 10.3233/CBM-2009-0615. PubMed PMID: 19414927.

42. Wu S, Zhang L, Zhong J, Zhang Z. Dual contrast magnetic resonance imaging tracking of iron-labeled cells in vivo. *Cytotherapy*. 2010;12(7):859-69. doi: 10.3109/14653241003587652. PubMed PMID: 20184501.

43. Gessner R, Dayton PA. Advances in molecular imaging with ultrasound. *Molecular imaging*. 2010;9(3):117-27. PubMed PMID: 20487678; PMCID: 2935327.

44. Deshpande N, Needles A, Willmann JK. Molecular ultrasound imaging: current status and future directions. *Clinical radiology*. 2010;65(7):567-81. doi: 10.1016/j.crad.2010.02.013. PubMed PMID: 20541656; PMCID: 3144865.

45. Willmann JK, van Bruggen N, Dinkelborg LM, Gambhir SS. Molecular imaging in drug development. *Nature reviews Drug discovery*. 2008;7(7):591-607. doi: 10.1038/nrd2290. PubMed PMID: 18591980.

46. Willmann JK, Kimura RH, Deshpande N, Lutz AM, Cochran JR, Gambhir SS. Targeted contrast-enhanced ultrasound imaging of tumor angiogenesis with contrast microbubbles conjugated to integrin-binding knottin peptides. *J Nucl Med.* 2010;51(3):433-40. doi: 10.2967/jnumed.109.068007. PubMed PMID: 20150258; PMCID: 4111897.
47. Herment A, Guglielmi JP, Dumeé P, Peronneau P, Delouche P. Limitations of ultrasound imaging and image restoration. *Ultrasonics.* 1987;25(5):267-73. PubMed PMID: 3310352.
48. Phelps ME, Hoffman EJ, Mullani NA, Ter-Pogossian MM. Application of annihilation coincidence detection to transaxial reconstruction tomography. *J Nucl Med.* 1975;16(3):210-24. PubMed PMID: 1113170.
49. Ter-Pogossian MM, Phelps ME, Hoffman EJ, Mullani NA. A positron-emission transaxial tomograph for nuclear imaging (PETT). *Radiology.* 1975;114(1):89-98. doi: 10.1148/114.1.89. PubMed PMID: 1208874.
50. Lucignani G, Paganelli G, Bombardieri E. The use of standardized uptake values for assessing FDG uptake with PET in oncology: a clinical perspective. *Nucl Med Commun.* 2004;25(7):651-6. PubMed PMID: 15208491.
51. Acton PD, Zhuang H, Alavi A. Quantification in PET. *Radiologic clinics of North America.* 2004;42(6):1055-62, viii. doi: 10.1016/j.rcl.2004.08.010. PubMed PMID: 15488557.
52. De Wever W, Meylaerts L, De Ceuninck L, Stroobants S, Verschakelen JA. Additional value of integrated PET-CT in the detection and characterization of lung

metastases: correlation with CT alone and PET alone. *Eur Radiol.* 2007;17(2):467-73. doi: 10.1007/s00330-006-0362-7. PubMed PMID: 17180333.

53. Gayed I, Vu T, Iyer R, Johnson M, Macapinlac H, Swanston N, Podoloff D. The role of 18F-FDG PET in staging and early prediction of response to therapy of recurrent gastrointestinal stromal tumors. *J Nucl Med.* 2004;45(1):17-21. PubMed PMID: 14734662.

54. Groheux D, Espie M, Giacchetti S, Hindie E. Performance of FDG PET/CT in the clinical management of breast cancer. *Radiology.* 2013;266(2):388-405. doi: 10.1148/radiol.12110853. PubMed PMID: 23220901.

55. Subedi N, Scarsbrook A, Darby M, Korde K, Mc Shane P, Muers MF. The clinical impact of integrated FDG PET-CT on management decisions in patients with lung cancer. *Lung Cancer.* 2009;64(3):301-7. doi: 10.1016/j.lungcan.2008.09.006. PubMed PMID: 19004519.

56. Barrington SF, Mikhaeel NG, Kostakoglu L, Meignan M, Hutchings M, Mueller SP, Schwartz LH, Zucca E, Fisher RI, Trotman J, Hoekstra OS, Hicks RJ, O'Doherty MJ, Hustinx R, Biggi A, Cheson BD. Role of imaging in the staging and response assessment of lymphoma: consensus of the International Conference on Malignant Lymphomas Imaging Working Group. *J Clin Oncol.* 2014;32(27):3048-58. doi: 10.1200/JCO.2013.53.5229. PubMed PMID: 25113771.

57. Moskowitz CH, Schoder H, Teruya-Feldstein J, Sima C, Iasonos A, Portlock CS, Straus D, Noy A, Palomba ML, O'Connor OA, Horwitz S, Weaver SA, Meikle JL, Filippa DA, Caravelli JF, Hamlin PA, Zelenetz AD. Risk-adapted dose-dense immunochemotherapy determined by interim FDG-PET in Advanced-stage diffuse large

B-Cell lymphoma. *J Clin Oncol.* 2010;28(11):1896-903. doi: 10.1200/JCO.2009.26.5942. PubMed PMID: 20212248; PMCID: PMC3651601.

58. Agress H, Jr., Cooper BZ. Detection of clinically unexpected malignant and premalignant tumors with whole-body FDG PET: histopathologic comparison. *Radiology.* 2004;230(2):417-22. doi: 10.1148/radiol.2302021685. PubMed PMID: 14699176.

59. Minamimoto R, Senda M, Jinnouchi S, Terauchi T, Yoshida T, Murano T, Fukuda H, Iinuma T, Uno K, Nishizawa S, Tsukamoto E, Iwata H, Inoue T, Oguchi K, Nakashima R, Inoue T. The current status of an FDG-PET cancer screening program in Japan, based on a 4-year (2006-2009) nationwide survey. *Ann Nucl Med.* 2013;27(1):46-57. doi: 10.1007/s12149-012-0660-x. PubMed PMID: 23086544; PMCID: PMC4328108.

60. Ide M, Suzuki Y. Is whole-body FDG-PET valuable for health screening? *For. Eur J Nucl Med Mol Imaging.* 2005;32(3):339-41. doi: 10.1007/s00259-005-1774-3. PubMed PMID: 15726352.

61. Chen YK, Ding HJ, Su CT, Shen YY, Chen LK, Liao AC, Hung TZ, Hu FL, Kao CH. Application of PET and PET/CT imaging for cancer screening. *Anticancer Res.* 2004;24(6):4103-8. PubMed PMID: 15736459.

62. Kubota R, Yamada S, Kubota K, Ishiwata K, Tamahashi N, Ido T. Intratumoral distribution of fluorine-18-fluorodeoxyglucose in vivo: high accumulation in macrophages and granulation tissues studied by microautoradiography. *J Nucl Med.* 1992;33(11):1972-80. PubMed PMID: 1432158.

63. McGuirt WF, Williams DW, 3rd, Keyes JW, Jr., Greven KM, Watson NE, Jr., Geisinger KR, Cappellari JO. A comparative diagnostic study of head and neck nodal metastases using positron emission tomography. *Laryngoscope*. 1995;105(4 Pt 1):373-5. doi: 10.1288/00005537-199504000-00006. PubMed PMID: 7715380.
64. Lopci E, Nanni C, Castellucci P, Montini GC, Allegri V, Rubello D, Chierichetti F, Ambrosini V, Fanti S. Imaging with non-FDG PET tracers: outlook for current clinical applications. *Insights into imaging*. 2010;1(5-6):373-85. doi: 10.1007/s13244-010-0040-9. PubMed PMID: 22347930; PMCID: 3259359.
65. Nahrendorf M, Zhang H, Hembrador S, Panizzi P, Sosnovik DE, Aikawa E, Libby P, Swirski FK, Weissleder R. Nanoparticle PET-CT imaging of macrophages in inflammatory atherosclerosis. *Circulation*. 2008;117(3):379-87. doi: 10.1161/CIRCULATIONAHA.107.741181. PubMed PMID: 18158358; PMCID: 2663426.
66. Chen X, Hou Y, Tohme M, Park R, Khankaldyyan V, Gonzales-Gomez I, Bading JR, Laug WE, Conti PS. Pegylated Arg-Gly-Asp peptide: ⁶⁴Cu labeling and PET imaging of brain tumor alpha_vbeta₃-integrin expression. *J Nucl Med*. 2004;45(10):1776-83. PubMed PMID: 15471848.
67. Elsasser-Beile U, Reischl G, Wiehr S, Buhler P, Wolf P, Alt K, Shively J, Judenhofer MS, Machulla HJ, Pichler BJ. PET imaging of prostate cancer xenografts with a highly specific antibody against the prostate-specific membrane antigen. *J Nucl Med*. 2009;50(4):606-11. doi: 10.2967/jnumed.108.058487. PubMed PMID: 19289418.
68. Wu AM, Yazaki PJ, Tsai S, Nguyen K, Anderson AL, McCarthy DW, Welch MJ, Shively JE, Williams LE, Raubitschek AA, Wong JY, Toyokuni T, Phelps ME, Gambhir SS. High-resolution microPET imaging of carcinoembryonic antigen-positive xenografts

by using a copper-64-labeled engineered antibody fragment. Proceedings of the National Academy of Sciences of the United States of America. 2000;97(15):8495-500. doi: 10.1073/pnas.150228297. PubMed PMID: 10880576; PMCID: 26976.

69. Sampson UK, Dorbala S, Limaye A, Kwong R, Di Carli MF. Diagnostic accuracy of rubidium-82 myocardial perfusion imaging with hybrid positron emission tomography/computed tomography in the detection of coronary artery disease. Journal of the American College of Cardiology. 2007;49(10):1052-8. doi: 10.1016/j.jacc.2006.12.015. PubMed PMID: 17349884.

70. Yoshinaga K, Klein R, Tamaki N. Generator-produced rubidium-82 positron emission tomography myocardial perfusion imaging-From basic aspects to clinical applications. Journal of cardiology. 2010;55(2):163-73. doi: 10.1016/j.jjcc.2010.01.001. PubMed PMID: 20206068.

71. Dijkers EC, Kosterink JG, Rademaker AP, Perk LR, van Dongen GA, Bart J, de Jong JR, de Vries EG, Lub-de Hooge MN. Development and characterization of clinical-grade ⁸⁹Zr-trastuzumab for HER2/neu immunoPET imaging. J Nucl Med. 2009;50(6):974-81. doi: 10.2967/jnumed.108.060392. PubMed PMID: 19443585.

72. Al-Nahhas A, Win Z, Szyszko T, Singh A, Nanni C, Fanti S, Rubello D. Gallium-68 PET: a new frontier in receptor cancer imaging. Anticancer Res. 2007;27(6B):4087-94. PubMed PMID: 18225576.

73. Mojtahedi A, Thamake S, Tworowska I, Ranganathan D, Delpassand ES. The value of (68)Ga-DOTATATE PET/CT in diagnosis and management of neuroendocrine tumors compared to current FDA approved imaging modalities: a review of literature.

American journal of nuclear medicine and molecular imaging. 2014;4(5):426-34. PubMed PMID: 25143861; PMCID: 4138137.

74. Anderson CJ, Ferdani R. Copper-64 radiopharmaceuticals for PET imaging of cancer: advances in preclinical and clinical research. *Cancer biotherapy & radiopharmaceuticals*. 2009;24(4):379-93. doi: 10.1089/cbr.2009.0674. PubMed PMID: 19694573; PMCID: 2794299.

75. Bueno R, Richards WG, Swanson SJ, Jaklitsch MT, Lukanich JM, Mentzer SJ, Sugarbaker DJ. Nodal stage after induction therapy for stage IIIA lung cancer determines patient survival. *Ann Thorac Surg*. 2000;70(6):1826-31. PubMed PMID: 11156079.

76. Ryu JS, Choi NC, Fischman AJ, Lynch TJ, Mathisen DJ. FDG-PET in staging and restaging non-small cell lung cancer after neoadjuvant chemoradiotherapy: correlation with histopathology. *Lung Cancer*. 2002;35(2):179-87. PubMed PMID: 11804691.

77. Clayton F. Pathologic correlates of survival in 378 lymph node-negative infiltrating ductal breast carcinomas. Mitotic count is the best single predictor. *Cancer*. 1991;68(6):1309-17. PubMed PMID: 1651805.

78. Tubiana M, Pejovic MH, Chavaudra N, Contesso G, Malaise EP. The long-term prognostic significance of the thymidine labelling index in breast cancer. *Int J Cancer*. 1984;33(4):441-5. PubMed PMID: 6706431.

79. Elston CW, Ellis IO. Pathological prognostic factors in breast cancer. I. The value of histological grade in breast cancer: experience from a large study with long-term follow-up. *Histopathology*. 1991;19(5):403-10. PubMed PMID: 1757079.

80. Hoffman JG. Theory of the mitotic index and its application to tissue growth measurement. *Bull Math Biophys.* 1949;11(2):139-44. PubMed PMID: 18133368.
81. Beresford MJ, Wilson GD, Makris A. Measuring proliferation in breast cancer: practicalities and applications. *Breast Cancer Res.* 2006;8(6):216. doi: 10.1186/bcr1618. PubMed PMID: 17164010; PMCID: PMC1797032.
82. van Diest PJ, Baak JP, Matze-Cok P, Wisse-Brekelmans EC, van Galen CM, Kurver PH, Bellot SM, Fijnheer J, van Gorp LH, Kwee WS, et al. Reproducibility of mitosis counting in 2,469 breast cancer specimens: results from the Multicenter Morphometric Mammary Carcinoma Project. *Hum Pathol.* 1992;23(6):603-7. PubMed PMID: 1592381.
83. van Diest PJ, van der Wall E, Baak JP. Prognostic value of proliferation in invasive breast cancer: a review. *J Clin Pathol.* 2004;57(7):675-81. doi: 10.1136/jcp.2003.010777. PubMed PMID: 15220356; PMCID: PMC1770351.
84. Gratzner HG. Monoclonal antibody to 5-bromo- and 5-iododeoxyuridine: A new reagent for detection of DNA replication. *Science.* 1982;218(4571):474-5. PubMed PMID: 7123245.
85. Sklarew RJ, Hoffman J, Post J. A rapid in vitro method for measuring cell proliferation in human breast cancer. *Cancer.* 1977;40(5):2299-302. PubMed PMID: 336186.
86. Clark GM, Dressler LG, Owens MA, Pounds G, Oldaker T, McGuire WL. Prediction of relapse or survival in patients with node-negative breast cancer by DNA flow cytometry. *N Engl J Med.* 1989;320(10):627-33. doi: 10.1056/NEJM198903093201003. PubMed PMID: 2918874.

87. Gerdes J, Schwab U, Lemke H, Stein H. Production of a mouse monoclonal antibody reactive with a human nuclear antigen associated with cell proliferation. *Int J Cancer*. 1983;31(1):13-20. PubMed PMID: 6339421.
88. Gerdes J, Lemke H, Baisch H, Wacker HH, Schwab U, Stein H. Cell cycle analysis of a cell proliferation-associated human nuclear antigen defined by the monoclonal antibody Ki-67. *J Immunol*. 1984;133(4):1710-5. PubMed PMID: 6206131.
89. Gerdes J, Li L, Schlueter C, Duchrow M, Wohlenberg C, Gerlach C, Stahmer I, Kloth S, Brandt E, Flad HD. Immunobiochemical and molecular biologic characterization of the cell proliferation-associated nuclear antigen that is defined by monoclonal antibody Ki-67. *Am J Pathol*. 1991;138(4):867-73. PubMed PMID: 2012175; PMCID: PMC1886092.
90. Drach J, Gattringer C, Glassl H, Drach D, Huber H. The biological and clinical significance of the KI-67 growth fraction in multiple myeloma. *Hematol Oncol*. 1992;10(2):125-34. PubMed PMID: 1592363.
91. Ueda T, Aozasa K, Tsujimoto M, Ohsawa M, Uchida A, Aoki Y, Ono K, Matsumoto K. Prognostic significance of Ki-67 reactivity in soft tissue sarcomas. *Cancer*. 1989;63(8):1607-11. PubMed PMID: 2647278.
92. Bouzubar N, Walker KJ, Griffiths K, Ellis IO, Elston CW, Robertson JF, Blamey RW, Nicholson RI. Ki67 immunostaining in primary breast cancer: pathological and clinical associations. *Br J Cancer*. 1989;59(6):943-7. PubMed PMID: 2472168; PMCID: PMC2246720.

93. Scholzen T, Gerdes J. The Ki-67 protein: from the known and the unknown. *J Cell Physiol.* 2000;182(3):311-22. doi: 10.1002/(SICI)1097-4652(200003)182:3<311::AID-JCP1>3.0.CO;2-9. PubMed PMID: 10653597.
94. Friberg S, Mattson S. On the growth rates of human malignant tumors: implications for medical decision making. *J Surg Oncol.* 1997;65(4):284-97. PubMed PMID: 9274795.
95. Junttila MR, de Sauvage FJ. Influence of tumour micro-environment heterogeneity on therapeutic response. *Nature.* 2013;501(7467):346-54. doi: 10.1038/nature12626. PubMed PMID: 24048067.
96. Schroeder T, Yuan H, Viglianti BL, Peltz C, Asopa S, Vujaskovic Z, Dewhirst MW. Spatial heterogeneity and oxygen dependence of glucose consumption in R3230Ac and fibrosarcomas of the Fischer 344 rat. *Cancer Res.* 2005;65(12):5163-71. doi: 10.1158/0008-5472.CAN-04-3900. PubMed PMID: 15958560.
97. Serganova I, Doubrovin M, Vider J, Ponomarev V, Soghomonyan S, Beresten T, Ageyeva L, Serganov A, Cai S, Balatoni J, Blasberg R, Gelovani J. Molecular imaging of temporal dynamics and spatial heterogeneity of hypoxia-inducible factor-1 signal transduction activity in tumors in living mice. *Cancer Res.* 2004;64(17):6101-8. doi: 10.1158/0008-5472.CAN-04-0842. PubMed PMID: 15342393.
98. Heppner GH. Tumor heterogeneity. *Cancer Res.* 1984;44(6):2259-65. PubMed PMID: 6372991.
99. Swanton C. Intratumor heterogeneity: evolution through space and time. *Cancer research.* 2012;72(19):4875-82. doi: 10.1158/0008-5472.CAN-12-2217. PubMed PMID: 23002210; PMCID: 3712191.

100. Fidler IJ. Tumor heterogeneity and the biology of cancer invasion and metastasis. *Cancer Res.* 1978;38(9):2651-60. PubMed PMID: 354778.
101. Chung JK, Lee YJ, Kim SK, Jeong JM, Lee DS, Lee MC. Comparison of [18F]fluorodeoxyglucose uptake with glucose transporter-1 expression and proliferation rate in human glioma and non-small-cell lung cancer. *Nucl Med Commun.* 2004;25(1):11-7. PubMed PMID: 15061260.
102. Buck AK, Halter G, Schirrmeister H, Kotzerke J, Wurziger I, Glatting G, Mattfeldt T, Neumaier B, Reske SN, Hetzel M. Imaging proliferation in lung tumors with PET: 18F-FLT versus 18F-FDG. *J Nucl Med.* 2003;44(9):1426-31. PubMed PMID: 12960187.
103. Christman D, Crawford EJ, Friedkin M, Wolf AP. Detection of DNA synthesis in intact organisms with positron-emitting (methyl- 11 C)thymidine. *Proceedings of the National Academy of Sciences of the United States of America.* 1972;69(4):988-92. PubMed PMID: 4554538; PMCID: PMC426610.
104. Shields AF, Larson SM, Grunbaum Z, Graham MM. Short-term thymidine uptake in normal and neoplastic tissues: studies for PET. *J Nucl Med.* 1984;25(7):759-64. PubMed PMID: 6610731.
105. Shields AF, Mankoff DA, Link JM, Graham MM, Eary JF, Kozawa SM, Zheng M, Lewellen B, Lewellen TK, Grierson JR, Krohn KA. Carbon-11-thymidine and FDG to measure therapy response. *J Nucl Med.* 1998;39(10):1757-62. PubMed PMID: 9776283.
106. Bading JR, Shields AF. Imaging of cell proliferation: status and prospects. *J Nucl Med.* 2008;49 Suppl 2:64S-80S. doi: 10.2967/jnumed.107.046391. PubMed PMID: 18523066.

107. Shields AF, Lim K, Grierson J, Link J, Krohn KA. Utilization of labeled thymidine in DNA synthesis: studies for PET. *J Nucl Med.* 1990;31(3):337-42. PubMed PMID: 2308005.
108. Shields AF, Grierson JR, Dohmen BM, Machulla HJ, Stayanoff JC, Lawhorn-Crews JM, Obradovich JE, Muzik O, Mangner TJ. Imaging proliferation in vivo with [¹⁸F]-FLT and positron emission tomography. *Nat Med.* 1998;4(11):1334-6. doi: 10.1038/3337. PubMed PMID: 9809561.
109. Langen P, Etzold G, Hintsche R, Kowolik G. 3'-Deoxy-3'-fluorothymidine, a new selective inhibitor of DNA-synthesis. *Acta Biol Med Ger.* 1969;23(6):759-66. PubMed PMID: 5375478.
110. Flexner C, van der Horst C, Jacobson MA, Powderly W, Duncanson F, Ganes D, Barditch-Crovo PA, Petty BG, Baron PA, Armstrong D, et al. Relationship between plasma concentrations of 3'-deoxy-3'-fluorothymidine (alovudine) and antiretroviral activity in two concentration-controlled trials. *J Infect Dis.* 1994;170(6):1394-403. PubMed PMID: 7995977.
111. Lundgren B, Bottiger D, Ljungdahl-Stahle E, Norrby E, Stahle L, Wahren B, Oberg B. Antiviral effects of 3'-fluorothymidine and 3'-azidothymidine in cynomolgus monkeys infected with simian immunodeficiency virus. *J Acquir Immune Defic Syndr.* 1991;4(5):489-98. PubMed PMID: 2016686.
112. Paproski RJ, Ng AM, Yao SY, Graham K, Young JD, Cass CE. The role of human nucleoside transporters in uptake of 3'-deoxy-3'-fluorothymidine. *Molecular pharmacology.* 2008;74(5):1372-80. doi: 10.1124/mol.108.048900. PubMed PMID: 18669604.

113. Plotnik DA, McLaughlin LJ, Chan J, Redmayne-Titley JN, Schwartz JL. The role of nucleoside/nucleotide transport and metabolism in the uptake and retention of 3'-fluoro-3'-deoxythymidine in human B-lymphoblast cells. *Nuclear medicine and biology*. 2011;38(7):979-86. doi: 10.1016/j.nucmedbio.2011.03.009. PubMed PMID: 21982569; PMCID: 3190124.
114. Been LB, Suurmeijer AJ, Cobben DC, Jager PL, Hoekstra HJ, Elsinga PH. [18F]FLT-PET in oncology: current status and opportunities. *Eur J Nucl Med Mol Imaging*. 2004;31(12):1659-72. doi: 10.1007/s00259-004-1687-6. PubMed PMID: 15565331.
115. Grierson JR, Schwartz JL, Muzi M, Jordan R, Krohn KA. Metabolism of 3'-deoxy-3'-[F-18]fluorothymidine in proliferating A549 cells: validations for positron emission tomography. *Nuclear medicine and biology*. 2004;31(7):829-37. doi: 10.1016/j.nucmedbio.2004.06.004. PubMed PMID: 15464384.
116. Muzi M, Mankoff DA, Grierson JR, Wells JM, Vesselle H, Krohn KA. Kinetic modeling of 3'-deoxy-3'-fluorothymidine in somatic tumors: mathematical studies. *J Nucl Med*. 2005;46(2):371-80. PubMed PMID: 15695799.
117. Shields AF, Briston DA, Chandupatla S, Douglas KA, Lawhorn-Crews J, Collins JM, Mangner TJ, Heilbrun LK, Muzik O. A simplified analysis of [18F]3'-deoxy-3'-fluorothymidine metabolism and retention. *European journal of nuclear medicine and molecular imaging*. 2005;32(11):1269-75. doi: 10.1007/s00259-005-1813-0. PubMed PMID: 15991018.
118. Kong XB, Zhu QY, Vidal PM, Watanabe KA, Polsky B, Armstrong D, Ostrander M, Lang SA, Jr., Muchmore E, Chou TC. Comparisons of anti-human immunodeficiency

virus activities, cellular transport, and plasma and intracellular pharmacokinetics of 3'-fluoro-3'-deoxythymidine and 3'-azido-3'-deoxythymidine. *Antimicrobial agents and chemotherapy*. 1992;36(4):808-18. PubMed PMID: 1503443; PMCID: 189428.

119. Chalkidou A, Landau DB, Odell EW, Cornelius VR, O'Doherty MJ, Marsden PK. Correlation between Ki-67 immunohistochemistry and 18F-fluorothymidine uptake in patients with cancer: A systematic review and meta-analysis. *European journal of cancer*. 2012;48(18):3499-513. doi: 10.1016/j.ejca.2012.05.001. PubMed PMID: 22658807.

120. Hardy LW, Finer-Moore JS, Montfort WR, Jones MO, Santi DV, Stroud RM. Atomic structure of thymidylate synthase: target for rational drug design. *Science*. 1987;235(4787):448-55. PubMed PMID: 3099389.

121. McKinley ET, Ayers GD, Smith RA, Saleh SA, Zhao P, Washington MK, Coffey RJ, Manning HC. Limits of [18F]-FLT PET as a biomarker of proliferation in oncology. *PloS one*. 2013;8(3):e58938. doi: 10.1371/journal.pone.0058938. PubMed PMID: 23554961; PMCID: 3598948.

122. Moroz MA, Kochetkov T, Cai S, Wu J, Shamis M, Nair J, de Stanchina E, Serganova I, Schwartz GK, Banerjee D, Bertino JR, Blasberg RG. Imaging colon cancer response following treatment with AZD1152: a preclinical analysis of [18F]fluoro-2-deoxyglucose and 3'-deoxy-3'-[18F]fluorothymidine imaging. *Clin Cancer Res*. 2011;17(5):1099-110. doi: 10.1158/1078-0432.CCR-10-1430. PubMed PMID: 21245090; PMCID: 3079195.

123. Bruns CJ, Harbison MT, Davis DW, Portera CA, Tsan R, McConkey DJ, Evans DB, Abbruzzese JL, Hicklin DJ, Radinsky R. Epidermal growth factor receptor blockade

with C225 plus gemcitabine results in regression of human pancreatic carcinoma growing orthotopically in nude mice by antiangiogenic mechanisms. *Clin Cancer Res.* 2000;6(5):1936-48. PubMed PMID: 10815919.

124. Paproski RJ, Wuest M, Jans HS, Graham K, Gati WP, McQuarrie S, McEwan A, Mercer J, Young JD, Cass CE. Biodistribution and uptake of 3'-deoxy-3'-fluorothymidine in ENT1-knockout mice and in an ENT1-knockdown tumor model. *J Nucl Med.* 2010;51(9):1447-55. doi: 10.2967/jnumed.110.076356. PubMed PMID: 20720035.

125. Tsuji AB, Sogawa C, Sugyo A, Sudo H, Toyohara J, Koizumi M, Abe M, Hino O, Harada YN, Furukawa T, Suzuki K, Saga T. Comparison of conventional and novel PET tracers for imaging mesothelioma in nude mice with subcutaneous and intrapleural xenografts. *Nuclear medicine and biology.* 2009;36(4):379-88. doi: 10.1016/j.nucmedbio.2009.01.018. PubMed PMID: 19423005.

126. Perumal M, Pillai RG, Barthel H, Leyton J, Latigo JR, Forster M, Mitchell F, Jackman AL, Aboagye EO. Redistribution of nucleoside transporters to the cell membrane provides a novel approach for imaging thymidylate synthase inhibition by positron emission tomography. *Cancer Res.* 2006;66(17):8558-64. doi: 10.1158/0008-5472.CAN-06-0898. PubMed PMID: 16951168.

127. Nottebrock H, Then R. Thymidine concentrations in serum and urine of different animal species and man. *Biochemical pharmacology.* 1977;26(22):2175-9. PubMed PMID: 412502.

128. Zhang CC, Yan Z, Li W, Kuszpit K, Painter CL, Zhang Q, Lappin PB, Nichols T, Lira ME, Affolter T, Fahey NR, Cullinane C, Spilker M, Zasadny K, O'Brien P, Buckman D, Wong A, Christensen JG. [(18)F]FLT-PET imaging does not always "light up"

proliferating tumor cells. *Clin Cancer Res.* 2012;18(5):1303-12. doi: 10.1158/1078-0432.CCR-11-1433. PubMed PMID: 22170262.

129. Li KM, Rivory LP, Hoskins J, Sharma R, Clarke SJ. Altered deoxyuridine and thymidine in plasma following capecitabine treatment in colorectal cancer patients. *British journal of clinical pharmacology.* 2007;63(1):67-74. doi: 10.1111/j.1365-2125.2006.02710.x. PubMed PMID: 16827816; PMCID: 2000712.

130. Lee SJ, Yeo JS, Lee HJ, Lee EJ, Kim SY, Jang SJ, Lee JJ, Ryu JS, Moon DH. Thymidine phosphorylase influences [(18)F]fluorothymidine uptake in cancer cells and patients with non-small cell lung cancer. *Eur J Nucl Med Mol Imaging.* 2014;41(7):1327-35. doi: 10.1007/s00259-014-2712-z. PubMed PMID: 24562648.

131. Schelhaas S, Wachsmuth L, Viel T, Honess DJ, Heinzmann K, Smith DM, Hermann S, Wagner S, Kuhlmann MT, Muller-Tidow C, Kopka K, Schober O, Schafers M, Schneider R, Aboagye EO, Griffiths J, Faber C, Jacobs AH. Variability of Proliferation and Diffusion in Different Lung Cancer Models as Measured by 3'-Deoxy-3'-(1)(8)F-Fluorothymidine PET and Diffusion-Weighted MR Imaging. *J Nucl Med.* 2014;55(6):983-8. doi: 10.2967/jnumed.113.133348. PubMed PMID: 24777288.

132. Rasey JS, Grierson JR, Wiens LW, Kolb PD, Schwartz JL. Validation of FLT uptake as a measure of thymidine kinase-1 activity in A549 carcinoma cells. *J Nucl Med.* 2002;43(9):1210-7. PubMed PMID: 12215561.

133. Piper AA, Tattersall MH, Fox RM. The activities of thymidine metabolising enzymes during the cell cycle of a human lymphocyte cell line LAZ-007 synchronised by centrifugal elutriation. *Biochim Biophys Acta.* 1980;633(3):400-9. PubMed PMID: 6260157.

134. Sherley JL, Kelly TJ. Regulation of human thymidine kinase during the cell cycle. *The Journal of biological chemistry*. 1988;263(17):8350-8. PubMed PMID: 3372530.
135. Ellims PH, Van der Weyden MB, Medley G. Thymidine kinase isoenzymes in human malignant lymphoma. *Cancer Res*. 1981;41(2):691-5. PubMed PMID: 7448815.
136. Munch-Petersen B, Cloos L, Jensen HK, Tyrsted G. Human thymidine kinase 1. Regulation in normal and malignant cells. *Adv Enzyme Regul*. 1995;35:69-89. PubMed PMID: 7572355.
137. Barthel H, Perumal M, Latigo J, He Q, Brady F, Luthra SK, Price PM, Aboagye EO. The uptake of 3'-deoxy-3'-[18F]fluorothymidine into L5178Y tumours in vivo is dependent on thymidine kinase 1 protein levels. *European journal of nuclear medicine and molecular imaging*. 2005;32(3):257-63. doi: 10.1007/s00259-004-1611-0. PubMed PMID: 15791434.
138. Keen H, Pichler B, Kukuk D, Duchamp O, Raguin O, Shannon A, Whalley N, Jacobs V, Bales J, Gingles N, Ricketts SA, Wedge SR. An evaluation of 2-deoxy-2-[18F]fluoro-D-glucose and 3'-deoxy-3'-[18F]-fluorothymidine uptake in human tumor xenograft models. *Molecular imaging and biology : MIB : the official publication of the Academy of Molecular Imaging*. 2012;14(3):355-65. doi: 10.1007/s11307-011-0504-4. PubMed PMID: 21761255.
139. Seitz U, Wagner M, Neumaier B, Wawra E, Glatting G, Leder G, Schmid RM, Reske SN. Evaluation of pyrimidine metabolising enzymes and in vitro uptake of 3'-[[18F]fluoro-3'-deoxythymidine ([[18F]FLT) in pancreatic cancer cell lines. *Eur J Nucl Med Mol Imaging*. 2002;29(9):1174-81. doi: 10.1007/s00259-002-0851-0. PubMed PMID: 12192562.

140. von Forstner C, Egberts JH, Ammerpohl O, Niedzielska D, Buchert R, Mikecz P, Schumacher U, Peldschus K, Adam G, Pilarsky C, Grutzmann R, Kalthoff H, Henze E, Brenner W. Gene expression patterns and tumor uptake of ¹⁸F-FDG, ¹⁸F-FLT, and ¹⁸F-FEC in PET/MRI of an orthotopic mouse xenotransplantation model of pancreatic cancer. *J Nucl Med*. 2008;49(8):1362-70. doi: 10.2967/jnumed.107.050021. PubMed PMID: 18632830.
141. Barthel H, Cleij MC, Collingridge DR, Hutchinson OC, Osman S, He Q, Luthra SK, Brady F, Price PM, Aboagye EO. 3'-deoxy-3'-[¹⁸F]fluorothymidine as a new marker for monitoring tumor response to antiproliferative therapy in vivo with positron emission tomography. *Cancer Res*. 2003;63(13):3791-8. PubMed PMID: 12839975.
142. van Waarde A, Been LB, Ishiwata K, Dierckx RA, Elsinga PH. Early response of sigma-receptor ligands and metabolic PET tracers to 3 forms of chemotherapy: an in vitro study in glioma cells. *J Nucl Med*. 2006;47(9):1538-45. PubMed PMID: 16954564.
143. Sala R, Nguyen QD, Patel CB, Mann D, Steinke JH, Vilar R, Aboagye EO. Phosphorylation status of thymidine kinase 1 following antiproliferative drug treatment mediates 3'-deoxy-3'-[¹⁸F]-fluorothymidine cellular retention. *PloS one*. 2014;9(7):e101366. doi: 10.1371/journal.pone.0101366. PubMed PMID: 25003822; PMCID: 4086825.
144. Viel T, Schelhaas S, Wagner S, Wachsmuth L, Schwegmann K, Kuhlmann M, Faber C, Kopka K, Schafers M, Jacobs AH. Early assessment of the efficacy of temozolomide chemotherapy in experimental glioblastoma using [¹⁸F]FLT-PET imaging. *PloS one*. 2013;8(7):e67911. doi: 10.1371/journal.pone.0067911. PubMed PMID: 23861829; PMCID: 3701682.

145. Buck AK, Kratochwil C, Glatting G, Juweid M, Bommer M, Tepsic D, Vogg AT, Mattfeldt T, Neumaier B, Moller P, Reske SN. Early assessment of therapy response in malignant lymphoma with the thymidine analogue [18F]FLT. *Eur J Nucl Med Mol Imaging*. 2007;34(11):1775-82. doi: 10.1007/s00259-007-0452-z. PubMed PMID: 17541585.
146. Herrmann K, Buck AK, Schuster T, Rudelius M, Wester HJ, Graf N, Scheuerer C, Peschel C, Schwaiger M, Dechow T, Keller U. A pilot study to evaluate 3'-deoxy-3'-18F-fluorothymidine pet for initial and early response imaging in mantle cell lymphoma. *J Nucl Med*. 2011;52(12):1898-902. doi: 10.2967/jnumed.111.094698. PubMed PMID: 22065875.
147. Graf N, Herrmann K, den Hollander J, Fend F, Schuster T, Wester HJ, Senekowitsch-Schmidtke R, zum Buschenfelde CM, Peschel C, Schwaiger M, Dechow T, Buck AK. Imaging proliferation to monitor early response of lymphoma to cytotoxic treatment. *Molecular imaging and biology : MIB : the official publication of the Academy of Molecular Imaging*. 2008;10(6):349-55. doi: 10.1007/s11307-008-0162-3. PubMed PMID: 18704591.
148. Kwak W, Ha YS, Soni N, Lee W, Park SI, Ahn H, An GI, Kim IS, Lee BH, Yoo J. Apoptosis imaging studies in various animal models using radio-iodinated peptide. *Apoptosis : an international journal on programmed cell death*. 2015;20(1):110-21. doi: 10.1007/s10495-014-1059-z. PubMed PMID: 25430587.
149. Wu CY, Chou LS, Chan PC, Ho CH, Lin MH, Shen CC, Liu RS, Lin WJ, Wang HE. Monitoring tumor response with radiolabeled nucleoside analogs in a hepatoma-bearing mouse model early after doxisome((R)) treatment. *Molecular imaging and*

biology : MIB : the official publication of the Academy of Molecular Imaging. 2013;15(3):326-35. doi: 10.1007/s11307-012-0604-9. PubMed PMID: 23247923.

150. Vanderhoek M, Juckett MB, Perlman SB, Nickles RJ, Jeraj R. Early assessment of treatment response in patients with AML using [(18)F]FLT PET imaging. *Leukemia research*. 2011;35(3):310-6. doi: 10.1016/j.leukres.2010.06.010. PubMed PMID: 20832860; PMCID: 3319294.

151. Stronach EA, Alfraidi A, Rama N, Datler C, Studd JB, Agarwal R, Guney TG, Gourley C, Hennessy BT, Mills GB, Mai A, Brown R, Dina R, Gabra H. HDAC4-regulated STAT1 activation mediates platinum resistance in ovarian cancer. *Cancer Res*. 2011;71(13):4412-22. doi: 10.1158/0008-5472.CAN-10-4111. PubMed PMID: 21571862; PMCID: 3130134.

152. Lee SJ, Kim SY, Chung JH, Oh SJ, Ryu JS, Hong YS, Kim TW, Moon DH. Induction of thymidine kinase 1 after 5-fluorouracil as a mechanism for 3'-deoxy-3'-[18F]fluorothymidine flare. *Biochemical pharmacology*. 2010;80(10):1528-36. doi: 10.1016/j.bcp.2010.08.004. PubMed PMID: 20723540.

153. Hong IK, Kim SY, Chung JH, Lee SJ, Oh SJ, Lee SJ, Oh J, Ryu JS, Kim TW, Kim DY, Moon DH. 3'-Deoxy-3'-[18F]fluorothymidine positron emission tomography imaging of thymidine kinase 1 activity after 5-fluorouracil treatment in a mouse tumor model. *Anticancer Res*. 2014;34(2):759-66. PubMed PMID: 24511010.

154. Dittmann H, Dohmen BM, Kehlbach R, Bartusek G, Pritzkow M, Sarbia M, Bares R. Early changes in [18F]FLT uptake after chemotherapy: an experimental study. *Eur J Nucl Med Mol Imaging*. 2002;29(11):1462-9. doi: 10.1007/s00259-002-0925-z. PubMed PMID: 12397465.

155. Saito Y, Furukawa T, Arano Y, Fujibayashi Y, Saga T. Comparison of semiquantitative fluorescence imaging and PET tracer uptake in mesothelioma models as a monitoring system for growth and therapeutic effects. *Nuclear medicine and biology*. 2008;35(8):851-60. doi: 10.1016/j.nucmedbio.2008.08.002. PubMed PMID: 19026946.
156. Paproski RJ, Young JD, Cass CE. Predicting gemcitabine transport and toxicity in human pancreatic cancer cell lines with the positron emission tomography tracer 3'-deoxy-3'-fluorothymidine. *Biochemical pharmacology*. 2010;79(4):587-95. doi: 10.1016/j.bcp.2009.09.025. PubMed PMID: 19788890.
157. Kenny LM, Contractor KB, Stebbing J, Al-Nahhas A, Palmieri C, Shousha S, Coombes RC, Aboagye EO. Altered tissue 3'-deoxy-3'-[18F]fluorothymidine pharmacokinetics in human breast cancer following capecitabine treatment detected by positron emission tomography. *Clin Cancer Res*. 2009;15(21):6649-57. doi: 10.1158/1078-0432.CCR-09-1213. PubMed PMID: 19861447.
158. Frings V, van der Veldt AA, Boellaard R, Herder GJ, Giovannetti E, Honeywell R, Peters GJ, Thunnissen E, Hoekstra OS, Smit EF. Pemetrexed induced thymidylate synthase inhibition in non-small cell lung cancer patients: a pilot study with 3'-deoxy-3'-[(1)(8)F]fluorothymidine positron emission tomography. *PloS one*. 2013;8(5):e63705. doi: 10.1371/journal.pone.0063705. PubMed PMID: 23717468; PMCID: 3663749.
159. Hong YS, Kim HO, Kim KP, Lee JL, Kim HJ, Lee SJ, Lee SJ, Oh SJ, Kim JS, Ryu JS, Moon DH, Kim TW. 3'-Deoxy-3'-18F-fluorothymidine PET for the early prediction of response to leucovorin, 5-fluorouracil, and oxaliplatin therapy in patients

with metastatic colorectal cancer. *J Nucl Med.* 2013;54(8):1209-16. doi: 10.2967/jnumed.112.117010. PubMed PMID: 23804324.

160. Tehrani OS, Shields AF. PET imaging of proliferation with pyrimidines. *J Nucl Med.* 2013;54(6):903-12. doi: 10.2967/jnumed.112.112201. PubMed PMID: 23674576.

161. Direcks WG, Berndsen SC, Proost N, Peters GJ, Balzarini J, Spreeuwenberg MD, Lammertsma AA, Molthoff CF. [18F]FDG and [18F]FLT uptake in human breast cancer cells in relation to the effects of chemotherapy: an in vitro study. *Br J Cancer.* 2008;99(3):481-7. doi: 10.1038/sj.bjc.6604523. PubMed PMID: 18665170; PMCID: 2527810.

162. Ye YX, Calcagno C, Binderup T, Courties G, Keliher EJ, Wojtkiewicz GR, Iwamoto Y, Tang J, Perez-Medina C, Mani V, Ishino S, Johnbeck CB, Knigge U, Fayad ZA, Libby P, Weissleder R, Tawakol A, Dubey S, Belanger AP, Di Carli MF, Swirski FK, Kjaer A, Mulder WJ, Nahrendorf M. Imaging Macrophage and Hematopoietic Progenitor Proliferation in Atherosclerosis. *Circulation research.* 2015;117(10):835-45. doi: 10.1161/CIRCRESAHA.115.307024. PubMed PMID: 26394773; PMCID: 4619168.

163. Zhao S, Kuge Y, Kohanawa M, Takahashi T, Zhao Y, Yi M, Kanegae K, Seki K, Tamaki N. Usefulness of 11C-methionine for differentiating tumors from granulomas in experimental rat models: a comparison with 18F-FDG and 18F-FLT. *J Nucl Med.* 2008;49(1):135-41. doi: 10.2967/jnumed.107.044578. PubMed PMID: 18077525.

164. Cobben DC, van der Laan BF, Maas B, Vaalburg W, Suurmeijer AJ, Hoekstra HJ, Jager PL, Elsinga PH. 18F-FLT PET for visualization of laryngeal cancer: comparison with 18F-FDG PET. *J Nucl Med.* 2004;45(2):226-31. PubMed PMID: 14960640.

165. Troost EG, Vogel WV, Merkx MA, Slootweg PJ, Marres HA, Peeters WJ, Bussink J, van der Kogel AJ, Oyen WJ, Kaanders JH. 18F-FLT PET does not discriminate between reactive and metastatic lymph nodes in primary head and neck cancer patients. *J Nucl Med.* 2007;48(5):726-35. doi: 10.2967/jnumed.106.037473. PubMed PMID: 17475960.
166. Abbruzzese JL, Schmidt S, Raber MN, Levy JK, Castellanos AM, Legha SS, Krakoff IH. Phase I trial of 1-(2'-deoxy-2'-fluoro-1-beta-D-arabinofuranosyl)-5-methyluracil (FMAU) terminated by severe neurologic toxicity. *Investigational new drugs.* 1989;7(2-3):195-201. PubMed PMID: 2793372.
167. Bading JR, Shahinian AH, Vail A, Bathija P, Koszalka GW, Koda RT, Alauddin MM, Fissekis JD, Conti PS. Pharmacokinetics of the thymidine analog 2'-fluoro-5-methyl-1-beta-D-arabinofuranosyluracil (FMAU) in tumor-bearing rats. *Nuclear medicine and biology.* 2004;31(4):407-18. doi: 10.1016/j.nucmedbio.2004.01.001. PubMed PMID: 15093810.
168. Tehrani OS, Muzik O, Heilbrun LK, Douglas KA, Lawhorn-Crews JM, Sun H, Mangner TJ, Shields AF. Tumor imaging using 1-(2'-deoxy-2'-18F-fluoro-beta-D-arabinofuranosyl)thymine and PET. *J Nucl Med.* 2007;48(9):1436-41. doi: 10.2967/jnumed.107.042762. PubMed PMID: 17785728.
169. Collins JM, Klecker RW, Katki AG. Suicide prodrugs activated by thymidylate synthase: rationale for treatment and noninvasive imaging of tumors with deoxyuridine analogues. *Clin Cancer Res.* 1999;5(8):1976-81. PubMed PMID: 10473074.

170. Munch-Petersen B, Tyrsted G. Induction of thymidine kinases in phytohaemagglutinin-stimulated human lymphocytes. *Biochim Biophys Acta*. 1977;478(3):364-75. PubMed PMID: 911839.
171. Arner ES, Spasokoukotskaja T, Eriksson S. Selective assays for thymidine kinase 1 and 2 and deoxycytidine kinase and their activities in extracts from human cells and tissues. *Biochem Biophys Res Commun*. 1992;188(2):712-8. PubMed PMID: 1359886.
172. Berk AJ, Meyer BJ, Clayton DA. Mitochondrial-specific thymidine kinase. *Archives of biochemistry and biophysics*. 1973;154(2):563-5. PubMed PMID: 4632422.
173. Koch J, Storstad EL. Incorporation of [3H]thymidine into nuclear and mitochondrial DNA in synchronized mammalian cells. *European journal of biochemistry / FEBS*. 1967;3(1):1-6. PubMed PMID: 6079770.
174. Sun H, Sloan A, Mangner TJ, Vaishampayan U, Muzik O, Collins JM, Douglas K, Shields AF. Imaging DNA synthesis with [18F]FMAU and positron emission tomography in patients with cancer. *Eur J Nucl Med Mol Imaging*. 2005;32(1):15-22. doi: 10.1007/s00259-004-1713-8. PubMed PMID: 15586282.
175. Eiseman JL, Brown-Proctor C, Kinahan PE, Collins JM, Anderson LW, Joseph E, Hamburger DR, Pan SS, Mathis CA, Egorin MJ, Klecker RW. Distribution of 1-(2-deoxy-2-fluoro-beta-D-arabinofuranosyl) uracil in mice bearing colorectal cancer xenografts: rationale for therapeutic use and as a positron emission tomography probe for thymidylate synthase. *Clin Cancer Res*. 2004;10(19):6669-76. doi: 10.1158/1078-0432.CCR-03-0686. PubMed PMID: 15475457.

176. Klecker RW, Katki AG, Collins JM. Toxicity, metabolism, DNA incorporation with lack of repair, and lactate production for 1-(2'-fluoro-2'-deoxy-beta-D-arabinofuranosyl)-5-iodouracil in U-937 and MOLT-4 cells. *Molecular pharmacology*. 1994;46(6):1204-9. PubMed PMID: 7808443.
177. Sun H, Collins JM, Mangner TJ, Muzik O, Shields AF. Imaging [18F]FAU [1-(2'-deoxy-2'-fluoro-beta-D-arabinofuranosyl) uracil] in dogs. *Nuclear medicine and biology*. 2003;30(1):25-30. PubMed PMID: 12493539.
178. Sun H, Collins JM, Mangner TJ, Muzik O, Shields AF. Imaging the pharmacokinetics of [F-18]FAU in patients with tumors: PET studies. *Cancer chemotherapy and pharmacology*. 2006;57(3):343-8. doi: 10.1007/s00280-005-0037-0. PubMed PMID: 16001172.
179. Wang H, Oliver P, Nan L, Wang S, Wang Z, Rhie JK, Zhang R, Hill DL. Radiolabeled 2'-fluorodeoxyuracil-beta-D-arabinofuranoside (FAU) and 2'-fluoro-5-methyldeoxyuracil-beta -D-arabinofuranoside (FMAU) as tumor-imaging agents in mice. *Cancer chemotherapy and pharmacology*. 2002;49(5):419-24. doi: 10.1007/s00280-002-0433-7. PubMed PMID: 11976837.
180. Allegra CJ, Paik S, Colangelo LH, Parr AL, Kirsch I, Kim G, Klein P, Johnston PG, Wolmark N, Wieand HS. Prognostic value of thymidylate synthase, Ki-67, and p53 in patients with Dukes' B and C colon cancer: a National Cancer Institute-National Surgical Adjuvant Breast and Bowel Project collaborative study. *J Clin Oncol*. 2003;21(2):241-50. PubMed PMID: 12525515.
181. Aschele C, Lonardi S, Monfardini S. Thymidylate Synthase expression as a predictor of clinical response to fluoropyrimidine-based chemotherapy in advanced

colorectal cancer. *Cancer treatment reviews*. 2002;28(1):27-47. doi: 10.1053/ctrv.2002.0253. PubMed PMID: 12027413.

182. Ichikawa W, Uetake H, Shirota Y, Yamada H, Nishi N, Nihei Z, Sugihara K, Hirayama R. Combination of dihydropyrimidine dehydrogenase and thymidylate synthase gene expressions in primary tumors as predictive parameters for the efficacy of fluoropyrimidine-based chemotherapy for metastatic colorectal cancer. *Clin Cancer Res*. 2003;9(2):786-91. PubMed PMID: 12576451.

183. Johnston PG, Fisher ER, Rockette HE, Fisher B, Wolmark N, Drake JC, Chabner BA, Allegra CJ. The role of thymidylate synthase expression in prognosis and outcome of adjuvant chemotherapy in patients with rectal cancer. *J Clin Oncol*. 1994;12(12):2640-7. PubMed PMID: 7989939.

184. Popat S, Matakidou A, Houlston RS. Thymidylate synthase expression and prognosis in colorectal cancer: a systematic review and meta-analysis. *J Clin Oncol*. 2004;22(3):529-36. doi: 10.1200/JCO.2004.05.064. PubMed PMID: 14752076.

185. Shields AF, Li J, Wiegand RA, Lawhorn-Crews J, Douglas K, Mangner TJ, LoRusso PM. Use of [18F]FAU and PET to Evaluate Hepatic Toxicity in Patients Receiving FAU in a Phase I Therapeutic Trial. *World Molecular Imaging Congress*; September 19, 2013; Savannah, GA2013.

186. Li J, Kim S, Shields AF, Douglas KA, McHugh CI, Lawhorn-Crews JM, Wu J, Mangner TJ, LoRusso PM. Integrating Dynamic Positron Emission Tomography and Conventional Pharmacokinetic Studies to Delineate Plasma and Tumor Pharmacokinetics of FAU, a Prodrug Bioactivated by Thymidylate Synthase. *J Clin Pharmacol*. 2016. doi: 10.1002/jcph.751. PubMed PMID: 27095537.

187. Wang Z, Malone MH, He H, McColl KS, Distelhorst CW. Microarray analysis uncovers the induction of the proapoptotic BH3-only protein Bim in multiple models of glucocorticoid-induced apoptosis. *The Journal of biological chemistry*. 2003;278(26):23861-7. doi: 10.1074/jbc.M301843200. PubMed PMID: 12676946.
188. Barnes PJ. Anti-inflammatory actions of glucocorticoids: molecular mechanisms. *Clinical science*. 1998;94(6):557-72. PubMed PMID: 9854452.
189. Lecocq FR, Mebane D, Madison LL. The Acute Effect of Hydrocortisone on Hepatic Glucose Output and Peripheral Glucose Utilization. *The Journal of clinical investigation*. 1964;43:237-46. doi: 10.1172/JCI104908. PubMed PMID: 14162532; PMCID: 289517.
190. Hollenberg SM, Weinberger C, Ong ES, Cerelli G, Oro A, Lebo R, Thompson EB, Rosenfeld MG, Evans RM. Primary structure and expression of a functional human glucocorticoid receptor cDNA. *Nature*. 1985;318(6047):635-41. PubMed PMID: 2867473.
191. Weinberger C, Hollenberg SM, Ong ES, Harmon JM, Brower ST, Cidlowski J, Thompson EB, Rosenfeld MG, Evans RM. Identification of human glucocorticoid receptor complementary DNA clones by epitope selection. *Science*. 1985;228(4700):740-2. PubMed PMID: 2581314.
192. McKenna NJ, Xu J, Nawaz Z, Tsai SY, Tsai MJ, O'Malley BW. Nuclear receptor coactivators: multiple enzymes, multiple complexes, multiple functions. *The Journal of steroid biochemistry and molecular biology*. 1999;69(1-6):3-12. PubMed PMID: 10418975.

193. Lu NZ, Cidlowski JA. The origin and functions of multiple human glucocorticoid receptor isoforms. *Annals of the New York Academy of Sciences*. 2004;1024:102-23. doi: 10.1196/annals.1321.008. PubMed PMID: 15265776.
194. Bamberger CM, Schulte HM, Chrousos GP. Molecular determinants of glucocorticoid receptor function and tissue sensitivity to glucocorticoids. *Endocrine reviews*. 1996;17(3):245-61. doi: 10.1210/edrv-17-3-245. PubMed PMID: 8771358.
195. Jonat C, Rahmsdorf HJ, Park KK, Cato AC, Gebel S, Ponta H, Herrlich P. Antitumor promotion and antiinflammation: down-modulation of AP-1 (Fos/Jun) activity by glucocorticoid hormone. *Cell*. 1990;62(6):1189-204. PubMed PMID: 2169351.
196. Scheinman RI, Gualberto A, Jewell CM, Cidlowski JA, Baldwin AS, Jr. Characterization of mechanisms involved in transrepression of NF-kappa B by activated glucocorticoid receptors. *Molecular and cellular biology*. 1995;15(2):943-53. PubMed PMID: 7823959; PMCID: 231982.
197. Oakley RH, Sar M, Cidlowski JA. The human glucocorticoid receptor beta isoform. Expression, biochemical properties, and putative function. *The Journal of biological chemistry*. 1996;271(16):9550-9. PubMed PMID: 8621628.
198. Oakley RH, Webster JC, Sar M, Parker CR, Jr., Cidlowski JA. Expression and subcellular distribution of the beta-isoform of the human glucocorticoid receptor. *Endocrinology*. 1997;138(11):5028-38. doi: 10.1210/endo.138.11.5501. PubMed PMID: 9348235.
199. Oakley RH, Jewell CM, Yudt MR, Bofetiado DM, Cidlowski JA. The dominant negative activity of the human glucocorticoid receptor beta isoform. Specificity and

mechanisms of action. *The Journal of biological chemistry*. 1999;274(39):27857-66. PubMed PMID: 10488132.

200. Vietti TJ, Sullivan MP, Berry DH, Haddy TB, Haggard ME, Blattner RJ. The Response of Acute Childhood Leukemia to an Initial and a Second Course of Prednisone. *The Journal of pediatrics*. 1965;66:18-26. PubMed PMID: 14250052.

201. Koizumi S, Fujimoto T. Improvement in treatment of childhood acute lymphoblastic leukemia: a 10-year study by the Children's Cancer and Leukemia Study Group. *International journal of hematology*. 1994;59(2):99-112. PubMed PMID: 8018909.

202. Tormo M, Terol MJ, Marugan I, Solano C, Benet I, Garcia-Conde J. Treatment of stage I and II Hodgkin's disease with NOVP (mitoxantrone, vincristine, vinblastine, prednisone) and radiotherapy. *Leukemia & lymphoma*. 1999;34(1-2):137-42. doi: 10.3109/10428199909083389. PubMed PMID: 10350341.

203. Santoro A, Balzarotti M, Tondini C, Zanini M, Giardini R, Latteri F, Rampinelli I, Bufalino R. Dose-escalation of CHOP in non-Hodgkin's lymphoma. *Annals of oncology : official journal of the European Society for Medical Oncology / ESMO*. 1999;10(5):519-25. PubMed PMID: 10416000.

204. Barlogie B, Smith L, Alexanian R. Effective treatment of advanced multiple myeloma refractory to alkylating agents. *N Engl J Med*. 1984;310(21):1353-6. doi: 10.1056/NEJM198405243102104. PubMed PMID: 6546971.

205. Schwartzman RA, Cidlowski JA. Mechanism of tissue-specific induction of internucleosomal deoxyribonucleic acid cleavage activity and apoptosis by

glucocorticoids. *Endocrinology*. 1993;133(2):591-9. doi: 10.1210/endo.133.2.8393769. PubMed PMID: 8393769.

206. Hala M, Hartmann BL, Bock G, Geley S, Kofler R. Glucocorticoid-receptor-gene defects and resistance to glucocorticoid-induced apoptosis in human leukemic cell lines. *Int J Cancer*. 1996;68(5):663-8. doi: 10.1002/(SICI)1097-0215(19961127)68:5<663::AID-IJC17>3.0.CO;2-2. PubMed PMID: 8938150.

207. Schlossmacher G, Stevens A, White A. Glucocorticoid receptor-mediated apoptosis: mechanisms of resistance in cancer cells. *The Journal of endocrinology*. 2011;211(1):17-25. doi: 10.1530/JOE-11-0135. PubMed PMID: 21602312.

208. Herr I, Buchler MW, Mattern J. Glucocorticoid-mediated apoptosis resistance of solid tumors. *Results and problems in cell differentiation*. 2009;49:191-218. doi: 10.1007/400_2008_20. PubMed PMID: 19132324.

209. Glick RD, Medary I, Aronson DC, Scotto KW, Swendeman SL, La Quaglia MP. The effects of serum depletion and dexamethasone on growth and differentiation of human neuroblastoma cell lines. *Journal of pediatric surgery*. 2000;35(3):465-72. PubMed PMID: 10726691.

210. Goya L, Maiyar AC, Ge Y, Firestone GL. Glucocorticoids induce a G1/G0 cell cycle arrest of Con8 rat mammary tumor cells that is synchronously reversed by steroid withdrawal or addition of transforming growth factor-alpha. *Molecular endocrinology*. 1993;7(9):1121-32. doi: 10.1210/mend.7.9.8247014. PubMed PMID: 8247014.

211. Sanchez I, Goya L, Vallerga AK, Firestone GL. Glucocorticoids reversibly arrest rat hepatoma cell growth by inducing an early G1 block in cell cycle progression. *Cell*

growth & differentiation : the molecular biology journal of the American Association for Cancer Research. 1993;4(3):215-25. PubMed PMID: 8466859.

212. Braunschweiger PG, Ting HL, Schiffer LM. Correlation between glucocorticoid receptor content and the antiproliferative effect of dexamethasone in experimental solid tumors. *Cancer Res.* 1983;43(10):4757-61. PubMed PMID: 6883333.

213. Braunschweiger PG, Ting HL, Schiffer LM. Receptor-mediated antiproliferative effects of corticosteroids in Lewis lung tumors. *European journal of cancer & clinical oncology.* 1984;20(3):427-33. PubMed PMID: 6538502.

214. Freshney RI, Sherry A, Hassanzadah M, Freshney M, Crilly P, Morgan D. Control of cell proliferation in human glioma by glucocorticoids. *Br J Cancer.* 1980;41(6):857-66. PubMed PMID: 7426310; PMCID: 2010353.

215. Hofmann J, Kaiser U, Maasberg M, Havemann K. Glucocorticoid receptors and growth inhibitory effects of dexamethasone in human lung cancer cell lines. *Eur J Cancer.* 1995;31A(12):2053-8. PubMed PMID: 8562165.

216. Zibera C, Gibelli N, Butti G, Pedrazzoli P, Carbone M, Magrassi L, Robustelli della Cuna G. Proliferative effect of dexamethasone on a human glioblastoma cell line (HU 197) is mediated by glucocorticoid receptors. *Anticancer Res.* 1992;12(5):1571-4. PubMed PMID: 1444223.

217. Allegra JC, Lippman ME, Thompson EB, Simon R, Barlock A, Green L, Huff KK, Do HM, Aitken SC. Distribution, frequency, and quantitative analysis of estrogen, progesterone, androgen, and glucocorticoid receptors in human breast cancer. *Cancer Res.* 1979;39(5):1447-54. PubMed PMID: 427788.

218. Liu SH, Ota-Brun M, Webb TE. Glucocorticoid receptors in human tumors. *Cancer letters*. 1980;10(3):269-75. PubMed PMID: 7191771.
219. Mattern J, Buchler MW, Herr I. Cell cycle arrest by glucocorticoids may protect normal tissue and solid tumors from cancer therapy. *Cancer biology & therapy*. 2007;6(9):1345-54. PubMed PMID: 18087223.
220. Drewinko B, Patchen M, Yang LY, Barlogie B. Differential killing efficacy of twenty antitumor drugs on proliferating and nonproliferating human tumor cells. *Cancer Res*. 1981;41(6):2328-33. PubMed PMID: 7237431.
221. Carollo M, Parente L, D'Alessandro N. Dexamethasone-induced cytotoxic activity and drug resistance effects in androgen-independent prostate tumor PC-3 cells are mediated by lipocortin 1. *Oncology research*. 1998;10(5):245-54. PubMed PMID: 9802059.
222. Weller M, Schmidt C, Roth W, Dichgans J. Chemotherapy of human malignant glioma: prevention of efficacy by dexamethasone? *Neurology*. 1997;48(6):1704-9. PubMed PMID: 9191791.
223. Wolff JE, Denecke J, Jurgens H. Dexamethasone induces partial resistance to cisplatin in C6 glioma cells. *Anticancer Res*. 1996;16(2):805-9. PubMed PMID: 8687132.
224. Patki M, Gadgeel S, Huang Y, McFall T, Shields AF, Matherly LH, Bepler G, Ratnam M. Glucocorticoid receptor status is a principal determinant of variability in the sensitivity of non-small-cell lung cancer cells to pemetrexed. *Journal of thoracic oncology : official publication of the International Association for the Study of Lung*

Cancer. 2014;9(4):519-26. doi: 10.1097/JTO.000000000000111. PubMed PMID: 24736075; PMCID: 4075060.

225. Marini G, Murray S, Goldhirsch A, Gelber RD, Castiglione-Gertsch M, Price KN, Tattersall MH, Rudenstam CM, Collins J, Lindtner J, Cavalli F, Cortes-Funes H, Gudgeon A, Forbes JF, Galligioni E, Coates AS, Senn HJ. The effect of adjuvant prednisone combined with CMF on patterns of relapse and occurrence of second malignancies in patients with breast cancer. International (Ludwig) Breast Cancer Study Group. *Annals of oncology : official journal of the European Society for Medical Oncology / ESMO*. 1996;7(3):245-50. PubMed PMID: 8740787.

226. Postmus PE, Smit EF, Haaxma-Reiche H, van Zandwijk N, Ardizzoni A, Quoix E, Kirkpatrick A, Sahmoud T, Giaccone G. Teniposide for brain metastases of small-cell lung cancer: a phase II study. European Organization for Research and Treatment of Cancer Lung Cancer Cooperative Group. *J Clin Oncol*. 1995;13(3):660-5. PubMed PMID: 7884426.

227. Tchekmedyan NS. Clinical approaches to nutritional support in cancer. *Current opinion in oncology*. 1993;5(4):633-8. PubMed PMID: 8364079.

228. Lai YL, Fang FM, Yeh CY. Management of anorexic patients in radiotherapy: a prospective randomized comparison of megestrol and prednisolone. *Journal of pain and symptom management*. 1994;9(4):265-8. PubMed PMID: 8089543.

229. Weissman DE. Glucocorticoid treatment for brain metastases and epidural spinal cord compression: a review. *J Clin Oncol*. 1988;6(3):543-51. PubMed PMID: 3280744.

230. Aapro MS. Corticosteroids as antiemetics. Recent results in cancer research *Fortschritte der Krebsforschung Progres dans les recherches sur le cancer*. 1988;108:102-11. PubMed PMID: 3051200.
231. Lilly E. Alimta (pemetrexed) package insert 2005.
232. Society AC. Cancer Facts & Figures 2016. Atlanta, GA: 2016.
233. Hanna N, Shepherd FA, Fossella FV, Pereira JR, De Marinis F, von Pawel J, Gatzemeier U, Tsao TC, Pless M, Muller T, Lim HL, Desch C, Szondy K, Gervais R, Shaharyar, Manegold C, Paul S, Paoletti P, Einhorn L, Bunn PA, Jr. Randomized phase III trial of pemetrexed versus docetaxel in patients with non-small-cell lung cancer previously treated with chemotherapy. *J Clin Oncol*. 2004;22(9):1589-97. doi: 10.1200/JCO.2004.08.163. PubMed PMID: 15117980.
234. Patel JD, Socinski MA, Garon EB, Reynolds CH, Spigel DR, Olsen MR, Hermann RC, Jotte RM, Beck T, Richards DA, Guba SC, Liu J, Frimodt-Moller B, John WJ, Obasaju CK, Pennella EJ, Bonomi P, Govindan R. PointBreak: a randomized phase III study of pemetrexed plus carboplatin and bevacizumab followed by maintenance pemetrexed and bevacizumab versus paclitaxel plus carboplatin and bevacizumab followed by maintenance bevacizumab in patients with stage IIIB or IV nonsquamous non-small-cell lung cancer. *J Clin Oncol*. 2013;31(34):4349-57. doi: 10.1200/JCO.2012.47.9626. PubMed PMID: 24145346; PMCID: 4881367.
235. Reck M, Heigener DF, Mok T, Soria JC, Rabe KF. Management of non-small-cell lung cancer: recent developments. *Lancet*. 2013;382(9893):709-19. doi: 10.1016/S0140-6736(13)61502-0. PubMed PMID: 23972814.

236. Scagliotti GV, Parikh P, von Pawel J, Biesma B, Vansteenkiste J, Manegold C, Serwatowski P, Gatzemeier U, Digumarti R, Zukin M, Lee JS, Mellempgaard A, Park K, Patil S, Rolski J, Goksel T, de Marinis F, Simms L, Sugarman KP, Gandara D. Phase III study comparing cisplatin plus gemcitabine with cisplatin plus pemetrexed in chemotherapy-naive patients with advanced-stage non-small-cell lung cancer. *J Clin Oncol*. 2008;26(21):3543-51. doi: 10.1200/JCO.2007.15.0375. PubMed PMID: 18506025.
237. Chattopadhyay S, Moran RG, Goldman ID. Pemetrexed: biochemical and cellular pharmacology, mechanisms, and clinical applications. *Molecular cancer therapeutics*. 2007;6(2):404-17. doi: 10.1158/1535-7163.MCT-06-0343. PubMed PMID: 17308042.
238. Shih C, Habeck LL, Mendelsohn LG, Chen VJ, Schultz RM. Multiple folate enzyme inhibition: mechanism of a novel pyrrolopyrimidine-based antifolate LY231514 (MTA). *Adv Enzyme Regul*. 1998;38:135-52. PubMed PMID: 9762351.
239. Rusthoven JJ, Eisenhauer E, Butts C, Gregg R, Dancey J, Fisher B, Iglesias J. Multitargeted antifolate LY231514 as first-line chemotherapy for patients with advanced non-small-cell lung cancer: A phase II study. National Cancer Institute of Canada Clinical Trials Group. *J Clin Oncol*. 1999;17(4):1194. PubMed PMID: 10561178.
240. Alimta(R) [package insert]. Eli Lilly and Company, Inc., Indianapolis, IN; 2004. . Available from: <http://pi.lilly.com/us/alimta-pi.pdf>.
241. Basch E, Prestrud AA, Hesketh PJ, Kris MG, Feyer PC, Somerfield MR, Chesney M, Clark-Snow RA, Flaherty AM, Freundlich B, Morrow G, Rao KV, Schwartz RN, Lyman GH, American Society of Clinical O. Antiemetics: American Society of Clinical

- Oncology clinical practice guideline update. *J Clin Oncol*. 2011;29(31):4189-98. doi: 10.1200/JCO.2010.34.4614. PubMed PMID: 21947834; PMCID: 4876353.
242. Vilasco M, Communal L, Mourra N, Courtin A, Forgez P, Gompel A. Glucocorticoid receptor and breast cancer. *Breast Cancer Res Treat*. 2011;130(1):1-10. doi: 10.1007/s10549-011-1689-6. PubMed PMID: 21818591.
243. Schaaf MJ, Cidlowski JA. Molecular mechanisms of glucocorticoid action and resistance. *The Journal of steroid biochemistry and molecular biology*. 2002;83(1-5):37-48. PubMed PMID: 12650700.
244. Gerlinger M, Rowan AJ, Horswell S, Larkin J, Endesfelder D, Gronroos E, Martinez P, Matthews N, Stewart A, Tarpey P, Varela I, Phillimore B, Begum S, McDonald NQ, Butler A, Jones D, Raine K, Latimer C, Santos CR, Nohadani M, Eklund AC, Spencer-Dene B, Clark G, Pickering L, Stamp G, Gore M, Szallasi Z, Downward J, Futreal PA, Swanton C. Intratumor heterogeneity and branched evolution revealed by multiregion sequencing. *N Engl J Med*. 2012;366(10):883-92. doi: 10.1056/NEJMoa1113205. PubMed PMID: 22397650.
245. Tehrani OS, Douglas KA, Lawhorn-Crews JM, Shields AF. Tracking cellular stress with labeled FMAU reflects changes in mitochondrial TK2. *European journal of nuclear medicine and molecular imaging*. 2008;35(8):1480-8. doi: 10.1007/s00259-008-0738-9. PubMed PMID: 18265975.
246. Shields AF, Lawhorn-Crews JM, Briston DA, Zalzal S, Gadgeel S, Douglas KA, Mangner TJ, Heilbrun LK, Muzik O. Analysis and reproducibility of 3'-Deoxy-3'-[18F]fluorothymidine positron emission tomography imaging in patients with non-small cell lung cancer. *Clinical cancer research : an official journal of the American*

Association for Cancer Research. 2008;14(14):4463-8. doi: 10.1158/1078-0432.CCR-07-5243. PubMed PMID: 18628460.

247. Freedman LP, Gibson MC, Wisman R, Ethier SP, Soule HR, Reid YA, Neve RM. The culture of cell culture practices and authentication--Results from a 2015 Survey. *Biotechniques*. 2015;59(4):189-90, 92. doi: 10.2144/000114344. PubMed PMID: 26458546.

248. Jackman AL, Calvert AH. Folate-based thymidylate synthase inhibitors as anticancer drugs. *Annals of oncology : official journal of the European Society for Medical Oncology / ESMO*. 1995;6(9):871-81. PubMed PMID: 8624289.

249. Schmitz JC, Grindey GB, Schultz RM, Priest DG. Impact of dietary folic acid on reduced folates in mouse plasma and tissues. Relationship to dideazatetrahydrofolate sensitivity. *Biochemical pharmacology*. 1994;48(2):319-25. PubMed PMID: 8053927.

250. Jackman AL, Taylor GA, Calvert AH, Harrap KR. Modulation of anti-metabolite effects. Effects of thymidine on the efficacy of the quinazoline-based thymidylate synthetase inhibitor, CB3717. *Biochemical pharmacology*. 1984;33(20):3269-75. PubMed PMID: 6487375.

251. Taylor GA, Jackman AL, Calvert AH, Harrap KR. Plasma nucleoside and base levels following treatment with the new thymidylate synthetase inhibitor CB 3717. *Adv Exp Med Biol*. 1984;165 Pt B:379-82. PubMed PMID: 6720435.

252. Cao S, McGuire JJ, Rustum YM. Antitumor activity of ZD1694 (tomudex) against human head and neck cancer in nude mouse models: role of dosing schedule and plasma thymidine. *Clin Cancer Res*. 1999;5(7):1925-34. PubMed PMID: 10430100.

253. van der Wilt CL, Backus HH, Smid K, Comijn L, Veerman G, Wouters D, Voorn DA, Priest DG, Bunni MA, Mitchell F, Jackman AL, Jansen G, Peters GJ. Modulation of both endogenous folates and thymidine enhance the therapeutic efficacy of thymidylate synthase inhibitors. *Cancer Res.* 2001;61(9):3675-81. PubMed PMID: 11325838.
254. Shields AF, Grierson JR, Muzik O, Stayanoff JC, Lawhorn-Crews JM, Obradovich JE, Mangner TJ. Kinetics of 3'-deoxy-3'-[F-18]fluorothymidine uptake and retention in dogs. *Molecular imaging and biology : MIB : the official publication of the Academy of Molecular Imaging.* 2002;4(1):83-9. PubMed PMID: 14538051.
255. Wiegand R, Wu J, Shields AF, Lorusso P, Li J. Simultaneous determination of 1-(2'-deoxy-2'-fluoro-beta-D-arabinofuranosyl) uracil (FAU) and 1-(2'-deoxy-2'-fluoro-beta-D-arabinofuranosyl) 5-methyluracil (FMAU) in human plasma by liquid chromatography/tandem mass spectrometry. *J Chromatogr B Analyt Technol Biomed Life Sci.* 2012;891-892:64-70. doi: 10.1016/j.jchromb.2012.02.030. PubMed PMID: 22410089; PMCID: PMC3760386.
256. Dandona P, Mohanty P, Hamouda W, Aljada A, Kumbkarni Y, Garg R. Effect of dexamethasone on reactive oxygen species generation by leukocytes and plasma interleukin-10 concentrations: a pharmacodynamic study. *Clinical pharmacology and therapeutics.* 1999;66(1):58-65. doi: 10.1016/S0009-9236(99)70054-8. PubMed PMID: 10430110.
257. Bhadri VA, Cowley MJ, Kaplan W, Trahair TN, Lock RB. Evaluation of the NOD/SCID xenograft model for glucocorticoid-regulated gene expression in childhood B-cell precursor acute lymphoblastic leukemia. *BMC Genomics.* 2011;12:565. doi: 10.1186/1471-2164-12-565. PubMed PMID: 22093874; PMCID: 3228854.

258. Leonard MO, Godson C, Brady HR, Taylor CT. Potentiation of glucocorticoid activity in hypoxia through induction of the glucocorticoid receptor. *J Immunol.* 2005;174(4):2250-7. PubMed PMID: 15699159.
259. Gridelli C, Kaukel E, Gregorc V, Migliorino MR, Muller TR, Manegold C, Favaretto A, Martoni A, Caffo O, Schmittl A, Rossi A, Russo F, Peterson P, Munoz M, Reck M. Single-agent pemetrexed or sequential pemetrexed/gemcitabine as front-line treatment of advanced non-small cell lung cancer in elderly patients or patients ineligible for platinum-based chemotherapy: a multicenter, randomized, phase II trial. *Journal of thoracic oncology : official publication of the International Association for the Study of Lung Cancer.* 2007;2(3):221-9. doi: 10.1097/JTO.0b013e318031cd62. PubMed PMID: 17410045.
260. Cetin K, Ettinger DS, Hei YJ, O'Malley CD. Survival by histologic subtype in stage IV nonsmall cell lung cancer based on data from the Surveillance, Epidemiology and End Results Program. *Clinical epidemiology.* 2011;3:139-48. doi: 10.2147/CLEP.S17191. PubMed PMID: 21607015; PMCID: 3096514.
261. Liu Y, Yin TJ, Zhou R, Zhou S, Fan L, Zhang RG. Expression of thymidylate synthase predicts clinical outcomes of pemetrexed-containing chemotherapy for non-small-cell lung cancer: a systemic review and meta-analysis. *Cancer chemotherapy and pharmacology.* 2013;72(5):1125-32. doi: 10.1007/s00280-013-2299-2. PubMed PMID: 24067998.
262. Wynes MW, Konopa K, Singh S, Reyna-Asuncion B, Ranger-Moore J, Sternau A, Christoph DC, Dziadziuszko R, Jassem J, Hirsch FR. Thymidylate synthase protein expression by IHC and gene copy number by SISH correlate and show great variability

in non-small cell lung cancer. *Journal of thoracic oncology : official publication of the International Association for the Study of Lung Cancer*. 2012;7(6):982-92. doi: 10.1097/JTO.0b013e31824fe95a. PubMed PMID: 22551903; PMCID: 3645942.

263. Lu YS, Lien HC, Yeh PY, Kuo SH, Chang WC, Kuo ML, Cheng AL. Glucocorticoid receptor expression in advanced non-small cell lung cancer: clinicopathological correlation and in vitro effect of glucocorticoid on cell growth and chemosensitivity. *Lung cancer*. 2006;53(3):303-10. doi: 10.1016/j.lungcan.2006.05.005. PubMed PMID: 16806572.

264. Koukourakis GV, Kouloulis V, Koukourakis MJ, Zacharias GA, Zabatis H, Kouvaris J. Efficacy of the oral fluorouracil pro-drug capecitabine in cancer treatment: a review. *Molecules*. 2008;13(8):1897-922. PubMed PMID: 18794792.

265. Simplicio AL, Clancy JM, Gilmer JF. Prodrugs for amines. *Molecules*. 2008;13(3):519-47. PubMed PMID: 18463563.

266. Budman DR, Meropol NJ, Reigner B, Creaven PJ, Lichtman SM, Berghorn E, Behr J, Gordon RJ, Osterwalder B, Griffin T. Preliminary studies of a novel oral fluoropyrimidine carbamate: capecitabine. *J Clin Oncol*. 1998;16(5):1795-802. PubMed PMID: 9586893.

267. Miwa M, Ura M, Nishida M, Sawada N, Ishikawa T, Mori K, Shimma N, Umeda I, Ishitsuka H. Design of a novel oral fluoropyrimidine carbamate, capecitabine, which generates 5-fluorouracil selectively in tumours by enzymes concentrated in human liver and cancer tissue. *Eur J Cancer*. 1998;34(8):1274-81. PubMed PMID: 9849491.

268. Schuetz JD, Wallace HJ, Diasio RB. 5-Fluorouracil incorporation into DNA of CF-1 mouse bone marrow cells as a possible mechanism of toxicity. *Cancer Res.* 1984;44(4):1358-63. PubMed PMID: 6704957.
269. Soloviev D, Lewis D, Honess D, Aboagye E. [(18)F]FLT: an imaging biomarker of tumour proliferation for assessment of tumour response to treatment. *Eur J Cancer.* 2012;48(4):416-24. doi: 10.1016/j.ejca.2011.11.035. PubMed PMID: 22209266.
270. Buck AK, Schirrmeister H, Hetzel M, Von Der Heide M, Halter G, Glatting G, Mattfeldt T, Liewald F, Reske SN, Neumaier B. 3-deoxy-3-[(18)F]fluorothymidine-positron emission tomography for noninvasive assessment of proliferation in pulmonary nodules. *Cancer Res.* 2002;62(12):3331-4. PubMed PMID: 12067968.
271. Schwartz JL, Tamura Y, Jordan R, Grierson JR, Krohn KA. Monitoring tumor cell proliferation by targeting DNA synthetic processes with thymidine and thymidine analogs. *J Nucl Med.* 2003;44(12):2027-32. PubMed PMID: 14660729.
272. Mangner TJ, Klecker RW, Anderson L, Shields AF. Synthesis of 2'-deoxy-2'-[18F]fluoro-beta-D-arabinofuranosyl nucleosides, [18F]FAU, [18F]FMAU, [18F]FBAU and [18F]FIAU, as potential PET agents for imaging cellular proliferation. Synthesis of [18F]labelled FAU, FMAU, FBAU, FIAU. *Nuclear medicine and biology.* 2003;30(3):215-24. PubMed PMID: 12745012.
273. Weber WA, Gatsonis CA, Mozley PD, Hanna LG, Shields AF, Aberle DR, Govindan R, Torigian DA, Karp JS, Yu JQ, Subramaniam RM, Halvorsen RA, Siegel BA, team AR, team MKR. Repeatability of 18F-FDG PET/CT in Advanced Non-Small Cell Lung Cancer: Prospective Assessment in 2 Multicenter Trials. *J Nucl Med.*

2015;56(8):1137-43. doi: 10.2967/jnumed.114.147728. PubMed PMID: 25908829; PMCID: PMC4699428.

274. Lee SJ, Choi YL, Park YH, Kim ST, Cho EY, Ahn JS, Im YH. Thymidylate synthase and thymidine phosphorylase as predictive markers of capecitabine monotherapy in patients with anthracycline- and taxane-pretreated metastatic breast cancer. *Cancer chemotherapy and pharmacology*. 2011;68(3):743-51. doi: 10.1007/s00280-010-1545-0. PubMed PMID: 21170649.

275. Kluza J, Marchetti P, Gallego MA, Lancel S, Fournier C, Loyens A, Beauvillain JC, Bailly C. Mitochondrial proliferation during apoptosis induced by anticancer agents: effects of doxorubicin and mitoxantrone on cancer and cardiac cells. *Oncogene*. 2004;23(42):7018-30. doi: 10.1038/sj.onc.1207936. PubMed PMID: 15273722.

276. Mancini M, Anderson BO, Caldwell E, Sedghinasab M, Paty PB, Hockenbery DM. Mitochondrial proliferation and paradoxical membrane depolarization during terminal differentiation and apoptosis in a human colon carcinoma cell line. *J Cell Biol*. 1997;138(2):449-69. PubMed PMID: 9230085; PMCID: 2138196.

ABSTRACT**IMAGING ANTI-PROLIFERATIVE COMPOUNDS WITH FLT-PET**

by

CHRISTOPHER I. MCHUGH**August 2016****Advisor:** Dr. Anthony F. Shields**Major:** Cancer Biology**Degree:** Doctor of Philosophy

Imaging is critical in the detection and management of malignancies, and positron emission tomography (PET) is an imaging approach that provides information regarding cancer physiology through the tracking of molecular pathways and receptors. 3'-fluoro-3'-deoxythymidine (FLT) is a PET tracer designed to image cellular proliferation, which is a hallmark of cancer. FLT has been used to study the response of cancer to a variety of treatments such as chemotherapy, targeted agents, and radiation.

Here we explored FLT retention as a biomarker to monitor the anti-proliferative effect of the synthetic glucocorticoid (GC) dexamethasone (Dex) on non-small cell lung cancer (NSCLC). The basis for this work was the recent finding that Dex can cause reversible cell cycle arrest in a subset of NSCLC cells leading to chemotherapy resistance. A similar phenomenon has been shown in several other solid tumor models treated with GCs. Through studies of cell line models, human xenografts, and NSCLC patients, we observed that although the susceptibility to Dex-mediated cell cycle arrest is variable between cancers, it could be detected using FLT-PET. We also examined the FLT 'flare' phenomenon, in which FLT uptake is transiently increased following

treatment with drugs that reduce cellular thymidine synthesis. Two routinely used chemotherapeutic agents, pemetrexed and capecitabine, were found to produce marked increases in FLT accumulation, though the effect was variable in patients treated with capecitabine.

The success of FLT led to the introduction of other thymidine analog PET tracers including 1-(2'-deoxy-2'-fluoro- β -D-arabinofuranosyl) thymidine (FMAU) and 1-(2'-deoxy-2'-fluoro- β -D-arabinofuranosyl) uracil (FAU). Uptake of FMAU has been shown to be related to mitochondrial mass and cellular stress, while FAU is a prodrug that requires activation by thymidylate synthase. Although capecitabine treatment produced a change from baseline in patients imaged with FLT, tracer retention was unchanged in patients imaged with FMAU and FAU, highlighting the differences in imaging properties between the tracers.

In summary, FLT continues to show promise as a tool for the non-invasive monitoring of cellular proliferation, and may be a useful biomarker for the prediction of GC sensitivity in solid tumors.

AUTOBIOGRAPHICAL STATEMENT

CHRISTOPHER I. MCHUGH

I enrolled in the MD/PhD program at the Wayne State University School of Medicine in the summer of 2011. After two years of medical school and a couple of graduate rotations I joined the research group of Dr. Anthony Shields. Although I didn't know much about imaging at the time, I was interested in Dr. Shields' work with positron emission tomography (PET) as a way to assess cancer therapy, an approach with which I was completely unfamiliar. In addition, I felt that Dr. Shields' would be an especially good mentor for me since he is a practicing physician-scientist.

My work in the Shields laboratory has been the study of thymidine analog PET tracers, with a focus on 3'-fluoro-3'-deoxythymidine (FLT). Specifically, the goal of my studies was to use PET to monitor the response of cancer to chemotherapy. With Dr. Shields' guidance, I gained an understanding of the field of nuclear imaging and developed my technical laboratory skills. I also learned to analyze patient and animal PET and computed tomography (CT) images. Throughout my training I collaborated with several clinical and scientific faculty at the Karmanos Cancer Institute, which helped to broaden my knowledge of chemotherapy and cancer as a whole.

I was able to present my work twice at international imaging conferences, as well as internal meetings at Wayne State. In the coming years I will conclude my medical training and seek a research-focused residency position. Ultimately, I would like to be a faculty member at a major research hospital.